A CASE STUDY OF LARGE SCALE ATMOSPHERIC BLOCKING AND A PROPOSED INSTABILITY MECHANISM

Francis X. Crum

Colorado State University

DEPARTMENT OF ATMOSPHERIC SCIENCE

PAPER NO. 431

A CASE STUDY OF LARGE SCALE ATMOSPHERIC BLOCKING

AND A PROPOSED INSTABILITY MECHANISM

by

Francis X. Crum

Department of Atmospheric Science
Colorado State University
Fort Collins, CO 80523

This research was supported by the
National Science Foundation under
grants ATM-8609731 and ATM-8405059

Atmospheric Science Paper No. 431

September 1988

Abstract

Blocking is investigated from both an observational and a theoretical viewpoint. Climatological and synoptic descriptions of blocks are summarized. A review of blocking theories is presented consisting of a detailed critique of multiple-equilibria and modon research. Despite some attractive features, both of these theories have some deficiencies as explanations of observed blocks.

The main body of the work is in two parts, the first of which is a case study of blocking using isentropic analysis, with particular emphasis on the distribution and evolution of potential vorticity on isentropic surfaces. Analysis of the Montgomery streamfunction on an isentropic surface is preferable to the more traditional analysis of geopotential height on a pressure surface for describing the evolution of the horizontal structure. Vertical cross sections during the mature phase show little tilt with height, a warm core and a high tropopause. Analysis of potential vorticity indicate that the block is a broad area of uniformly low potential vorticity. An EOF analysis added confirmation to this while illustrating well the development of the block. The two components of the potential vorticity – the absolute vorticity and the static stability – evolve in the same way as the potential vorticity itself, becoming smaller or larger as the potential vorticity becomes smaller or larger. Subjective interpretation of the potential vorticity maps indicate that the low potential vorticity air characterizing the block originates from well south of the block. Isentropic trajectory analysis verifies this and notes the relationship between the trajectories and the advection ahead of an intense cyclone that formed upstream of the block as the block developed. Selected moist trajectories are also computed.

The second part of the work is an examination of barotropic instability in the presence of downstream and asymmetric cross–stream variations in the basic state. Solutions are obtained with the non-divergent barotropic vorticity equation linearized about an arbitrary basic state. When downstream variation is present, the maximum amplitude of the unstable

streamfunction is always located downstream from the location of maximum latitudinal shear. This occurs because the unstable disturbance lags in adjusting to the local instability characteristics. The instability is sensitive to the degree of downstream variation with more concentration of streamfunction amplitude in specific regions of the channel, smaller disturbance scales and smaller growth rates when there is strong variation that when the flow is more parallel. The smaller growth rate for the downstream variation case results from the propagating disturbance being subjected to strong shear for only a finite time before moving into regions of lesser shear where it cannot grow as fast. Asymmetric cross-stream variation has little effect on the growth rate and frequency of the most unstable mode but significantly affects the structure of the instability. Larger amplitude and more pronounced tilt opposite to the shear occur on the side of the jet with the strongest shear. This can be expected from a theoretical consideration of the energetics. Instabilities in the presence of both downstream and asymmetric cross-stream variations combine the effects of each of those individual kinds of variations. An eigenvalue method and a time integration method were used to obtain these results. They compare favorably and complement one another. A single non-linear calculation shows that as the disturbances grow to finite amplitude, they split, with high centers moving to the north and low centers to the south. The disturbances also increase in scale and stabilize the mean flow without removing all the downstream variation.

Additional baroclinic and non-linear calculations are proposed to investigate the hypothesis that the development of blocking patterns may depend crucially on whether the large scale flow is conducive to an instability with blocking characteristics.

Acknowledgements

I thank my advisor, Dr. Duane E. Stevens, for his guidance, encouragement, and support of my research. I especially appreciate the freedom he gave me to pursue several different topics throughout my long association with him. My other committee members, Dr. Wayne Schubert, Dr. William Gray and Dr. Gerry Taylor contributed valuable advice during private meetings as well as at committee meetings. I have also benefited from several discussions with Dr. Richard Johnson.

There is a long list of students and research associates from whom I have learned much. Scott Fulton helped me to understand many numerical and mathematical techniques. His knowledge, enthusiasm and quality of work made a strong impression on me. Hung-Chi Kuo was always interested in my work – his questions helped me to more clearly formulate what I was doing and how I was doing it. George Young, Bob Merrill, Greg Holland, Mel Nicholls and Mark DeMaria were always willing to discuss any scientific question. The work ethics of Tim Stoker and Paul Ciesielski have set a high standard for me. Craig Tremback frequently helped me to unravel the complexities of the NCAR computer systems. These folks are also my friends and as such I've shared with them innumerable wonderful cycling trips, games and music making experiences.

I thank Gail Cordova for expertly typing this paper using the TEX typesetting system and for her able assistance in other secretarial matters.

I am also indebted to my church family. Many folks deserve my thanks for their prayers, support, Christian fellowship and genuine interest in my work. John McBride, Glenn Gilbert and Tom Glossi are especially deserving of mention.

My wife, Joanne, has been infinitely patient with me offering ongoing support and love. Her encouragement and prayers were probably the determining factor in finishing my dissertation and this paper. I also thank my family for upholding me throughout my many years of higher education.

The research reported in this work was funded by the National Science Foundation through grants ATM-8609731 and ATM-8405059. Computing support was provided by the National Center for Atmospheric Research.

TABLE OF CONTENTS

Chapter 1

INTRODUCTION AND REVIEW OF OBSERVATIONAL AND THEORETICAL BLOCKING RESEARCH

1.1 Introduction

Blocking events have long been recognized as significant features of the large scale flow in the atmosphere. They are not only theoretically interesting but of practical importance as well because they can influence the weather in a rather large region for a week to two weeks and sometimes even longer. Much attention has been devoted to documenting their climatological and synoptic characteristics, diagnosing what physical effects are important to their dynamics, and developing theories to account for these observations. In the following sections we review and evaluate some of this research. Section 1.2 is devoted to observations of blocking events, concentrating on a climatological and synoptic description along with diagnostic work. Section 1.3 is devoted to theories with emphasis on multiple equilibria concepts and modons. Conclusions and an overview of subsequent chapters is given in Section 1.4.

1.2 Observations of Blocking

1.2.1 Climatology

It would seem wise to begin a summary of blocking studies by giving a precise definition of the phenomena. However, in spite of the recent increase in research effort devoted to blocks, there is no single definition that all researchers find suitable. The classic definition is due to Rex (1950a) who requires a blocking case to exhibit the following characteristics at 500mb:

(a) the basic westerly current must split into two branches,

(b) each branch must transport appreciable mass,

(c) the double jet system must extend over at least 45° of longitude,

(d) a sharp transition from zonal type flow upstream to meridional type downstream must be observed across the current split, and

(e) the pattern must persist for at least 10 days.

This rather subjective definition can be contrasted with Dole and Gordon's (1983) much more objective definition of persistent anomalies which requires (for a positive anomaly) the normalized geopotential height deviation from a long term time mean to be greater than some specified magnitude M for a time not less than T days. Most other definitions are some modification of one of these. Despite this variety, there seems to be an informal consensus that defines blocks at middle and upper levels as strong, large scale, persistent and nearly stationary perturbations of the predominantly westerly flow. While it is common and traditional to think of the perturbations as ridges or dipole–like structures with a ridge to the north and a trough to the south, troughs which have the above characteristics have also been accepted as blocks. Researchers may argue over details, but they all seem to have in mind a fundamental picture of what constitutes a blocking pattern.

Blocking in the northern hemisphere tends to occur mostly in two areas: the northern Atlantic southeast of Greenland and the northern Pacific. The Atlantic geographical maximum is consistently documented (e.g. Rex, 1950b; Treidl, *et al.*, 1981; Charney, Schukla and Mo, 1981; Knox and Hay, 1985; Quiroz, 1987). In the Pacific region there seems to be some minor discrepancies with Rex (1950b) and Knox and Hay (1985), for example, showing a maximum around 150W while White and Clark (1975) and Lejenas and Økland (1983) document a maximum closer to 180W. Dole and Gordon's (1983) positive persistent anomalies have a maximum at about 160W. Each of these studies uses a different criteria for block identification which undoubtedly explains some of the differences. Rex acknowledges that data limitations may effect his results in the Pacific; other studies use different data sets yielding another source of discrepancies. It is not the

purpose of this summary to investigate these differences in detail; suffice it to say that there is a definite Pacific maximum in blocking activity. Finally, there is also a region of blocking activity near the Ural mountains as noted by Dole and Gordon (1983) and Shukla and Mo (1983).

Blocking patterns can occur at any time of year but are most prevalent during the spring and winter. Rex (1950b) notes a percentage of blocking days in a month that is roughly twice as large during the spring and winter than the summer and fall. Analyzing 664 blocking highs over a 32 year period, Treidl, *et al.*, (1981) noted that 205 blocks began in spring, 173 in winter, 147 in summer and 139 in fall. The geographical distribution of blocks does not change with season (Shukla and Mo, 1983).

The question of how often blocks occur is one that is hard to answer directly because of the variety of blocking definitions and techniques used to identify them. Beginning again with Rex (1950b), his statistics show one blocking case every two months in the Atlantic region and one case every four months in the Pacific. Rex's criteria are rather stringent so that he finds fewer blocks than in some other investigations. Treidl, et.al. (1981) find slightly more than two blocking events per month. These figures are averages and need to be adjusted accordingly for seasonal and geographical variations.

The duration of blocking events is subjected to the same problem as their frequency of occurrence. Rex (1950b) and Triedl, *et al.* (1981) find maxima at roughly two weeks and twelve days, respectively. Dole and Gordon (1983) find no preferred duration for their persistent anomalies, noting exponential frequency decay with increasing duration for sufficiently long durations.

In conclusion, the results of a climatology of blocking are a strong function of the methods used to identify blocking events. Nevertheless, certain general characteristics predominate: geographical maxima in blocking frequency in the north Atlantic and north Pacific, seasonal variation with maxima in spring and winter, an average of one to two blocking events per month with durations in the range of one to two weeks. Specific problems and reason for discrepancies have only been touched upon; the interested reader is referred to the references quoted herein for a much greater wealth of detail.

1.2.2 Synoptic characteristics

Having roughly defined blocks and documented the gross features of their climatology, a brief overview of their synoptic characteristics is now given.

It is the horizontal structure of blocking events that is addressed when formulating a definition of blocks. Thus, this structure has been defined previously as one of large scale perturbations to the predominately westerly flow, generally taking the form of ridges or dipole–like structures. Blocks have a barotropic structure in the vertical, exhibiting little tilt with height in their mature phase (Dole, 1986a). Strong surface highs are usually associated with ridging in the middle and upper troposphere.

Dole (1986b) describes in detail the life cycles of persistent anomalies in the Pacific region. He concludes that they often develop rapidly, in less than a week, with little evidence for a precursor until just prior to onset. The anomalies have substantial tilts with height during development, suggesting the importance of baroclinic effects during this stage. Breakdown is often rapid as well.

The dynamical balances of blocks have been studied by Mullen (1986). He used an anomaly type criterion to identify blocking events in a General Circulation Model (GCM). An advantage of using GCM output, instead of actual data, is the availability of a long record of high quality data containing many blocking events. The time–averaged vorticity and thermodynamic equations are considered. He finds that in the free atmosphere, the mean divergence and horizontal advection terms are the primary balance in the vorticity equation. The net effect of the time mean terms is to shift the block downstream. The eddy fluxes induce upstream movement and so oppose this tendency. In the thermodynamic equation, the primary balance is between the mean horizontal temperature advection and mean adiabatic heating or cooling. The net effect of the time mean terms is to maintain the thermal anomaly of the block. The eddies act to dissipate the thermal anomalies. The diabatic heating terms are small except near the surface. Finally, he suggests that processes affecting the vorticity balance may be more important than those affecting the heat balance.

Traveling synoptic scale storms appear to have an influence on blocking development. This was first documented by Berggren, *et al.* (1949) who show some interesting schematic illustrations of the effect of cyclone scale waves on the larger scale flow. Recent studies of this influence can be put into two categories: those which look at individual synoptic examples and those of a more statistical nature. The work of Colucci (1985, 1987) is a good example from the first category. He examines specific cases of intense cyclogenesis and notes their relationship to subsequent changes in the large scale flow. Intense cyclones located immediately upstream from a planetary scale ridge can favor development of an anticyclonic blocking vortex while similar cyclones upstream from a planetary scale trough can favor development of a cyclonic blocking vortex. When the planetary waves are of small amplitude, no response may be produced by cyclones. These studies can be contrasted with Mullen (1986, 1987) which are typical examples from the second category. In this type of study, the *net* effect of eddies on the time mean flow is calculated. Without going into detail, Mullen shows that the time–averaged vorticity and heat transports due to the transient eddies are an important part of the overall dynamical picture of the block. Illari (1984) notes that the time averaged eddy fluxes of quasi– geostrophic potential vorticity tend to balance the mean advection of potential vorticity. Hoskins, *et al.* (1983), using the powerful diagnostic technique of EP fluxes (Edmon *et al.*, 1980), come to similar conclusions. These studies are different from Colucci's in that only the net effect of many transients is known; information of the effect of any individual cyclone is not available. Both types of studies have value, the latter giving more quantitative proof that storms effect blocks while the former gives individual examples of that effect. Moreover, blocks are complex, and while an individual storm may be crucial to the evolution of one block, a sequence of storms may be the major influence in other cases (Shutts, 1986).

The general subject of scale interactions and energetics as they relate to blocking has been studied by Hansen and Chen (1982). They conclude that changes in ultralong waves during a blocking period are caused at least in part by non–linear interactions with cyclone scale waves. Additional work suggesting the presence of upscale transfer of energy as one of the differences between blocking and non–blocking periods is provided in Hansen

et al. (1984). More observational evidence for transient influence is found in Brown *et al.* (1986), and a numerical experiment suggesting that small scale traveling storms need to be resolved in order to predict blocking is given by Bengtsson (1981). In conclusion, there is a considerable body of evidence in support of cyclone scale waves having a significant impact on large–scale blocking flows.

1.3 Theories for blocking

Between the time of Rex's (1950a) tentative explanation of blocks as an example of an hydraulic jump, and the beginning of the last decade, there was little theoretical research devoted to blocking. This has changed with the recent appearance of numerous papers, possibly motivated by the extremely cold weather conditions during the North American winter of 1976 (Benzi and Wiin-Nielsen, 1986). Theoretical explanations for blocks fall into several categories; a useful review is given by Baines (1983). Benzi, Saltzman and Wiin-Nielsen (1986) provide a more up-to-date compilation of research results. Rather than attempt to summarize all this research, a critical, detailed review of two specific areas related to the author's interest is given. Accordingly, the following two subsections are devoted to multiple equilibria concepts and modons.

1.3.1 Multiple-equilibria

An obvious synoptic feature of blocking events, for which any complete dynamical theory must account, is their persistence: the large scale flow changes little over a period of a week or longer. A plausible explanation is provided by the multiple-equilibria theories. These theories suggest that the state of the atmosphere tends to be, excepting transition times, in one of several different regimes, each characterized by a different type of large scale flow pattern. Very often, one of these regimes resembles blocking flow. The term *multiple-equilibria* is generally used to refer to these ideas even though *equilibria* suggests a state with no time change. In its fullest development the theory allows not only for time changes associated with transitions between regimes but also for time changes within regimes that do not change the essential large scale character of the regime. Both observational and theoretical evidence exists in support of multiple–equilibria or multiple

regimes, though it is somewhat disputed. A review of the evidence is presented in this section.

The seminal work on multiple–equilibria is due to Charney and DeVore (1979). They demonstrated with a simple barotropic model including topographical and thermal driving that more that one stable, stationary solution can exist for given external forcings. One of these multiple–equilibria is a high index flow with a strong zonal velocity component, while another corresponds to low index flow with larger wave amplitudes. They suggest that blocking is an example of the low index equilibria. Källén (1981) extends the result to the sphere. Charney and Strauss (1980) make the extension to a baroclinic version of multiple–equilibria. Other studies (Hart, 1979; Wiin-Nielsen, 1979; Roads, 1980a, b) come to similar conclusions.

A problem with these early theories is that the equilibria are essentially global in nature. For example, the flow associated with the low index equilibrium looks essentially like a high amplitude planetary wave. In contrast, blocking events are most often local phenomena–strong, wavelike perturbations exist in the blocking region but the flow outside that region may be much more zonal. Malguzzi and Speranza (1981) have addressed this problem and demonstrated the existence of equilibrium solutions with blocking like flow in localized regions. In their analytical approach relying heavily on perturbation expansions, non-sinusoidal topography replaces the single topographic wave used by Charney and DeVore (1979). This change leads to the localized high amplitude flows.

Another criticism of the first theories is that they are highly truncated, or, equivalently, of low order. Can multiple-equilibria still be found as this assumption is relaxed? Källén (1982) integrates a high resolution barotropic model on a sphere and finds multiple steady states. Legras and Ghil (1985) document in detail the phase space structure of a similar high order barotropic model, again noting multiple steady state solutions. So it would seem that multiple-equilibria is not an artifact of highly truncated systems. As an additional comment on the question of localness, the stationary flow patterns found by Legras and Ghil (1985) are surprisingly realistic with local blocking structures. Thus, high resolution can also account for localized patterns.

Models with multiple-equilibria, by a strict definition of that term, cannot account for transitions between different types of flows: the model atmosphere eventually finds itself at one of the equilibria points where it stays forever. This is a consequence of the simplicity of the models where processes that can make the equilibrium states unstable, such as baroclinic instability or addition non-linear interactions arising from increased spectral resolution, are neglected. In more general models, the concept of multiple-equilibria is more accurately replaced by that of multiple regimes (Legras and Ghil, 1985). Significant work along these lines was done by Reinhold and Pierrehumbert (1982). By adding a synoptic scale wave to Charney and Strauss' (1980) low order model, they demonstrated the existence of multiple weather regimes. Each regime is characterized by a similar pattern of synoptic scale weather while the transitions between the regimes is due to the behavior of the synoptic scale transient wave. The larger scales are integrally associated with the organized behavior of the synoptic scale. This result also lends some theoretical support to the observations of scale interaction noted in Section 1.2. This type of temporal behavior can also be accomplished if the system is stochastically forced (Benzi et al., 1984). In that case a model trajectory in phase space spends some time near one stable equilibrium state before the forcing abruptly moves it to a region near a second stable equilibrium state.

The studies quoted so far lend theoretical support to the concept of multiple-equilibria. An opposing viewpoint can be found in the papers of Tung and Rosenthal (1985) and Cehelsky and Tung (1987). In the former paper, the authors pose the question of whether multiple-equilibria still exist in high order barotropic models when realistic topography, zonal wind forcing and damping are used. Regarding topography, they note that Charney et al. (1981) find multiple-equilibria with realistic topography; however, they show that only one equilibria exists when more wave modes are added to the model. Quoting Legras and Ghil (1985), they note that the parameter domain where multiple-equilibria can exist is reduced as more modes are taken into account. This may restrict multiple-equilibria to a region of parameter space that is physically unrealistic. For example, Legras and Ghil's counterpart to Charney and DeVore's result occurs when the

forcing parameter corresponds to a zonal jet with speed $150ms^{-1}$. There is some discussion and questioning of the physical meaning of forcing terms in a barotropic model. They conclude that some non-linear models can have multiple-equilibria but that they exist only for unrealistic parameter values associated with forcings that are ambiguous in a barotropic context.

Cehelsky and Tung (1987) extend this critical re-examination of multiple-equilibria to the baroclinic case where forcing terms have a stronger physical basis. They demonstrate that the result of Reinhold and Pierrehumbert (1982) is an artifact of their truncation. Specifically, as more wave modes are added in both spatial directions, the multiple weather regimes disappear. Only one regime is found when all the possible non- linearities are taken into account.

Tung and his co-workers do not claim to have disproved once and for all the theoretical existence of multiple-equilibria. Rather they have thoroughly examined the most commonly used models for a given set of parameters and have found only one equilibria or weather regime. In conclusion, there is only tentative evidence at present for the theoretical existence of realistic multiple equilibria.

Is there any observational evidence for multiple–equilibria or multiple regimes? Certainly, most meteorologists are aware that weather often tends to be generally dry for a period of time and then wetter for a period, or warm for a period and then colder. But is there quantitative evidence in support of these subjective observations? Dole and Gordon examined their geopotential anomalies to see of they tended to particular (possibly multiple) "preferred" values. They found no convincing evidence of such behavior. A similar viewpoint is borne out in most of Hoskins and Pearce (1983). In contrast, Sutera (1986) found that a measure of planetary wave amplitude exhibited a bimodal distribution. Hansen (1986) documented that the mode with larger wave amplitude had blocking characteristics similar to those found by Rex (1950b). Hansen and Sutera (1986) confirmed this result with a larger data set.

Thus there is some observational evidence for multiple quasi–equilibria; however, it disagrees with the original theory proposed by Charney and Devore (1979). That theory

predicts bimodal distributions not only for the wave amplitude but for the mean zonal wind as well. The observational evidence does not support bimodality in the zonal wind (Hansen and Sutera, 1986). These results have been partially reconciled by the work of Benzi, *et al.* (1984, 1986) who added wave-wave interaction to the Charney and DeVore model in such a way as to produce multiple values of the wave amplitude for the same value of the mean zonal wind. (See also Speranza, 1986.) Tung and Rosenthal (1985) also register some disagreement with this school of thought.

An interesting paper that examines the connection between statistical techniques to find multiple regimes and dynamical modelling is Mo and Ghil (1987). They analyze both a southern hemisphere geopotential height data set and the results of the Legras and Ghil (1985) model using Empirical Orthogonal Functions (EOF's). Multiple regimes exist in both the observational data set and in the model results. They conclude that the interpretation of EOF's in the context of non-linear dynamical models is that they point from the time mean (possibly never realized in either the model or the atmosphere) to the most populated regions of phase space. This means that the dominant EOF patterns are associated with the multiple regimes. This paper is very useful in describing how rather complicated non-linear theory permits interpretation of the statistics of observed low frequency variability while in turn showing how the statistical methods can shed light on the dynamics.

In conclusion, there is observational evidence for the existence of multiple quasi-equilibria in the atmosphere. Finding the evidence involves looking at the right quantities: bimodality is more likely to be observed in a global parameter such as wave amplitude than in a point measure of some variable such as geopotential height anomaly. The observational evidence is not always in agreement with theory, but research seems to be bringing the two together.

The dynamical systems approach, to give a mathematical term to the concepts discussed in this section, holds a lot of promise for understanding the low frequency variability of the atmosphere and hence for increasing our skill in long range forecasting of phenomena such as blocks. This view essentially explains low frequency variability as the result

of the inherent *internal* variability of the atmosphere. Changes in *external* parameters such as sea surface temperatures are not needed. In the last resort, what is an internal process and what is an external process is a function of the complexity of the model: a coupled ocean-atmosphere model, for example, may predict sea surface temperature from knowledge of other atmospheric and oceanic variables, thus making sea surface temperature variations part of the internal dynamics. The dynamical systems approach is also non-linear by nature. Only non-linearity in some form can induce the internal variability and multiple regimes that have been discussed. Moreover, this approach aids in understanding GCM results in those cases where linearization is not appropriate. Finally, this way of thinking suggests that although *individual* synoptic storms within a regime may not be predictable beyond a week or ten days, the statistics of each individual regime may be predictable. In conclusion, the dynamical systems approach is not without its problems, but it holds a lot of promise for understanding phenomena such as blocks. It is appropriate to end with a quote from Charney and DeVore (1979):

> " ...a stochastic, dynamical system approach, in which the location of equilibrium points, attractor sets, stable and unstable limit cycles, etc., and the study of the stochastic forcing of the system by various instabilities will become a useful tool for the investigation of large scale atmospheric phenomena. We believe that this approach can lead to a better understanding of large scale variability, predictability and climate. To know that a system is in the attractor basin of a stable or metastable equilibrium is to know that it will remain for a time. To know that a system is in a state of transition is to know that it will change more rapidly and be less predictable. Climate itself becomes a question of distributions among possible equilibrium states, and climate variations a matter of how boundary changes lead to altered distributions."

1.3.2 Modons

The multiple-equilibria theories attempt to account for one obvious synoptic feature of blocks; namely, their persistence. Another synoptic feature, common to many blocks,

is a localized, dipole structure in the horizontal with a high pressure region located north of a low pressure region. Solitary eddies, or, more colloquially, modons, offer a promising explanation for both these features. Modons are steadily propagating, localized, shape preserving solutions of fluid dynamics systems. The early work on modons is due to Stern (1975), Larichev and Reznik (1976) and Flierl, *et al.* (1980). Several steps are needed to establish an equivalence between modons and blocks. First, models which have modon solutions must be shown to be relevant to the real atmosphere. Second, there must be a way to make a steadily propagating modon stationary in a westerly flow such as exists in the real atmosphere. Furthermore, modons must be shown to remain reasonably coherent in the presence of sheared flow and smaller scale turbulence. Finally, modon generation must be addressed: how can a modon be formed from a flow that does not already contain one?

We first address the question of model relevance. The equivalent barotropic vorticity equation (hereafter called the EBVE) is the model equation that has been applied most frequently to study explicitly the relationship between modons and blocks (McWilliams, 1980; Baines, 1983; Haines and Marshall, 1987). This equation may be written

$$\nabla^2\psi_t - k^2\psi_t + J(\psi, \nabla^2\psi) + \beta\psi_x = 0 \tag{3.1}$$

where ψ is the streamfunction, β is the northward derivative of the coriolis parameter and k is a constant (which in an appropriate context is a Rossby radius of deformation). The difference between the EBVE and the barotropic vorticity equation is that the $k^2\psi_t$ term is absent in the latter. A valid interpretation of (3.1) is that it represents the quasi-geostrophic flow of a homogeneous shallow water fluid. Alternatively, it represents the flow of the internal vertical mode in a two layer quasi- geostrophic stratified atmosphere with rigid boundaries at top and bottom. Neither of these physical interpretations are appropriate to the study of blocks. As originally used, the equation represented an empirical correction to the barotropic vorticity equation that allowed for better prediction of long wave movement (Cressman, 1958). The traditional derivation is to vertically average the

quasi-geostrophic vorticity equation under the assumption that the streamfunction is separable in its vertical and horizontal dependence (Thompson, 1961). McWilliams (1980), who treats the derivation of the EBVE in some detail, notes that the problem with this approach is that it gives a value for k which is different than that required for the best prediction of long waves. When the technique is modified to take into account the thermodynamic equation, the value of k is consistent, but other inconsistencies are introduced. To avoid these problems, McWilliams (1980) offers an alternate derivation involving an expansion and projection of the quasi-geostrophic equations with empirically determined, orthogonal, vertical modes of the atmosphere. The most severe truncation of the resulting equations, where only one vertical mode is kept in the expansion, yields the EBVE. The value of k is consistent with the best prediction values and vertical averaging and the assumption of separability are avoided. The gravest empirical mode for geopotential has a variable amplitude with height, but does not change sign, so that the model represents an appropriate vertical structure for blocks. This approach seems to correct the defects of the previous interpretation, yet we believe some problems still remain. McWilliams claims that his procedure has the advantage of being based upon a complete set of basis functions; however, only one function is kept to arrive at the EBVE. The inclusion of additional basis functions would couple all the vertical modes together through the non-linear terms so that a flow initially containing only the gravest mode would eventually evolve into a much more complicated vertical structure. In conclusion, the variety of derivations and interpretations of the EBVE casts some doubt on its validity. We feel that there are still conceptual difficulties in deriving this model and interpreting it in terms of an atmosphere with vertical structure.

Accepting for the moment the relevance of the EBVE, we now turn to the problem of making equivalent modons stationary in a westerly background flow. In the last resort, this is done by doppler shifting the modon to a zero phase speed, but there are several subtleties that need to be taken into account Steadily translating solutions of the EBVE satisfy

$$J(\psi + cy, \nabla^2\psi - k^2\psi + \beta y) = 0 \tag{3.2}$$

where we have assumed $\psi(x,y,t) = \psi(x-ct,y)$. Modon solutions are derived from this starting point. In this case, the solution corresponds to an isolated dipole propagating uniformly to the west (for $c < 0$) in zero background flow. The interested reader is referred to Flierl *et al.* (1980) for details. Now suppose we separate the streamfunction into a part corresponding to constant westerly flow and a perturbation part by writing $\psi = -\bar{u}y + \psi'$. Substituting into (3.1) and looking for stationary solutions yields

$$J(\psi' - \bar{u}y, \nabla^2\psi' + \beta y) = 0 \tag{3.3}$$

or, after some manipulation,

$$J(\psi' - \bar{u}y, \nabla^2\psi' - k^2\psi' + k^2\bar{u}y + \beta y) = 0. \tag{3.4}$$

Neither of these is mathematically equivalent to (3.2) showing that it is not possible with the standard EBVE to doppler shift an westward moving modon to zero speed by adding a westerly background flow. As McWilliams states it, the EBVE is not Galilean invariant with respect to a coordinate transformation from a stationary to a moving reference frame.

There are solutions to this problem. McWilliams (1980) shows how his vertical mode expansion method can be extended to include a zonal mean flow. Also, the traditional derivation can be modified by first writing the streamfunction as a sum of mean and perturbation parts and then making the standard separability assumption on only the perturbation part (Haines and Marshall, 1987). The result of both methods is a new form of the EBVE given by

$$\nabla^2\psi'_t - k^2\psi'_t + J(\psi', \nabla^2\psi') + \bar{u}(\nabla^2\psi'_x - k^2\psi'_x) + \beta\psi'_x = 0. \tag{3.5}$$

Stationary solutions to this satisfy

$$J(\psi' - \bar{u}y, \nabla^2\psi' - k^2\psi' + \beta y) = 0, \tag{3.6}$$

which is mathematically equivalent to (3.2). Thus, the EBVE can be modified so that westward moving modons can be doppler shifted to zero by a uniform westerly wind.

The model defined by (3.5) has been used by McWilliams (1980) to study the consistency between modon dynamics and an observed blocking event in the north Atlantic. Very rough correspondence is found. A particular difficulty is that the vertical structure of the mean wind must be more barotropic than that of the block in order for modon solutions to exist. This seems questionable in the real atmosphere because blocks often form near regions of high baroclinicity and hence large vertical wind shears. There is also the problem of defining from observations exactly what is meant by the mean wind. Theoretical considerations dictate that it be the flow far away from the modon, but this flow is unlikely to be purely zonal. McWilliams also notes that there is a certain amount of transience associated with blocking structures: the structure may look like a modon in a time averaged sense, but instantaneous maps show a distorted pattern reflecting the influence of transients.

The problem of the vertical wind structures is addressed briefly by Baines (1983). He first modifies McWilliams' version of the EBVE to allow for topography and diabatic heating. When diabatic heating alone is considered he finds that the constraint requiring the mean flow to be more barotropic than the modon can be relaxed while still allowing for an appropriate modon solution. The dynamic balances imply a certain spatial pattern of diabatic heating. This pattern need not be overly complex; in fact, he argues that a rather simple and observable sea surface temperature pattern may be sufficient to account for it. Therefore, by adding some external forces, some of the inconsistencies between modons and observations of blocks can perhaps be rectified. Baines' work is by no means a complete theory in this respect, rather it suggests some possible directions.

The problem with transients is addressed in some detail by Haines and Marshall (1987). They apply the modified EBVE as discussed above. In one of their experiments, the model is initialized with a stationary analytical modon solution. Waves are generated by a wavemaker upstream from the modon. The result is quite realistic: tongues of potential vorticity are advected around the modon which also entrains some of this air and continuously fluctuates in position and structure. Sufficiently intense eddies may break down the vortex structure. The behavior is very realistic and consistent with instantaneous

maps of potential vorticity documented by Shutts (1986). This research clearly addresses and solves the transient problem with which McWilliams was concerned.

We have made some preliminary calculations with the EBVE addressing the observed dynamical balances of blocks. It was noted in Section 1.2 that the time mean terms in the vorticity equation want to move a block downstream while the effect of the eddies opposes this tendency. In an effort to simulate this process, we linearized the EBVE about a basic state containing a modon embedded in westerly flow and noted the pattern of eddy potential vorticity flux divergence produced by a series of waves impinging on the modon. Then we used the flux divergence pattern as forcing in the non-linear model to see if a modon with an eastward propagation speed could be held stationary. The results were encouraging: although the forcing distorted the modon structure somewhat, the tendency for eastward propagation could be reduced.

We summarize this research on the EBVE and modons by noting first, that nearly all studies that attempt to relate modons to blocking do so in the context of the equivalent barotropic model. Second, the model must be modified to allow for stationary modons to exist in westerly background flows as observed in the atmosphere. Third, conceptual difficulties regarding vertical wind structure and transient influences can be overcome. However, all this work must be evaluated in light of the questionable relevance of the equivalent barotropic model to the real atmosphere. Some of the results obtained with this model are realistic, but we must see if these results hold for more justifiable models before we can believe in a strong correspondence between modons and blocks.

Modon solutions have been found for several other models. Pure barotropic modons are solutions to (3.1) for $k = 0$. They were originally documented by Stern (1975) and Larichev and Reznik (1976). Flierl, et al. (1980) discuss them in the context of a two layer model. In contrast to equivalent modons, which can propagate to the east or west, barotropic modons, as originally formulated, can only move to the east. Therefore, they can only be doppler shifted to zero speed by a mean easterly flow uncharacteristic of middle latitudes. Furthermore, barotropic modons have a low north of a high, in contrast to observed dipole blocks. These characteristics preclude the association of these modons with

blocking events. Thus, it seems that in the context of barotropic theory, pure barotropic modons are untenable as a description of blocks, and equivalent modons describe some blocking features well, but come from an equation of questionable relevance. A solution to this dilemma has been provided recently by Verkley (1987) who derives a barotropic modon with appropriate north-south structure that can be stationary in westerly background flow. He accomplishes this by relaxing somewhat the degree of localness required in the solution so that the modon is less isolated and resembles more a Rossby-Haurwitz wave. This is not a drawback of the theory; instead, it is probably more realistic than the original result because blocks are more complicated than isolated dipoles embedded in an otherwise zonal flow. Unfortunately, Verkley concludes that some examples of his stationary modons are unstable to small perturbations, but suggests that other regions in "modon parameter space" may have better stability properties.

Baroclinic modons have been thoroughly studied by Flierl, *et al.* (1980) in a two layer quasi-geostrophic model. Using a multi-level model is an obvious way to circumvent the problems associated with the various barotropic models. However, Flierl, *et al.* find no two layer solutions that are appropriate as models of blocks. Either the modons have a baroclinic vertical structure where the geopotential anomaly changes sign with height, or, in the case of pure barotropic modons in the two layer atmosphere, they move only to the east. Neither situation is consistent with observations as blocks have a nearly barotropic vertical structure and are relatively stationary in a westerly background flows. Perhaps some of this incompatibility can be overcome in light of Verkley's (1987) results quoted above. Any solution to the barotropic vorticity equation is also a solution to the two layer quasi-geostrophic equations if the streamfunction in each layer is given by the barotropic streamfunction. Thus the two layer model admits a solution where the flow in each layer is described by Verkley's modon. However, this is not a particularly interesting solution because it uses a baroclinic model when none of the flow is baroclinic. Yet this approach might be a starting point for including mean winds with vertical structure

Modons are robust in the sense that they exist in a variety of geophysical systems. The original beta plane solutions of Flierl, et al. (1980) have been extended to the sphere

by Verkley (1984) and Tribbia (1984). Verkley (1987) derives his modified modons on the sphere as well. Swaters (1986) discusses the interaction of modons with topography starting with the purely barotropic eastward moving modons. He shows that as the modon moves into a region of shallower fluid, its speed decreases and its streamfunction and vorticity fields amplify. He suggests that topography can interact with a modon to capture and amplify it and hence lead to a blocking-like state. While topographic-modon interactions are inherently interesting, we would argue that blocks do not occur directly over mountain regions. Furthermore, his model admits only the unrealistic eastward moving modons with a low north of a high. Extensions of his theory to more realistic situations is necessary.

It is also appropriate to mention what Flierl, *et al.* (1980) call "riders". These are streamfunction fields that can be added to the basic modon without affecting the evolution. Their significance is that they are radially symmetric and so can dramatically alter the appearance of the radially asymmetric basic modon. Because of this, features which are actually modons may go unobserved.

Robustness of modons must be tested in another sense, that of stability to small perturbations. McWilliams, *et al.* (1981) have studied this for barotropic modons. Small amplitude perturbations do not affect the modons, but sufficiently strong perturbations can destroy them. The critical amplitude for destruction is a function of scale with larger scale perturbations being more efficient in destroying modons than smaller scale perturbations. The analytical work of Pierini (1985), set in the framework of equivalent barotropic dynamics, lends theoretical support to these numerical calculations. McWilliams, et al. also study the influence of dissipation with the result that dissipation causes a decrease in modon amplitude and propagation rate and an increase in meridional scale. These studies indicate that modons are relatively robust phenomena, but more work should be done, especially regarding robustness of baroclinic modons.

Robustness in the presence of horizontally sheared flow has also been investigated. We have done some preliminary calculations which show that equivalent modons in weak jet-like flow remain coherent on time scales of 10 days. Analytic equivalent modon solutions in

the presence of weak linear shear have been found by Swenson (1986). Sheared flow does not inhibit the existence of modons. As relevant baroclinic solutions become available, they should be tested for robustness to horizontal and vertical shear.

Finally, we address the question of modon generation. How can a modon evolve from a flow which does not already contain one? It is unlikely that coherent structures with exact physical balances of analytic modons can evolve from any flow: the analytical solution is too specific. The best we can hope for is the generation of vortex pairs similar to modons. McWilliams (1983) has suggested that modons can be generated from the interaction between two monopoles. Haines and Marshall (1987) suggest a less abstract mechanism. In the context of a transient/block interaction experiment they first compute the pattern of eddy potential vorticity flux divergence, $\nabla \cdot \overline{\mathbf{v}'q'}$, obtained by allowing linearized eddies generated by a wavemaker to propagate through a mean flow containing a stationary equivalent modon. Here, $\mathbf{v}'$ is the eddy vector velocity and q' the eddy potential vorticity. The eddy flux divergence pattern is then used to force the non-linear EBVE with no modon in the initial condition. Some Ekman dissipation is also included. The result is the generation of a local dipole structure with closed streamfunction contours whose intensity is limited by the friction. The relationship between the potential vorticity and the streamfunction is very similar to that for analytic equivalent modons. The dipole is not exactly steady: there is some time evolution. They conclude that a striking aspect of their study is the ease and vigor with which non- linear dipole structures can be excited by appropriate non-linear forcing. However, we believe their argument is somewhat circular: certain forcing patterns can generate modon-like features, but the forcing patterns themselves come from the effect of eddies impinging on an already existing modon. Their study is very intriguing in its suggestion that modons can be easily forced by eddies, but some sort of localized dipole structure must exist in order that the eddies can do the right thing. Perhaps eddies impinging on a weakly diffluent flow can enhance a split jet and lead to a dipole structure. In any case, it seems as though modon-like features can be excited, but you "have to have one to get one".

We are attracted by the idea that eddies can generate modons. This hypothesis is relevant to Colucci's (1987) work mentioned previously. It is conceivable that one or

more intense synoptic scale storms can transform a wavy large scale flow pattern into a localized dipole structure where modon dynamics can then account for its coherence and persistence. But much more work needs to be done along these lines; we believe the generation of modons is a pressing problem that is not well understood.

Before concluding, the work of Pierrehumbert and Malguzzi (1984) deserves mention. Using the EBVE they show that if an inviscid and unforced system has a closed streamline solution (such as a modon), then a weakly forced and damped system can possess both a high amplitude localized state and a zonal state for the same forcing. This suggests a sort of localized multiple-equilibria where global resonances involving topographic waves are not required. The high amplitude state predicted by this theory essentially explains Haines and Marshall's result quoted above.

In conclusion, modons are appealing as an explanation of the localized, persistent, dipole structure of some blocks. Most research relating modons to blocks has used the equivalent barotropic vorticity equation which we think is of questionable relevance to the real atmosphere. Nevertheless, modon solutions to this equation can behave quite realistically. The modon concept has been extended to the sphere and to include the influence of topography. A particular problem with the non-existence of stationary, pure barotropic modons in a westerly background flow has been recently solved. Baroclinic modons in a two layer model have been derived but have a vertical structure inconsistent with blocks. Modons are relatively robust to perturbations. Finally, much more work needs to be done to understand how modons are generated. It seems to us that the modon concept is useful and, at the same time, limited. The usefulness is in showing that reasonably relevant equations can have localized, dipole solutions. This is helpful for broad, speculative thinking such as saying that the observed behavior of blocks can be explained, at least in part, by internal, non-linear dynamics. But where does one go from here? Formation of blocks is a pressing problem and no combination of processes is likely to generate an exact, analytical modon. Aside from suggesting the rather general idea that blocks are non-linear, coherent structures, do modons really have relevance beyond the simple fact that they can exist?

1.4 Summary and Overview of Subsequent Work

We have reviewed research relating to observations of the blocking phenomenon. Recently there has been a renewed interest in isentropic analysis as a useful observational tool, specifically in regard to the analysis of potential vorticity on isentropic surfaces. However, this tool has not been widely applied to the study of blocks. This, briefly, is the motivation for Chapter 2 which reports on the results of a case study of blocking using isentropic analysis.

We have also reviewed in some detail two particular theories for blocking: multiple-equilibria and modons. Both were found to have some deficiencies which question their use as models for blocking. Therefore, we considered a third prominent theory for blocks which suggests that they are the result of instabilities of the large scale flow. The sensitivity of the instabilities to variations in the basic state might explain why blocking flows develop in some situations and not in others. Chapter 3 documents some of this sensitivity for the preliminary case of barotropic instability. Chapter 4 summarizes our train of research ideas and results, and suggests plausible directions for future study.

REFERENCES

Baines, P.G., 1983: A survey of blocking mechanisms, with application to the Australian region. *Aust. Meteor. Mag.*, **31**, 27-36.

Bengtsson, L., 1981: Numerical prediction of atmospheric blocking – a case study. *Tellus*, **33**, 19-42.

Benzi, R., A.R. Hansen, and A. Sutera, 1984: On stochastic perturbation of simple blocking models. *Quart. J. Roy. Meteor. Soc.*, **110**, 393-409.

Benzi, R., P. Malguzzi, A. Speranza and A. Sutera, 1984: The statistical properties of general atmospheric circulation: observational evidence and a minimal theory of bi-modality. *Quart. J. Roy. Meteor. Soc.*, **112**, 661-674.

Benzi, R. and A.C. Wiin-Nielsen, 1986: preface to *Adv. Geophys.*, 29.

Benzi, R., A. Speranza and A. Sutera, 1986: A minimal baroclinic model for the statistical properties of low frequency variability. *J. Atmos. Sci.*, **43**, 2962-2967.

Benzi, R., B. Saltzman and A.C. Wiin-Nielsen, Eds.,1986: Anomalous Atmospheric Flows and Blocking. *Adv. Geophys.*, **29**.

Berggren, B., B. Bolin, and C.-G. Rossby, 1949: An aerological study of zonal motion, its perturbations and break-down. *Tellus*, **1**, 14-37.

Brown, P.S. Jr., A.R. Hansen, and J. Pandolfo, 1986: Circulation regime- dependent nonlinear interactions during northern hemisphere winter. *J. Atmos. Sci.*, **43**, 476-485.

Cehelsky, P. and K.K. Tung, 1987: Theories of multiple-equilibria and weather regimes – A critical re-examination. Part II: Baroclinic two layer models. *J. Atmos. Sci.*, **44**, 3282-3303.

Charney, J.G. and J. DeVore, 1979: Multiple flow equilibria in the atmosphere and blocking. *J. Atmos. Sci.*, **36**, 1205-1216.

Charney, J.G. and D.M. Strauss, 1980: Form-drag instability, multiple- equilibria and propagating planetary waves in baroclinic, orographically forced planetary wave systems. *J. Atmos. Sci.*, **37**, 1157-1176.

Charney, J.G., J. Shukla and K.C. Mo, 1981: Comparison of a barotropic blocking theory with observations. *J. Atmos. Sci.*, **38**, 762-779.

Colucci, S.J., 1985: Explosive cyclogenesis and large scale circulation changes: Implications for atmospheric blocking. *J. Atmos. Sci.*, **42**, 2701-2717.

Colucci, S.J., 1987: Comparative diagnosis of blocking versus non-blocking planetary scale circulation changes during synoptic scale cyclogenesis. *J. Atmos. Sci.*, **44**, 124-139.

Cressman, G., 1958: Barotropic divergence and very long atmospheric waves. *Mon. Wea. Rev.*, **86**, 293-297.

Dole, R.M., 1986a: Persistent anomalies of the extratropical northern hemisphere wintertime circulation: Structure. *Mon. Wea. Rev.*, **114**, 178-207.

Dole, R.M., 1986b: The life cycles of persistent anomalies and blocking over the north Pacific. *Adv. Geophys.*, **29**, 31-69.

Dole, R.M. and N.D. Gordon, 1983: Persistent anomalies of the extratropical northern hemisphere wintertime circulation: Geographical distribution and regional persistence characteristics. *Mon. Wea. Rev.*, **111**, 1567- 1586.

Edmon, H.J., B.J. Hoskins and M.E. McIntyre, 1980: Eliassen-Palm cross- sections for the troposphere. *J. Atmos. Sci.*, **37**, 2600-2616.

Flierl, G.R., V.D. Larichev, J.C. McWilliams, and G.M. Reznik, 1980: The dynamics of baroclinic and barotropic solitary eddies. *Dyn. Atmos. Ocean*, **5**, 1-41.

Haines, K. and J. Marshall, 1987: Eddy-forced coherent structures as a prototype of atmospheric blocking. *Quart. J. Roy. Meteor. Soc.*, **113**, 681-704.

Hansen, A.R., 1986: Observational characteristics of atmospheric planetary waves with bimodal amplitude distributions. *Adv. Geophys.*, **29**, 101- 133.

Hansen, A.R. and T.-S. Chen, 1982: A spectral energetics analysis of atmospheric blocking. *Mon. Wea. Rev.*, **110**, 1146-1165.

Hansen, A.R. and A. Sutera, 1984: A comparison of the spectral energy and enstrophy budgets of blocking versus non-blocking periods. *Tellus*, **36**, 52-63.

Hansen, A.R. and A. Sutera, 1986: On the probability density distribution of planetary scale atmospheric wave amplitude. *J. Atmos. Sci.*, **43**, 3250- 3265.

Hart, J.E., 1979: Barotropic quasi-geostrophic flow over anisotropic mountains. *J. Atmos. Sci.*, **36**, 1736-1746.

Hoskins, B.J., I. James and G. White, 1983: The shape, propagation and mean flow interaction of large scale weather systems. *J. Atmos. Sci.*, **40**, 1595- 1612.

Hoskins, B. and R. Pearce, Eds.: *Large-scale dynamical processes in the atmosphere.* Academic, 1983, 397pp.

Illari, L., 1984: A diagnostic study of the potential vorticity in a warm blocking anticyclone. *J. Atmos. Sci.*, **41**, 3518-3526.

Källén, E., 1981: The non-linear effects of orographic and momentum forcing in a low order barotropic model. *J. Atmos. Sci.*, **38**, 2150-2163.

Källén, E., 1982: Bifurcation properties of quasi-geostrophic, barotropic models and their relation to atmospheric blocking. *Tellus*, **34**, 255-265.

Knox, J.L., and J.F. Hay, 1985: Blocking signatures in the northern hemisphere: Frequency distribution and interpretation. *J. Climatology*, **5**, 1-16.

Larichev, V. and G Reznik, 1976: Two-dimensional Rossby soliton: An exact solution. *Rep. U.S.S.R. Acad. Sci.*, **5**, 231.

Legras, B. and M. Ghil, 1985: Persistent anomalies, blocking and variations in atmospheric predictability. *J. Atmos. Sci.*, **42**, 433-471.

Lejanas, H. and H. Økland, 1983: Characteristics of northern hemisphere blocking as determined from a long time series of observational data. *Tellus*, **35**, 350-362.

Malguzzi, P. and A. Speranza, 1981: Local multiple-equilibria and regional atmospheric blocking. *J. Atmos. Sci.*, **38**, 1939-1948.

McWilliams, J.C., 1980: An application of equivalent modons to atmospheric blocking. *Dyn. Atmos. Ocean*, **5**, 43-66.

McWilliams, J.C., 1983: Interactions of isolated vortices II: Modon generation by monopole collision. *Geophys. Astrophys. Fluid Dyn.*, **24**, 1- 22.

McWilliams, J.C., G. R. Flierl, V.D. Larichev, and G.M. Reznik, 1981: Numerical studies of barotropic modons. *Dyn. Atmos. Ocean*, **5**, 219-238.

Mo, K.C. and M. Ghil, 1987: Statistics and dynamics of persistent anomalies. *J. Atmos. Sci.*, **44**, 877-901.

Mullen, S.L., 1986: The local balances of vorticity and heat for blocking anticyclones in a spectral general circulation model. *J. Atmos. Sci.*, **43**, 1406-1441.

Mullen, S.L., 1987: Transient eddy forcing of blocking flows. *J. Atmos. Sci.*, **44**, 3-22.

Pierini, S., 1985: On the stability of equivalent modons. *Dyn. Atmos. Ocean*, **9**, 273-281.

Pierrehumbert, R.T. and P. Malguzzi, 1984: Forced coherent structures and local multiple equilibria in a barotropic atmosphere. *J. Atmos. Sci.*, **41**, 246-257.

Quiroz, R.S., 1987: Traveling waves and regional transitions in blocking activity in the northern hemisphere. *Mon. Wea. Rev.*, **115**, 919-935.

Reinhold, B.B. and R.T. Pierrehumbert, 1982: Dynamics of weather regimes: Quasi-stationary waves and blocking. *Mon. Wea. Rev.*, **110**, 1105-1145.

Rex, D.F., 1950a: Blocking action in the middle troposphere and its effect upon regional climate. I. An aerological study of blocking action. *Tellus*, **2**, 196-211.

Rex, D.F., 1950b: Blocking action in the middle troposphere and its effect upon regional climate. II. The climatology of blocking action. *Tellus*, **2**, 275-301.

Roads, J.O., 1980a: Stable, near-resonant states forced by orography in a simple baroclinic model. *J. Atmos. Sci.*, **37**, 2381-2395.

Roads, J.O., 1980b: Stable, near-resonant states forced by perturbation heating in a simple baroclinic model. *J. Atmos. Sci.*, **37**, 1958-1967.

Shukla, J. and K.C. Mo, 1983: Seasonal and geographical variation of blocking. *Mon. Wea. Rev.*, **111**, 388-402.

Shutts, G.J., 1986: A case study of eddy forcing during an Atlantic blocking episode. *Adv Geophys.*, **29**, 135-162.

Speranza, A., 1986: Deterministic and statistical properties of northern hemisphere, middle latitude circulation: Minimal theoretical models. *Adv. Geophys.*, **29**, 199-225.

Stern, M.E., 1975: Minimal properties of planetary eddies. *J. Mar. Res.*, **33**, 1-13.

Sutera, A., 1986: Probability density distribution of large scale atmospheric flow. *Adv. Geophys.*, **29**, 227-249.

Swaters, G.E., 1986: Barotropic modon propagation over slowly varying topography. *Geophys. Astrophys. Fluid Dyn.*, **36**, 85-113.

Swenson, M., 1986: Equivalent modons in simple shear. *J. Atmos. Sci.*, **43**, 3177-3185.

Thompson, P., 1961: *Numerical Weather Analysis and Prediction.* Macmillan, New York, NY, 197pp.

Treidl, R.A., E.C. Birch, and P. Sajecki, 1981: Blocking action in the northern hemisphere: A climatological study. *Atmosphere: Atmos. Ocean*, **19**, 1- 23.

Tribbia, J.J., 1984: Modons in spherical geometry. *Geophys. Astrophys. Fluid Dyn.*, **30**, 131-168.

Tung, K.K. and A.J. Rosenthal, 1985: Theories of multiple-equilibria – A critical reexamination. Part I: Barotropic models. *J. Atmos. Sci.*, **42**, 2804-2819.

Verkley, W.T.M., 1984: The construction of barotropic modons on a sphere. *J. Atmos. Sci.*, **41**, 2492-2504.

Verkley, W.T.M., 1987: Stationary barotropic modons in westerly background flows. *J. Atmos. Sci.*, **44**, 2383-2398.

White, W.B. and N. E. Clark, 1975: On the development of blocking activity over the central north Pacific. *J. Atmos. Sci.*, **32**, 489-502.

Wiin-Nielson, A., 1979: Steady-states and stability properties of a low- order barotropic system with forcing and dissipation. *Tellus*, **31**, 375- 386.

Chapter 2

A CASE STUDY OF ATMOSPHERIC BLOCKING USING ISENTROPIC ANALYSIS

2.1 Introduction

Short term climatic events, such as blocking, have been of significant interest recently. By restricting the passage of cyclonic storms and their associated fronts through a given region, a block can influence the weather in that region for a week to ten days, sometimes even longer. Thus blocks are important because of the impact they have on medium range weather forecasts.

Most synoptic blocking studies (e.g., Rex, 1950; White and Clark, 1975; Colucci, et.al., 1981; Hansen and Chen, 1982; Illari, 1984; Colucci, 1985; Dole 1986) focus on the horizontal structure of blocks as seen on constant pressure maps, typically, geopotential at 500mb or 300mb and temperature at 850mb. Much has been learned from these studies about the characteristics that make blocking unique. First, blocks are relatively stationary, fluctuating only a few degrees about a central longitude. Second, they frequently have a meridional dipole structure with a high north of a low. (This is most common in North Atlantic blocks.) Finally, they persist for a long time compared with synoptic scale weather events and, once formed, are not easily destroyed by transient, synoptic scale disturbances, although such disturbances may play an important role in their maintainance (e.g., Illari, 1984).

A distinctly different synoptic approach is that of isentropic analysis. This technique was originally introduced by Rossby and collaborators in the late 1930's (e.g., Rossby, 1937; Namias, 1938) and has undergone a recent resurgence of interest not only for synoptic applications (Uccellini, 1976) but also for dynamical/ theoretical applications (Hoskins, et. al., 1985). However, it has not been frequently applied to blocking flows.

Isentropic analysis has several advantages over conventional pressure analysis. First, individual air parcels remain on isentropic surfaces in the absence of diabatic effects. Thus, isentropic analysis is a convenient framework for trajectory calculations. Also, analysis of moisture advection on an isentropic surface is often more revealing than on an isobaric surface and can lead to better prediction of thunderstorms (Namias, 1938; Uccellini, 1976). But, perhaps most importantly, isentropic analysis is the best way to examine the potential vorticity, first derived by Ertel (1942), and given by

$$P = \frac{1}{\rho}(\vec{\zeta_a} \cdot \nabla\theta). \tag{1.1}$$

Here, $\vec{\zeta_a}$ is the absolute, three dimensional vector vorticity, ρ the density and θ the potential temperature. The potential vorticity is significant for several reasons.

1. An air parcel conserves its potential vorticity as it moves about if frictional and diabatic effects are absent. These two constraints are difficult to satisfy yet are less restrictive than the conservation constraints on say, absolute vorticity or circulation.

2. The potential vorticity combines both the wind and mass fields into one quantity. This is in contrast to other sometimes conserved quantities like vorticity and circulation, which are kinematic—related only to the wind field, or potential temperature, which is related only to the mass field.

3. The distribution of potential vorticity controls the time evolution of many large scale dynamical processes and makes the dynamics highly visible. For example, Rossby wave propagation is related to the latitudinal gradient of potential vorticity. Also, a necessary condition for baroclinic instability (in the absence of surface temperature gradients) is that the northward gradient of the zonally averaged potential vorticity be less than zero. In the words of McIntyre and Palmer (1984), maps of the potential vorticity "are fundamentally the simplest and most useful way in which to visualize large scale dynamical processes."

4. Points (2) and (3) say that the distribution of a quantity combining both the wind and mass fields is a control on the evolution of many large scale processes. The

connecting link between these two points is the invertibility principle, discussed in depth by Hoskins, et. al., (1985). This principle states that knowledge of the potential vorticity distribution plus specification of boundary conditions, a reference state and a balance condition (such as quasi-geostrophy), is sufficient to determine both the wind and mass fields. It is the baroclinic analogue to obtaining the winds from the vorticity field in a barotropic fluid. The invertibility principle is a powerful concept because it allows the dynamicist to look at all the controlling physics at once and yet be able to separate that physics into its wind related and mass related components.

To see why the potential vorticity is best examined isentropically, note that with the hydrostatic approximation, the potential vorticity may be written in the two equivalent forms

$$P = -g\left\{-\frac{\partial v}{\partial p}\left(\frac{\partial \theta}{\partial x}\right)_p + \frac{\partial u}{\partial p}\left(\frac{\partial \theta}{\partial y}\right)_p + \left[\left(\frac{\partial v}{\partial x}\right)_p - \left(\frac{\partial u}{\partial y}\right)_p + f\right]\frac{\partial \theta}{\partial p}\right\}, \tag{1.2a}$$

or,

$$P = \frac{\left(\frac{\partial v}{\partial x}\right)_\theta - \left(\frac{\partial u}{\partial y}\right)_\theta + f}{-\frac{1}{g}\frac{\partial p}{\partial \theta}}. \tag{1.2b}$$

where u is the eastward velocity, v is the northward velocity, f the Coriolis parameter, g the acceleration of gravity and p the pressure. Subscripts indicate which vertical coordinate is held constant during differentiation. In either case, for adiabatic and frictionless flow, the potential vorticity is conserved following the motion, i.e.,

$$\frac{dP}{dt} = 0\,. \tag{1.3}$$

It is easily seen that the isentropic form for P (1.2b) is a mathematically simpler expression than the isobaric form (1.2a). But more importantly, predicting local changes of potential vorticity in isobaric coordinates requires knowledge of the vertical velocity ω ($\equiv dp/dt$). This is because individual air parcels do not generally remain on a pressure surface. In isentropic coordinates air parcels do remain on an isentropic surface (again in the absence

of diabatic effects) so that knowledge of only the horizontal wind field is necessary to predict local changes. For these reasons potential vorticity is best examined on isentropic surfaces.

This paper presents a case study, using isentropic analysis, of a blocking event that occurred over the North Atlantic in December of 1978. The results indicate that, for this block, isentropic analysis is preferable to the traditional pressure analysis for describing the evolution of the block. Both synoptic and dynamic understanding of the block is complemented and deepened by analysis of isentropic potential vorticity, and isentropic trajectories aid in visualizing the flow of air during the blocking period. Section 2.2 describes the methods of data analysis. The synoptic evolution of the block is shown in Section 2.3; isentropic and isobaric representations are compared. Section 2.4 presents the analysis of the potential vorticity on isentropic surfaces. Section 2.5 shows the results of some trajectory calculations and Section 2.6 contains the summary, conclusions and speculations on the nature of blocking.

2.2 Data Analysis

Isentropic analysis requires the construction of an isentropic data set consisting of gridpoint values of pressure, winds and the Montgomery streamfunction $M = c_pT + gz$ on a set of specified levels of constant potential temperature θ. Here, z is geopotential height, T is temperature and c_p is the specific heat of dry air at constant pressure. National Meteorological Center gridpoint data, available from the National Center for Atmospheric Research, was used to build this isentropic data set. Temperatures, geopotential heights and horizontal velocities at 12 hour intervals on 2.5 degree latitude by 2.5 degree longitude grids at 100mb, 150mb, 200mb, 250mb, 300mb, 400mb, 500mb, 700mb, 850mb, and 1000mb were collected for the period 16-30 December, 1978. Analysis was performed only for the Atlantic region 20N–87.5N, 100W–20E. The vertical profile of potential temperature was calculated at each gridpoint and checked for superadiabatic layers. When such layers occurred, the average value of θ in the layer was calculated and the θ at the top of the layer was replaced by the average value plus 0.2K and the θ at the bottom by the

average minus 0.2K. If the correction caused adjacent layers to become superadiabatic, the technique was applied to those layers. The process was repeated until no superadiabatic layers remained. Less than 0.5% of the θ profiles needed this correction.

Linear interpolation in $\ln p$ and the bisection iterative method (see e.g., Conte and deBoor, 1980) were used to find the pressure at θ levels in 5K increments between 400K and 250K. The u and v winds were then interpolated to these θ levels. The Montgomery streamfunction was calculated at each isentropic level by first calculating its value at 500mb and then integrating, both upward and downward, the hydrostatic equation

$$\frac{\partial M}{\partial \theta} = c_p \left(\frac{p}{p_{00}} \right)^{\kappa}, \tag{2.1}$$

where $\kappa = R/c_p$ (R is the gas constant) and p_{00} is a constant reference pressure (taken to be 1000mb). This method ensures that the geostrophic wind, proportional to the horizontal gradient of M, is determined as accurately as possible. If, for example, M is calculated by evaluating T from p and θ using Poisson's equation and interpolating z to a given θ surface, the consistency between the two terms in M, imposed by the hydrostatic and Poisson equations, is ignored. Following Danielson (1959), large errors in the calculated geostrophic winds can then result. With M properly evaluated, the isentropic data set is complete: u, v, p and M are known as functions of x, y, θ and time t.

2.3 Synoptic Analysis of the Block

The 300mb geopotential height and the Montgomery streamfunction at 315K for several times during the blocking episode are shown in Figures 2.1 and 2.2, respectively. For orientation, the pressure on the 315K surface typically ranges from approximately 600mb at 20N to 250-300mb in the region 60-80N. On 16 December at 1200 UTC a ridge is present in both fields in the east-central Atlantic with relatively zonal flow upstream. By 1200 UTC on 18 December, this ridge has moved eastward and a strong trough has developed off the coast of North America with a second ridge just downstream. Both the trough and the second ridge intensify so that at 1200 UTC on 21 December a strong blocking high is present in the north-central Atlantic with a closed contour on the streamfunction map. The classical dipole structure described by Rex (1950) is evident at 1200

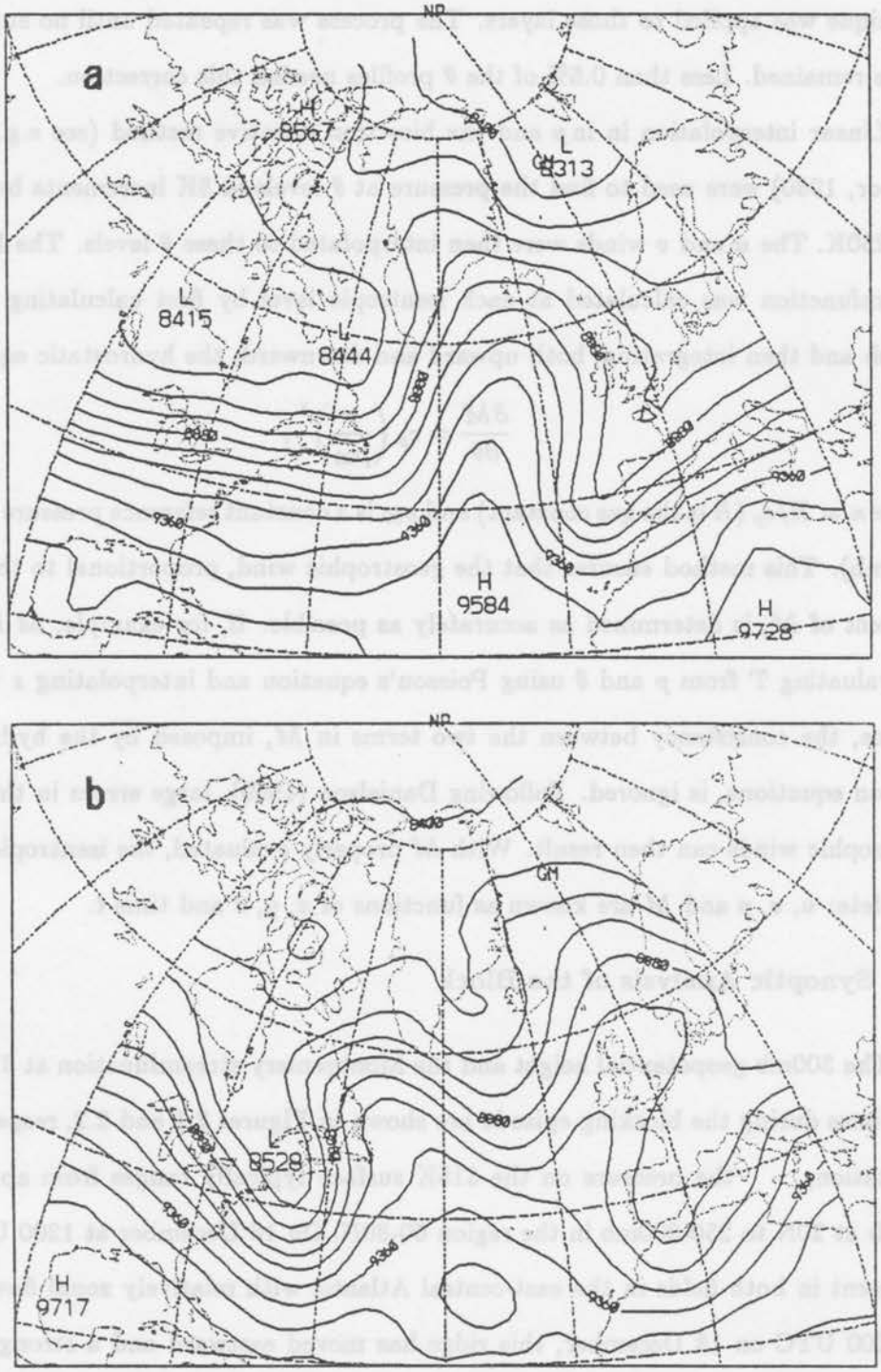

Figure 2.1: The 300mb geopotential height in meters for (a) 1200 UTC, 16 December, (b) 1200 UTC, 18 December, (c) 1200 UTC, 19 December, (d) 1200 UTC, 21 December (e) 1200 UTC, 25 December and (f) 1200 UTC, 29 December. Latitude/longitude lines are drawn at 20 degree increments.

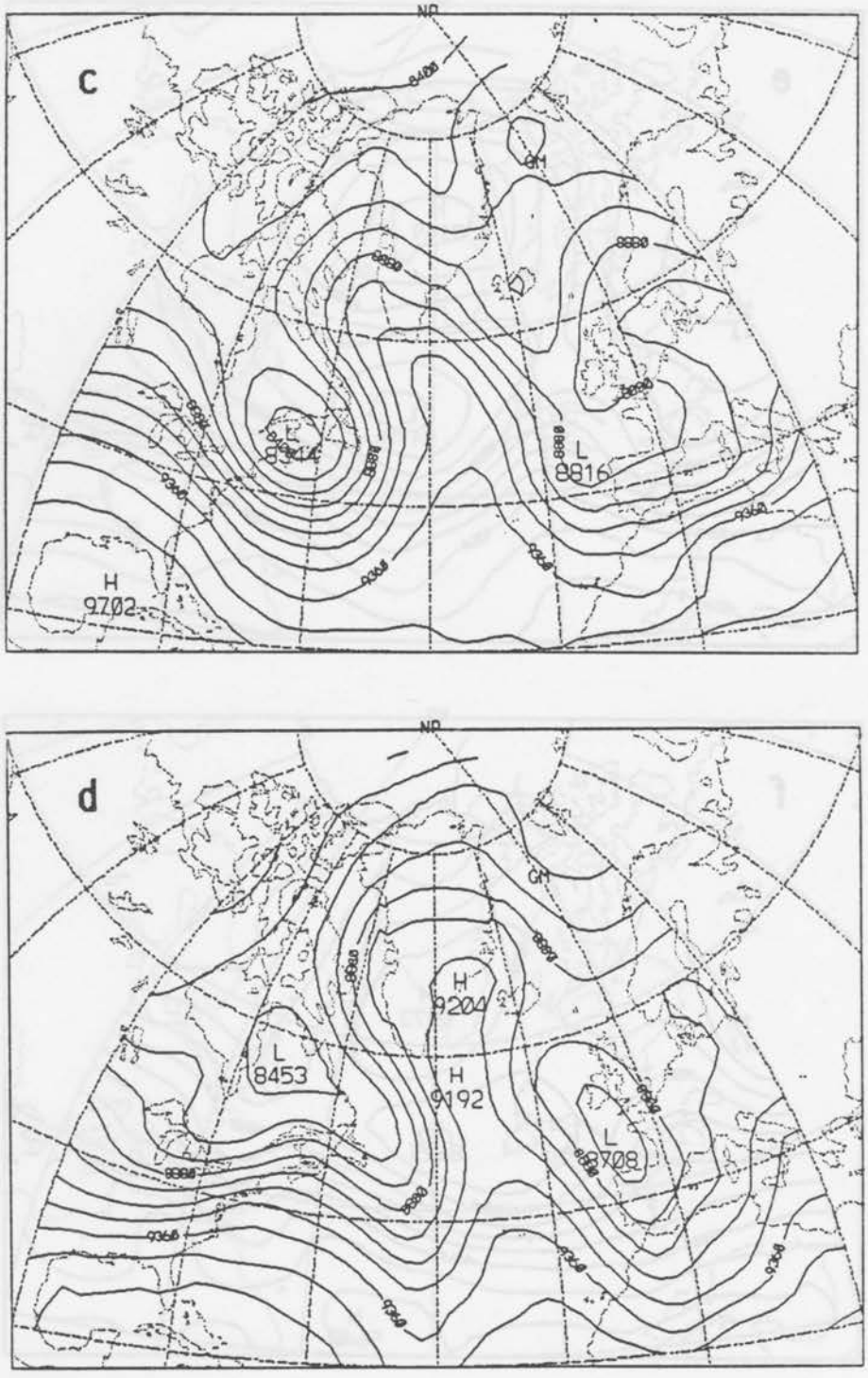

Figure 2.1: continued.

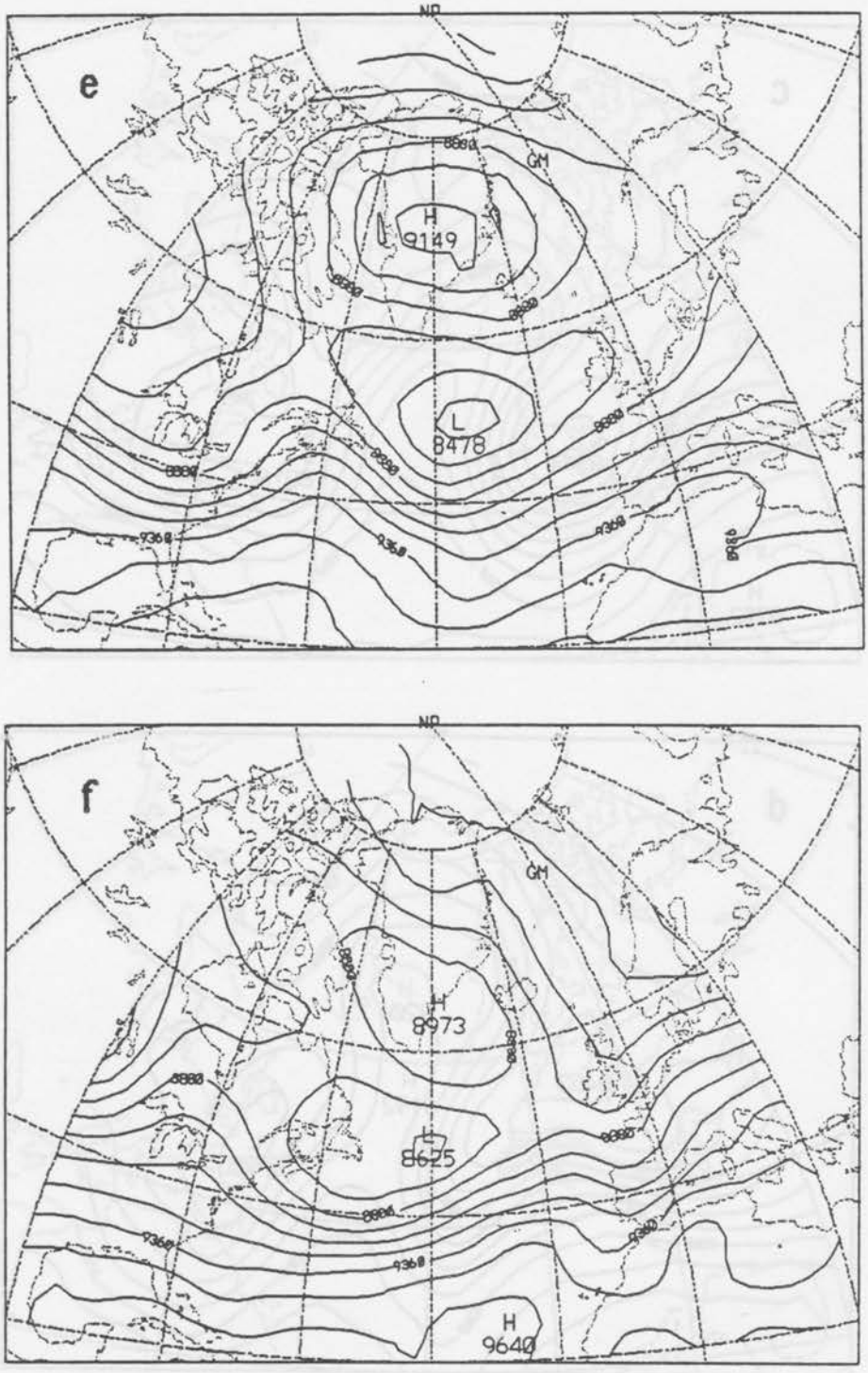

Figure 2.1: continued.

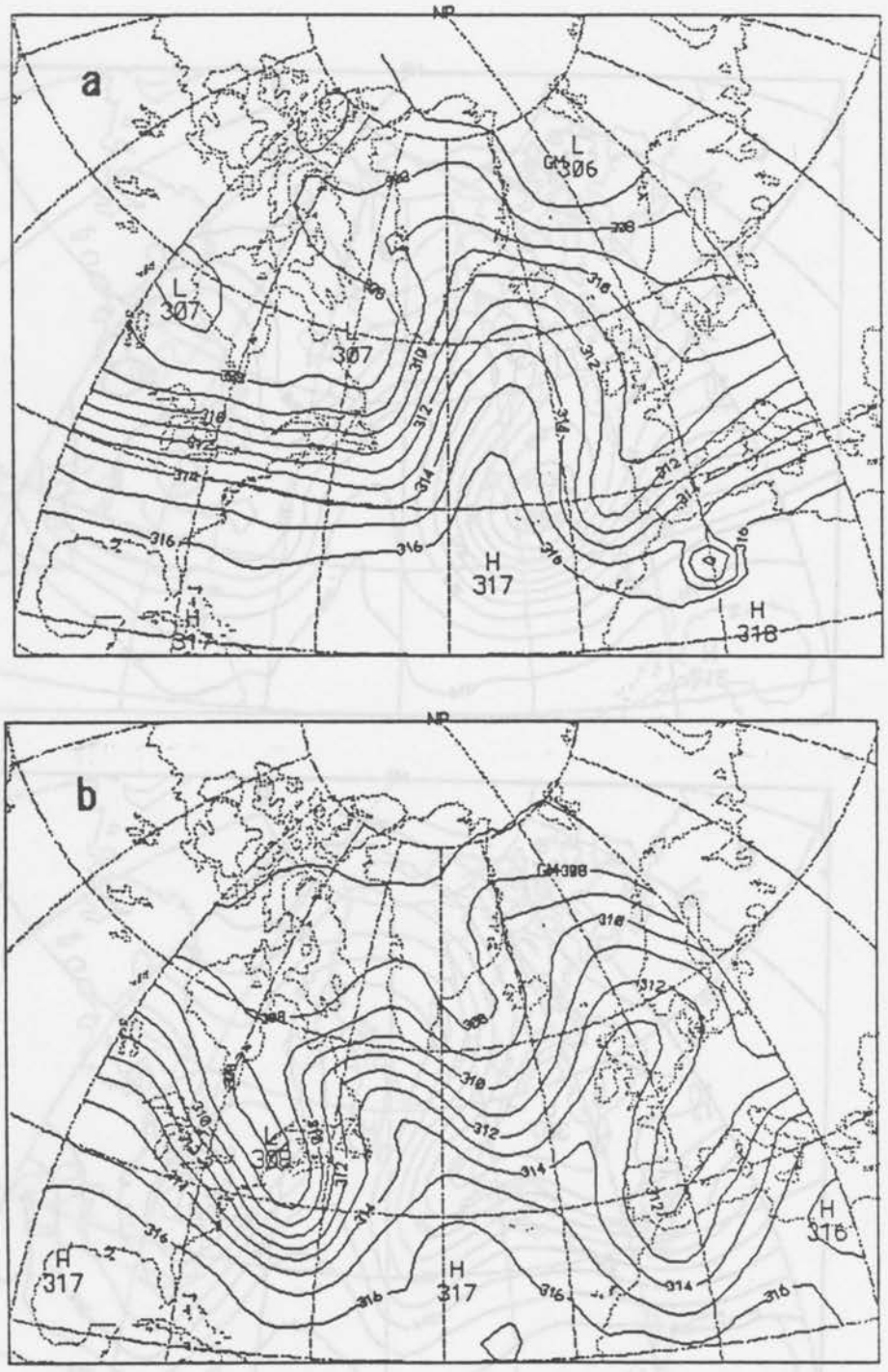

Figure 2.2: The 315K Montgomery streamfunction in units of $10^3 m^2 s^{-2}$ for (a) 1200 UTC, 16 December, (b) 1200 UTC, 18 December, (c) 1200 UTC, 19 December, (d) 1200 UTC, 21 December (e) 1200 UTC, 25 December and (f) 1200 UTC, 29 December.

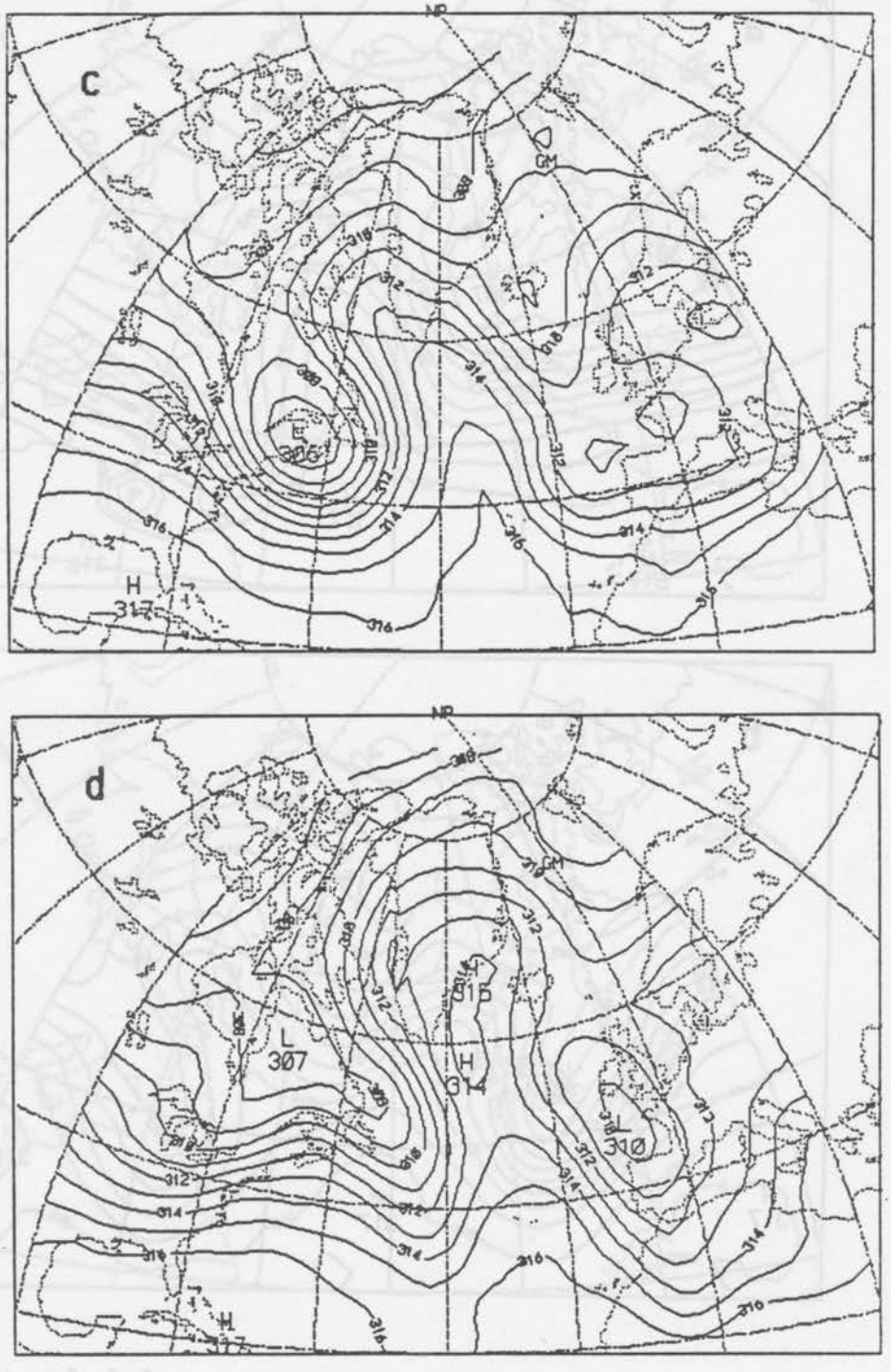

Figure 2.2: continued.

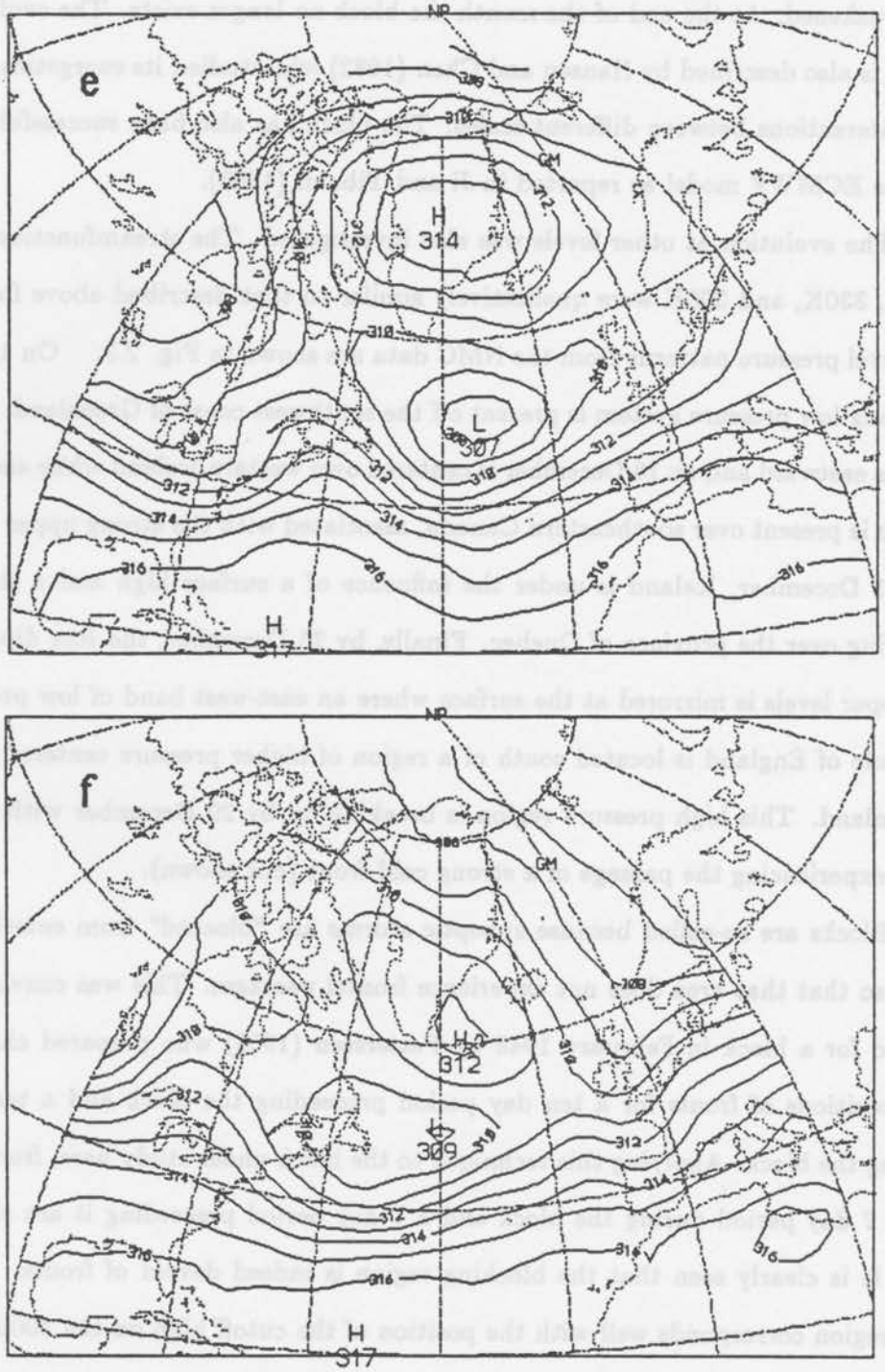

Figure 2.2: continued.

UTC on 25 December. The block occupies most of the area between the latitudes 60N and 80N and the longitudes 0W to 80W. By 1200 UTC on 29 December this structure has weakened. At the end of the month the block no longer exists. The evolution of this block is also described by Hansen and Chen (1982) who studied its energetics, focusing on the interactions between different scales. The block has also been successfully simulated by the ECMWF model as reported in Ji and Tibaldi (1983).

The evolution at other levels was also investigated. The streamfunction patterns at 350K, 330K, and 300K were qualitatively similar to that described above for 315K. The sea level pressure patterns from the NMC data are shown in Fig. 2.3. On 16 December, a strong low pressure system is present off the southwest coast of Greenland. This system moves eastward and on 18 December is centered over western Iceland while another intense storm is present over southeastern Canada, associated with the strong upper level trough. By 21 December, Iceland is under the influence of a surface high and a third storm is building over the province of Quebec. Finally, by 25 December, the Rex dipole structure at upper levels is mirrored at the surface where an east-west band of low pressure at the latitude of England is located south of a region of higher pressure centered over eastern Greenland. This high pressure region is breaking up by 29 December with the blocking area experiencing the passage of a strong cold front (not shown).

Blocks are so-called because synoptic storms are "blocked" from entering a certain area so that that area does not experience frontal passages. This was convincingly illustrated for a block in February 1948 by Petterssen (1956) who prepared charts showing the positions of fronts for a ten day period preceeding the block and a ten day period during the block. Applying this technique to the block under study here, frontal positions for a 7 day period during the block and a 7 day period preceeding it are shown in Fig. 2.4. It is clearly seen that the blocking region is indeed devoid of fronts. Futhermore, this region corresponds well with the position of the cutoff high on the 300mb and 315K streamfunction charts.

North-south and east-west cross sections through the mature stage of the block are shown in Fig. 2.5. Note that the block is warm core throughout most of the troposphere

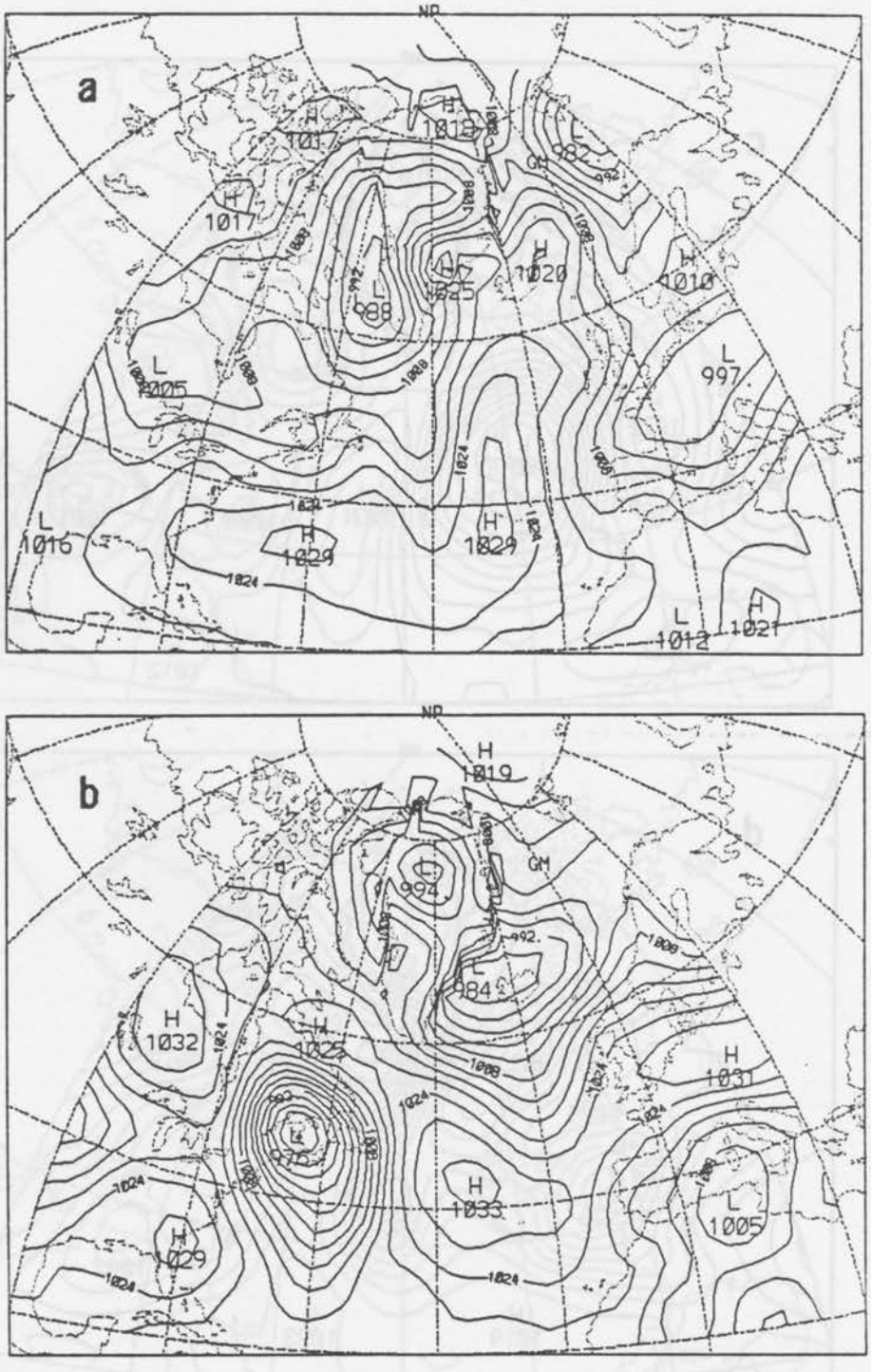

Figure 2.3: The sea level pressure patterns in mb for (a) 1200 UTC, 16 December, (b) 1200 UTC, 18 December, (c) 1200 UTC, 19 December, (d) 1200 UTC, 21 December (e) 1200 UTC, 25 December and (f) 1200 UTC, 29 December.

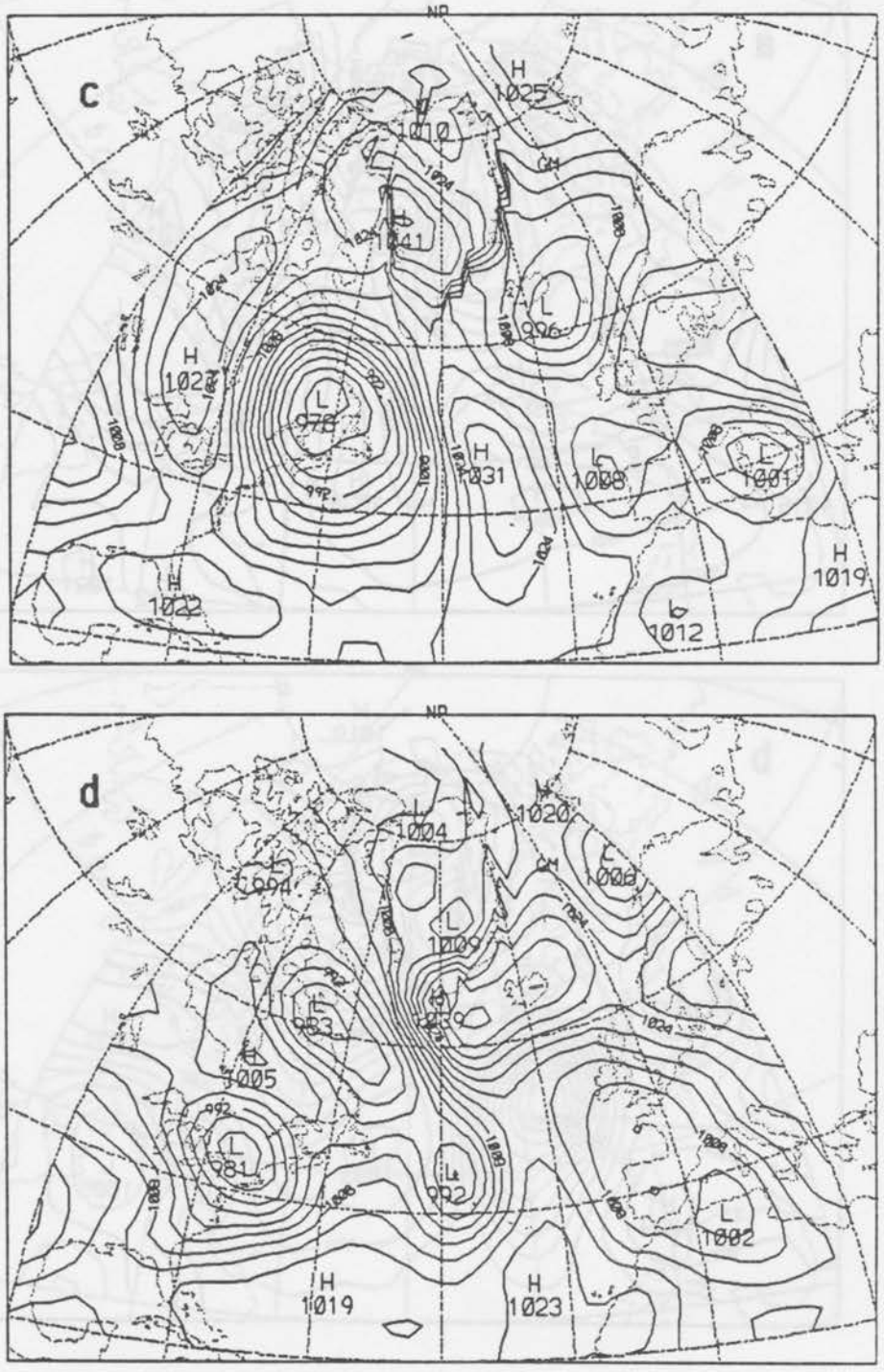

Figure 2.3: continued.

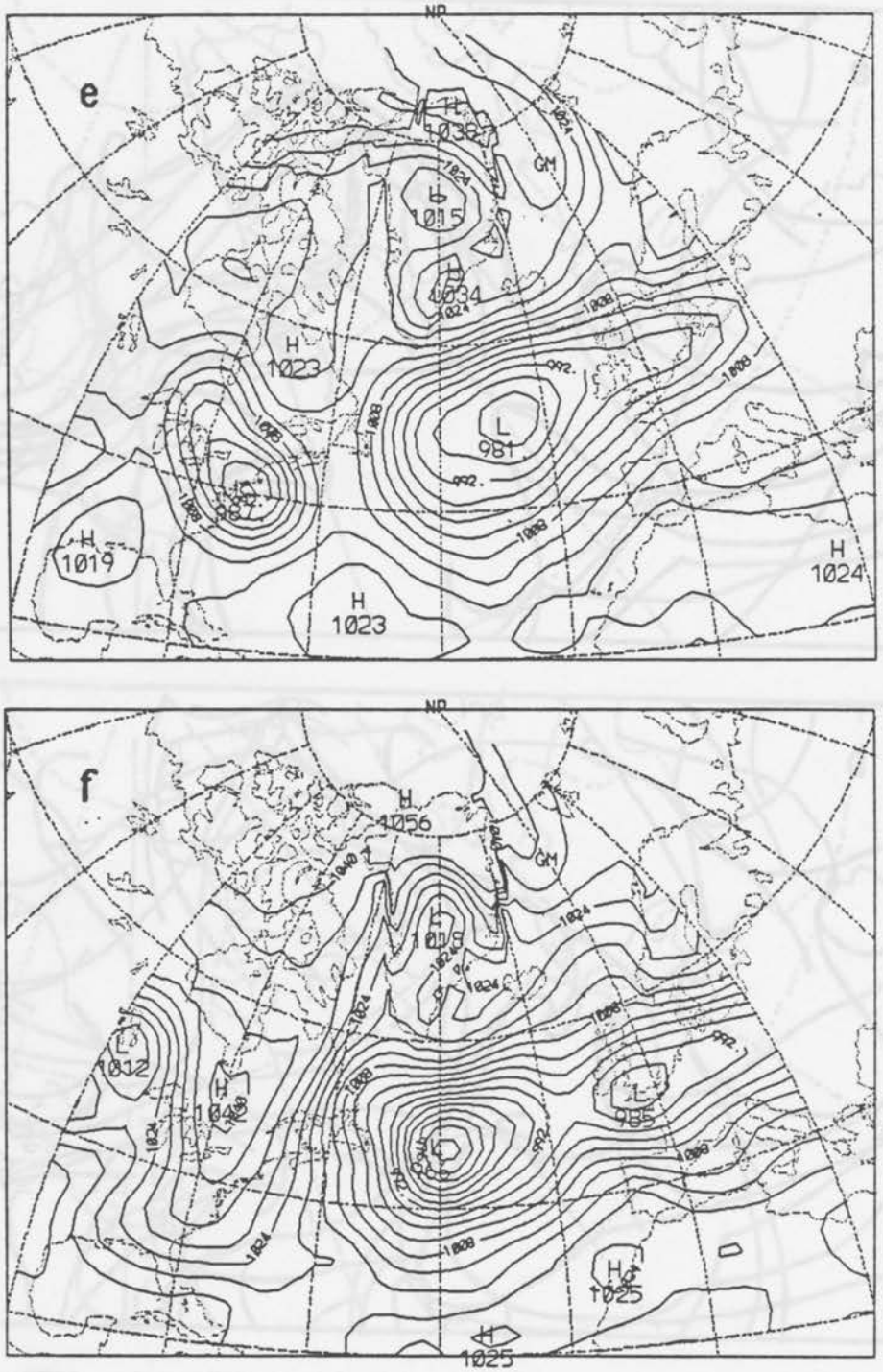

Figure 2.3: continued.

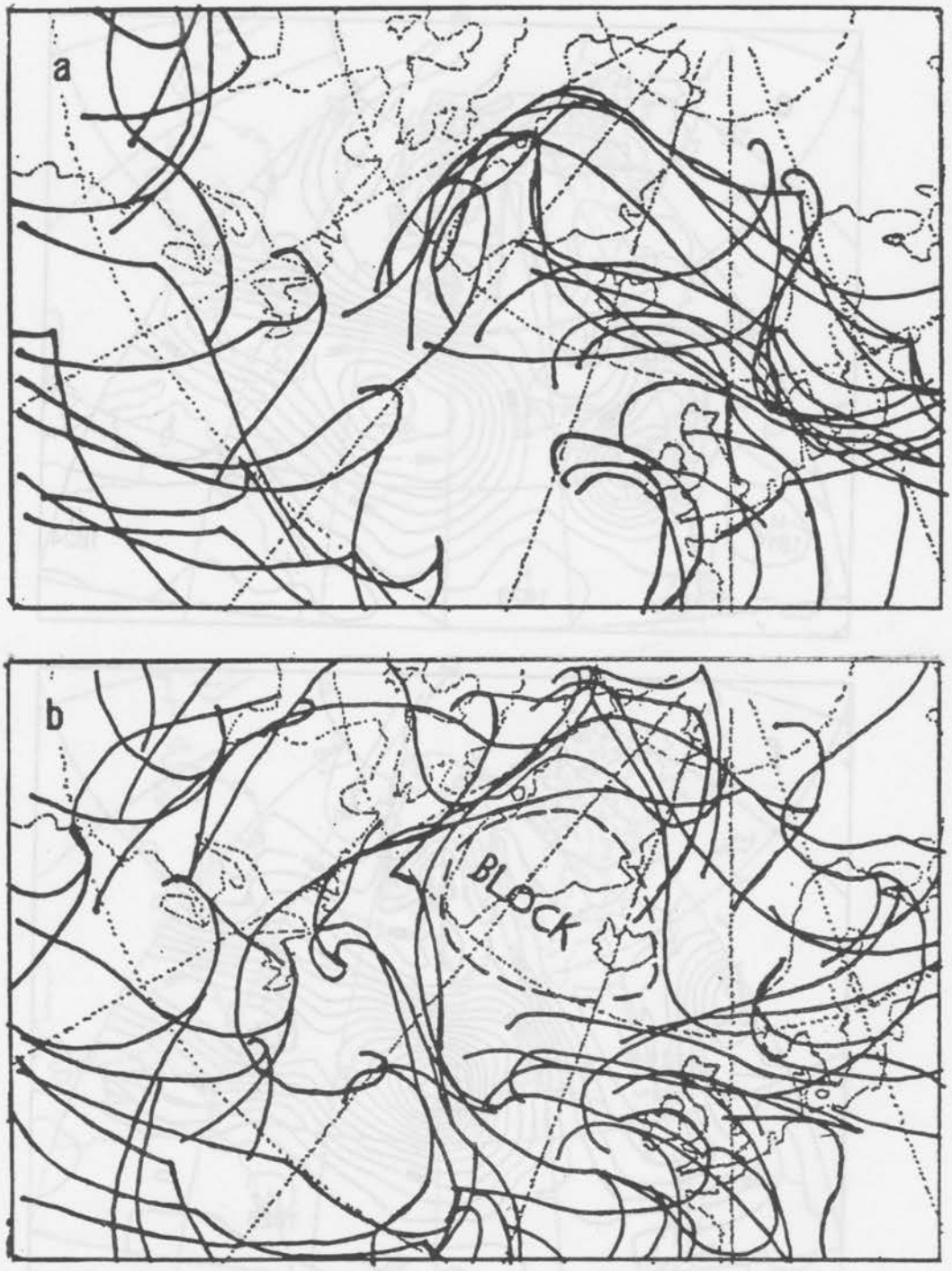

Figure 2.4: Frontal positions at 0600 UTC for (a) 10-16 December, 1978 and (b) 22-28 December, 1978. These are taken from *Meteorologische Abhandlungen*, Series B, Grundlagenmaterial, Freien Universität Berlin, Institut für Meteorologie, 1978.

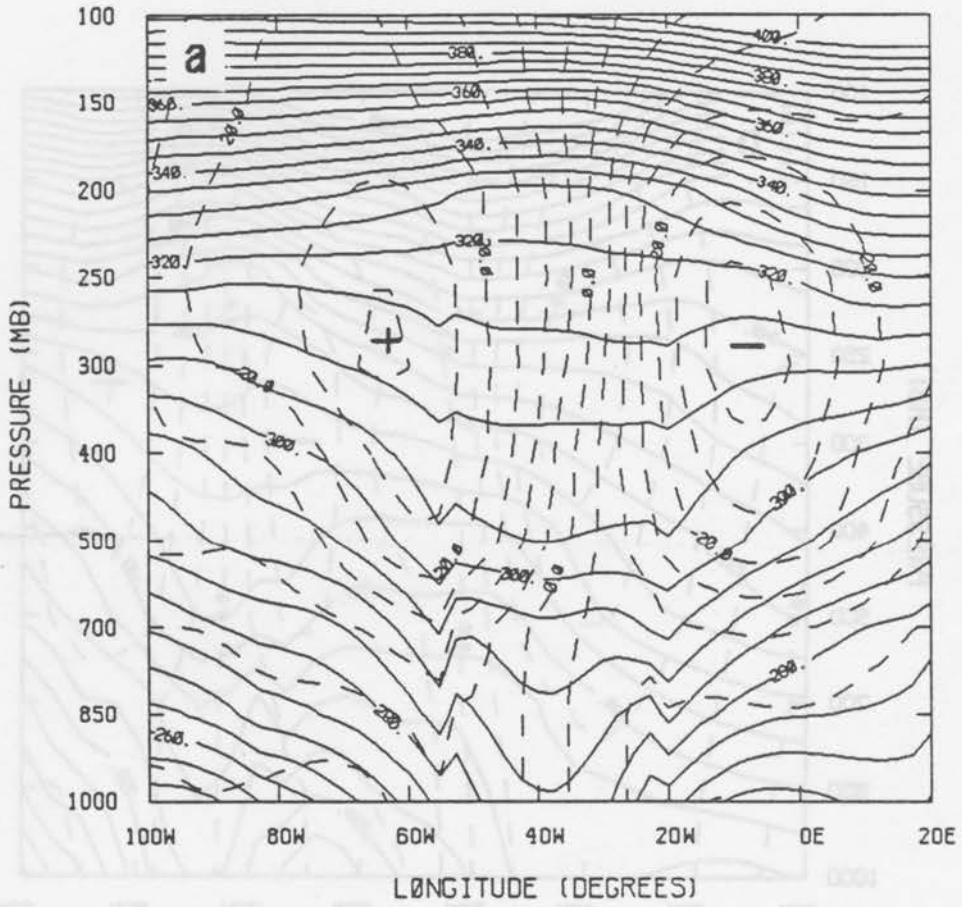

Figure 2.5: Cross-sections obtained by averaging the 1200 UTC data for the period 21-28 December, 1978; (a) east-west cross section at 70N, (b) north- south cross section at 37.5W. The solid lines are isentropes and the dashed lines the wind component perpendicular to the section.

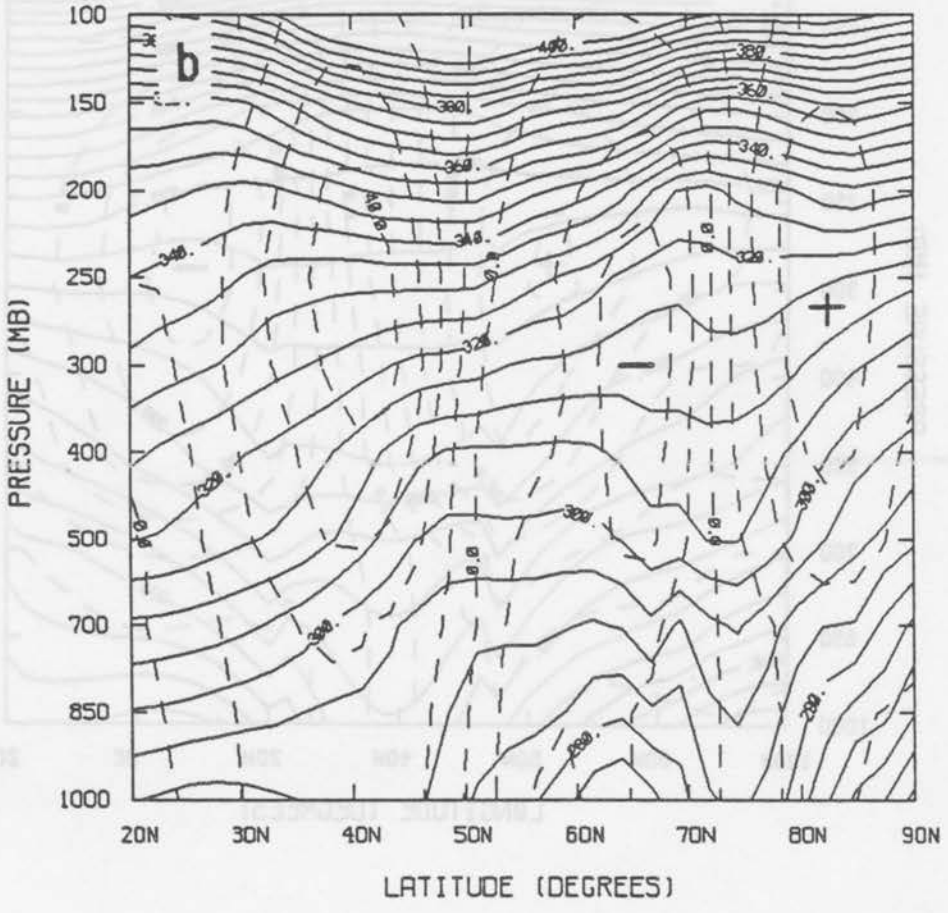

Figure 2.5: continued.

and cold core near the tropopause which may be identified by the level where the isentropes become more closely packed. The tropopause over the block is quite high compared to the surrounding regions. Strong upper level easterlies corresponding to the flow south of the high pressure region are present. During its mature stage, the block tilts little with height. This is consistent with Dole (1986) who showed that northern Pacific (PAC) persistent anomalies had less vertical tilt during the mature stage than during development.

Two particular observations can be drawn from the synoptic analysis of the block. First, the evolution of the block is just as easily seen with isentropic analysis as with isobaric analysis. In fact, the former analysis is preferable. Again, because air parcels in adiabatic motion stay on isentropic surfaces, isentropic analysis gives a three-dimensional picture of the motion not easily available from conventional pressure level analysis. [Two pieces of information not displayed here are necessary to see this three dimensional aspect of isentropic flow: (1) the instantaneous topography of isentropic surfaces and (2) the vertical movement of the isentropic surfaces.] Second, intense synoptic scale low pressure systems exist upstream from the block as it develops. Many previous studies (e.g., Sanders and Gyakum, 1980; Hansen and Chen, 1982; Colucci, 1985) have also noted this and suggested that such strong storms play an important role in the development of blocks. This second point will be taken up again in Section 2.5.

2.4 Isentropic Potential Vorticity Analysis

The potential vorticity on isentropic surface was calculated at several levels from (1.2b). The evolution of potential vorticity (hereafter PV) at 315K during the blocking period is shown in Fig. 2.6. The PV pattern evolves in a remarkably similar way to the streamfunction pattern. This is a consequence of the invertibility principle. By considering a simplified case of an isolated, circularly symmetric PV anomaly under gradient and hydrostatic balance, Hoskins, *et al.* (1985) deduce several characteristics of the associated wind and mass fields. These characteristics turn out to be robust (i.e., they are not restricted to a very specific form of PV anomaly) and hence allow for a qualitative inversion of a given PV field. One of these characteristics states that the circulation

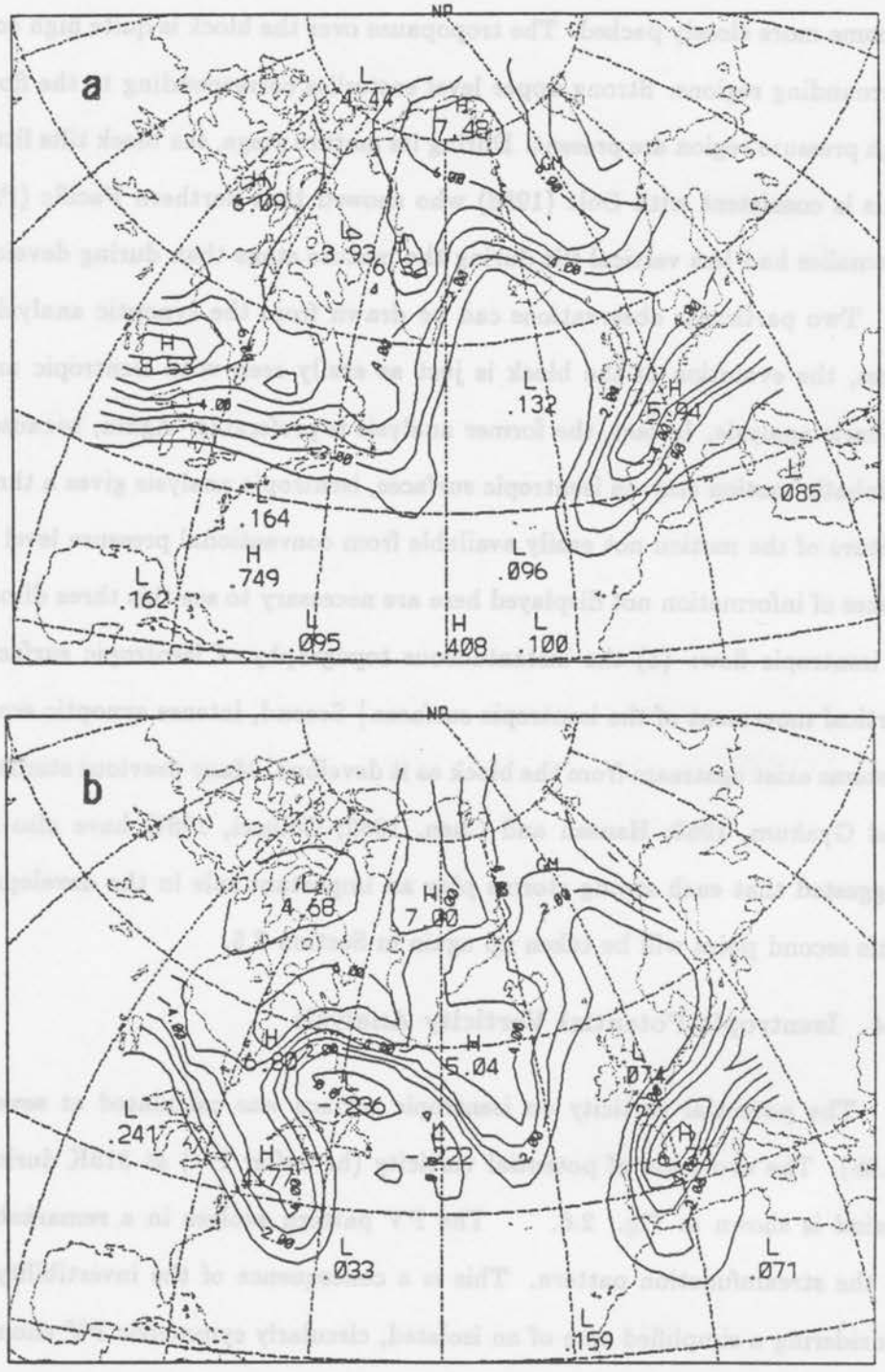

Figure 2.6: The potential vorticity at 315K for (a) 1200 UTC, 16 December, (b) 1200 UTC, 18 December, (c) 1200 UTC, 19 December, (d) 1200 UTC, 21 December (e) 1200 UTC, 25 December and (f) 1200 UTC, 29 December. The potential vorticity has been non-dimensionalized by dividing it by $10^6 m^2 K kg^{-1} s^{-1}$.

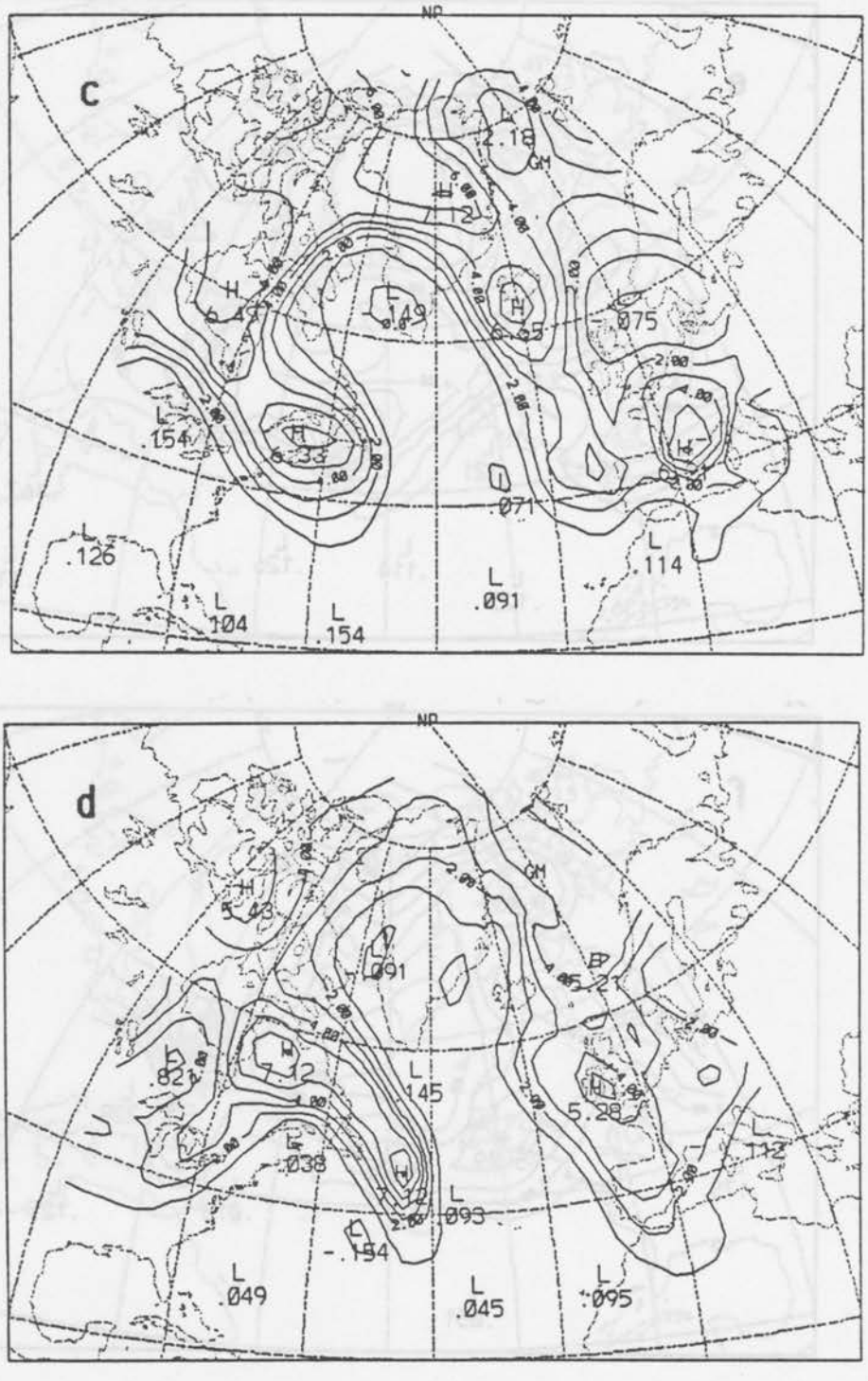

Figure 2.6: continued.

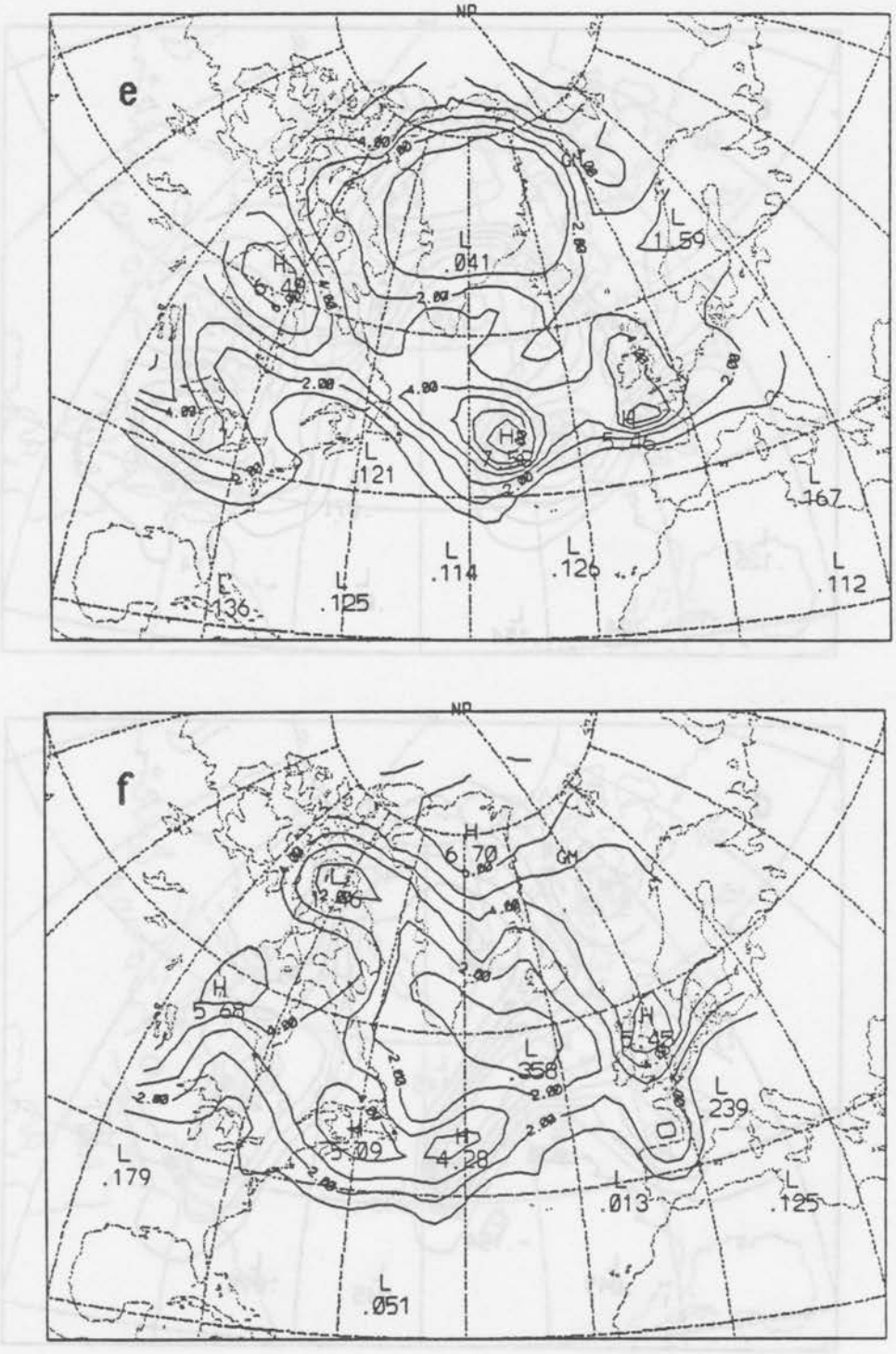

Figure 2.6: continued.

around an PV anomaly has the same sense as the anomaly. This means that the flow around a region of low potential vorticity is clockwise and the flow around a region of high potential vorticity is counterclockwise. Intuitively, this is expected, as low potential vorticity has low absolute vorticity (unless the term $(-1/g)\partial p/\partial\theta$ is extremely large) and hence is probably associated with high pressure, ridging and clockwise flow. Therefore, it is not surprising that the eastern Atlantic ridge of low potential vorticity air at 1200 UTC on 16 December is coincident with the ridge in the streamfunction pattern at the same time. Continuing the parallel evolution between PV and streamfunction, this ridge moves off to the east and by 18 December a trough of high potential vorticity air is present over the coast of North America with a ridge of low potential vorticity air just downstream. The trough intensifies and the ridge moves northward so that on 21 December a broad, uniform area of low potential vorticity in the North Atlantic corresponds to the blocking ridge. By 25 December, the PV pattern exhibits the dipole structure seen in the streamfunction and surface pressure fields. An area of low potential vorticity air has cutoff from the surrounding pattern. Finally, by 29 December, much higher PV air has moved into the blocking region. Maps of PV at 350K, 330K, and 300K show patterns which are qualitatively similar.

Figure 2.6 shows that the blocking region is characterized by a broad area of uniformly low potential vorticity. An Empirical Orthogonal Function (EOF) analysis of the 315K PV for the period 16-28 December, shown in Fig. 2.7, provides additional confirmation of this result. The first step in the EOF analysis is the calculation of the time mean field. This is plotted in Fig. 2.7a and shows the dominant influence that the block had during the period. The spatial variation away from the mean field is given by the EOF's. In this case, the first EOF explained 34.6% of the variance and the second 12.7%. The first EOF pattern (Fig. 2.7b) shows that the dominant region of variability away from the mean occurs in the blocking region. The temporal variation of a given EOF spatial pattern is described by the principal component time series corresponding to that EOF. The first principal component is plotted in Fig. 2.7c. Now the contribution to the total field from a single EOF is given by the mean field plus the product of the EOF with its

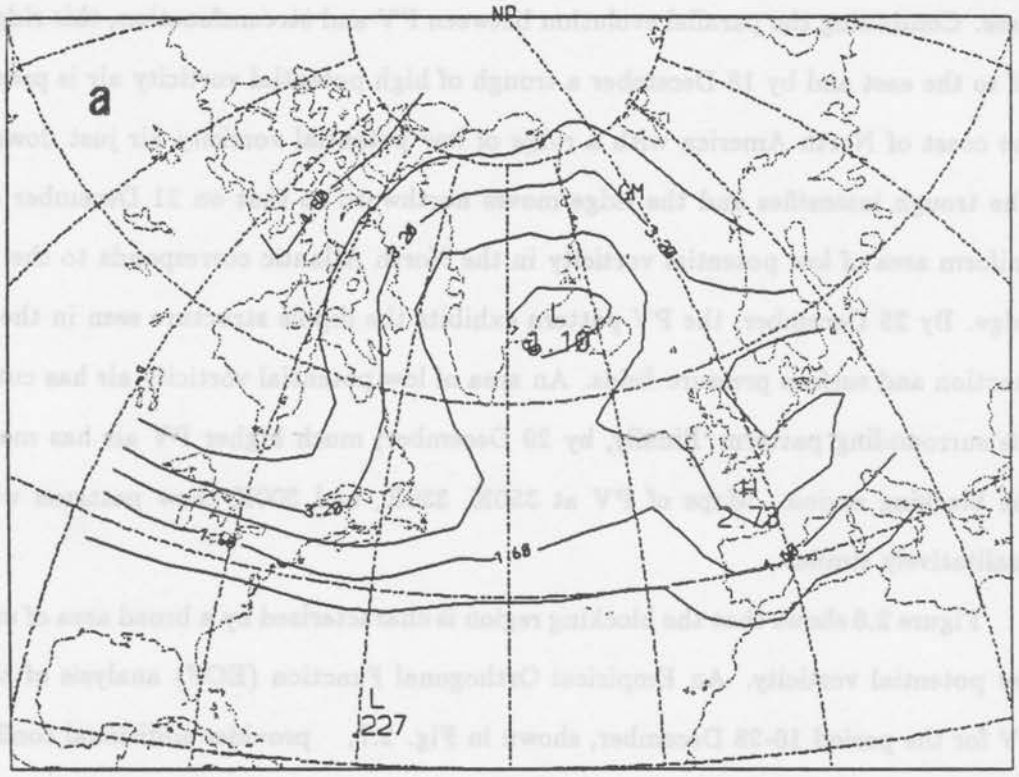

Figure 2.7: (a) The time mean potential vorticity field at 315K for the period 16-28 December, 1978, (b) the first EOF of potential vorticity, (c) the first principal component of potential vorticity, (d) the mean field plus the contribution from the first EOF for 1200 UTC, 18 December, and (e) the mean field plus the contribution from the first EOF for 1200 UTC, 25 December. The mean potential vorticity is non-dimensionalized as in Fig. 2.6. Values plotted for the first EOF have been multiplied by 10^3. Values on the abscissa of the principal component graph are the day of the month at 1200 UTC.

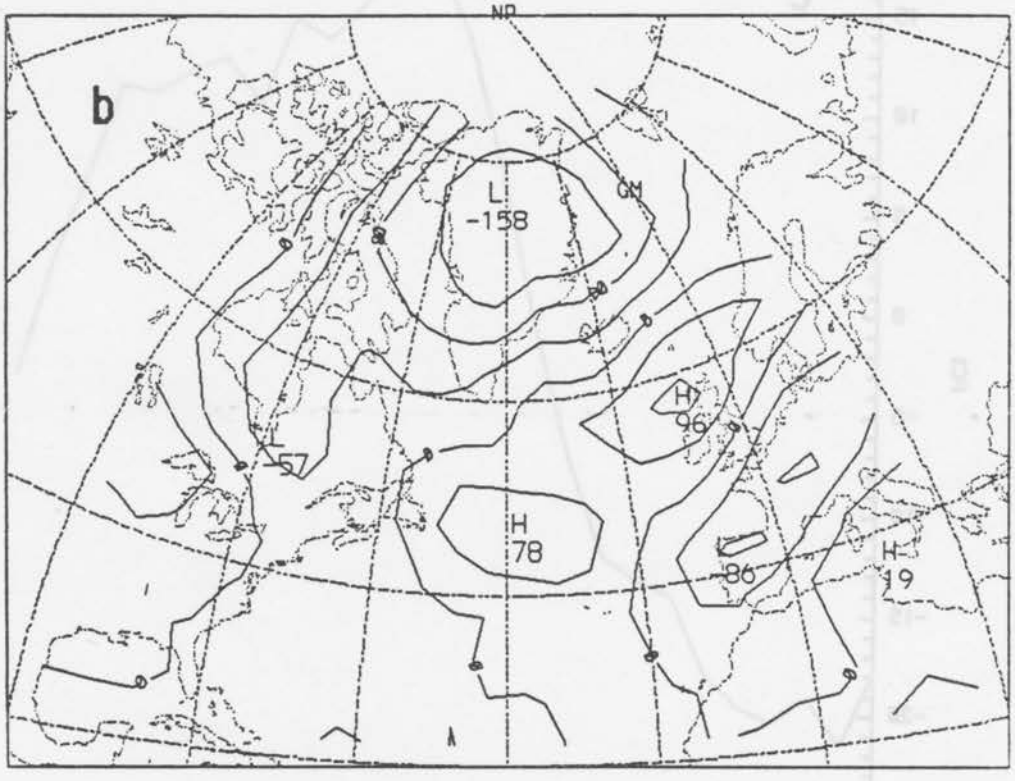

Figure 2.7: continued.

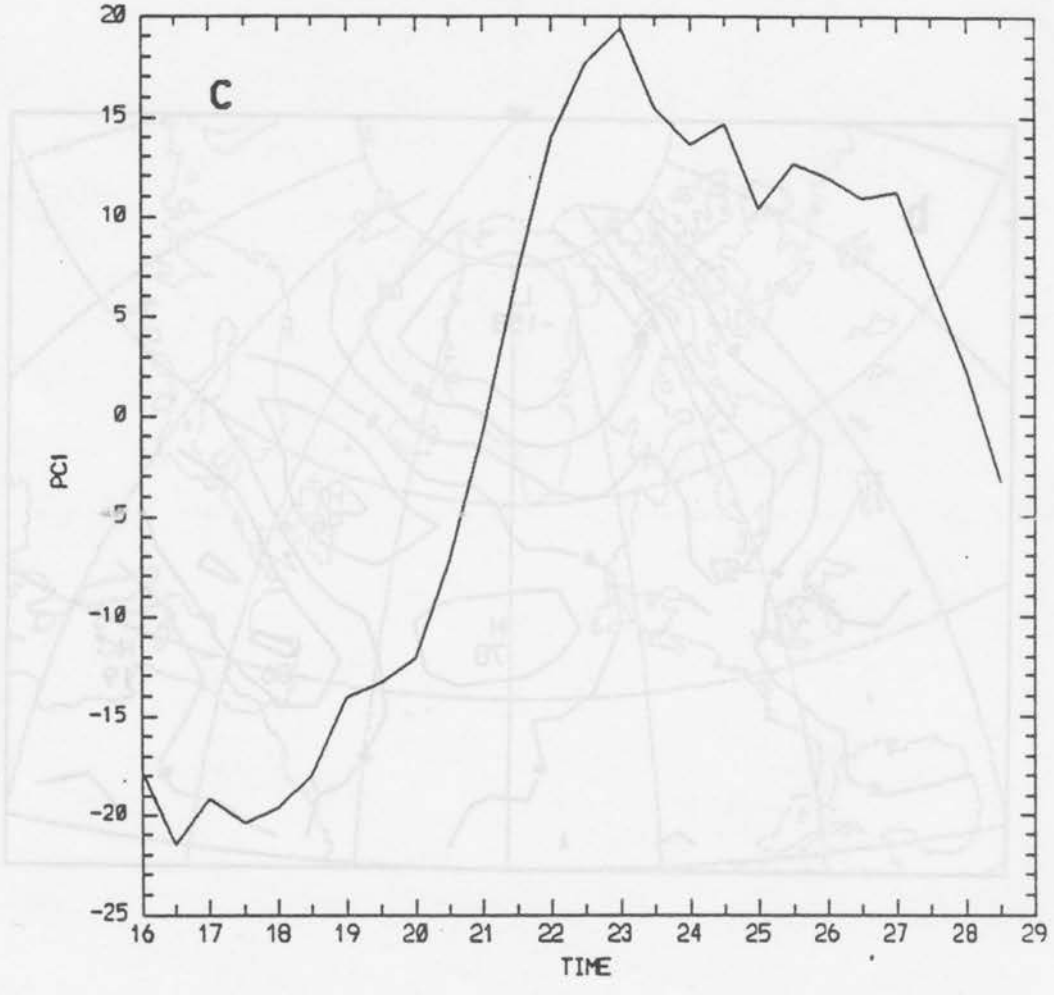

Figure 2.7: continued.

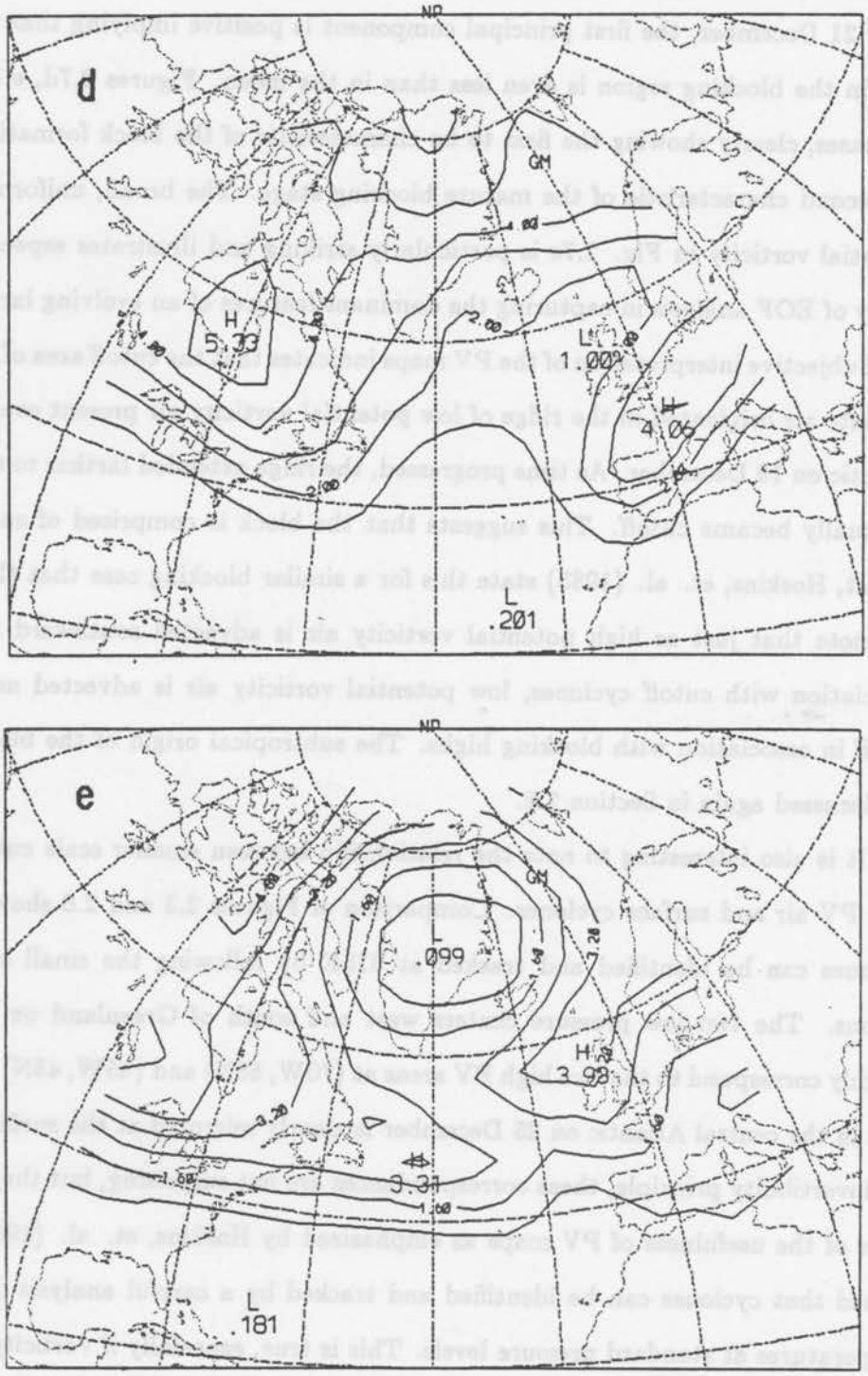

Figure 2.7: continued.

corresponding principal component. Before 21 December, the first principal component is negative; in the blocking region the total PV field is then higher than in the mean. After 21 December, the first principal component is positive implying that the total PV field in the blocking region is even less than in the mean. Figures 2.7d, e illustrate the two cases, clearly showing the first to be characteristic of the block formation stage and the second characteristic of the mature blocking stage. The broad, uniform area of low potential vorticity in Fig. 2.7e is particularly striking and illustrates especially well the utility of EOF analysis in capturing the dominant features of an evolving large scale field.

Subjective interpretation of the PV maps indicates that the cutoff area of low potential vorticity air originated in the ridge of low potential vorticity air present over the western Atlantic on 18 December. As time progressed, the ridge extended farther to the north and eventually became cutoff. This suggests that the block is comprised of subtropical air. In fact, Hoskins, et. al. (1985) state this for a similar blocking case that they examined and note that just as high potential vorticity air is advected southward and cutoff in association with cutoff cyclones, low potential vorticity air is advected northward and cutoff in association with blocking highs. The subtropical origin of the blocking air will be discussed again in Section 2.5.

It is also interesting to note the relationship between smaller scale cutoff regions of high PV air and surface cyclones. Comparison of Figures 2.3 and 2.6 show that surface cyclones can be identified and tracked at 315K by following the small scale high PV regions. The two low pressure centers west and south of Greenland on 21 December roughly correspond to the two high PV areas at (70W, 55N) and (45W, 45N). The high PV area in the central Atlantic on 25 December is clearly mirrored at the surface. In light of the invertibility principle, these correspondences are not surprising, but they do illustrate some of the usefulness of PV maps as emphasized by Hoskins, et. al. (1985). It can be argued that cyclones can be identified and tracked by a careful analysis of heights and temperatures at standard pressure levels. This is true, especially if vorticity contours are superimposed. However, this task seems easier on an PV map where anomalous features stand out more clearly. In addition, the potential vorticity reflects not only vorticity, a kinematic quantity, but also the temperature structure $\partial p/\partial \theta$, a thermodynamic quantity.

As mentioned previously, the invertibility principal allows the wind and mass fields to be determined from the potential vorticity field under appropriate constraints. Qualitative statements can be made by extrapolating the results from inversion of simple PV anomalies. One of these has already been encountered; namely, that the circulation around an PV anomaly has the same sense as the anomaly. This is a statement about the wind field. The analogous statement about the mass field says that the isentropic anomaly in static stability (relative to a basic state upon which the anomaly is superimposed) also has the same sense as the PV anomaly. Thus the blocking region, because it is an area of low potential vorticity, may be expected to be an area of low absolute vorticity and low static stability. It is interesting to determine the nature of this partitioning; i.e., is the blocking region of low potential vorticity mainly a consequence of low absolute vorticity, low stability, or a combination of both? Furthermore, how are changes in potential vorticity partitioned between absolute vorticity changes and stability changes?

Rather than answering these questions by performing an actual inversion of the potential vorticity field, the vorticity and stability are simply evaluated from the data. It proves convenient to think of the potential vorticity as the ratio of the vertical component of absolute vorticity $(\partial v/\partial x)_\theta - (\partial u/\partial y)_\theta + f$ to a measure of the inverse of stability $(-1/g)\partial p/\partial\theta$. This latter quantity may be called the pseudo-density in isentropic coordinates because the isentropic continuity equation may be written so that pseudo-density appears in the same place as density appears in the continuity equation in height coordinates. (See Schubert and Alworth, 1987, for an example of the use of pseudo-density in a modelling study.) A time series of maps of absolute vorticity and pseudo-density were examined. Fig. 2.8 shows these two quantities at 1200 UTC on 25 December. In agreement with the invertibility theory, the block is seen as a region of small absolute vorticity and large pseudo-density (or low stability). The time series of maps indicated that a ridge of low absolute vorticity and low stability air moved northward and eventually cutoff—the same general evolution seen in the streamfunction and potential vorticity fields.

To see this more clearly, the average potential vorticity, absolute vorticity and pseudo-density were calculated for the nine points (separated by 2.5deg longitude, 2.5deg latitude)

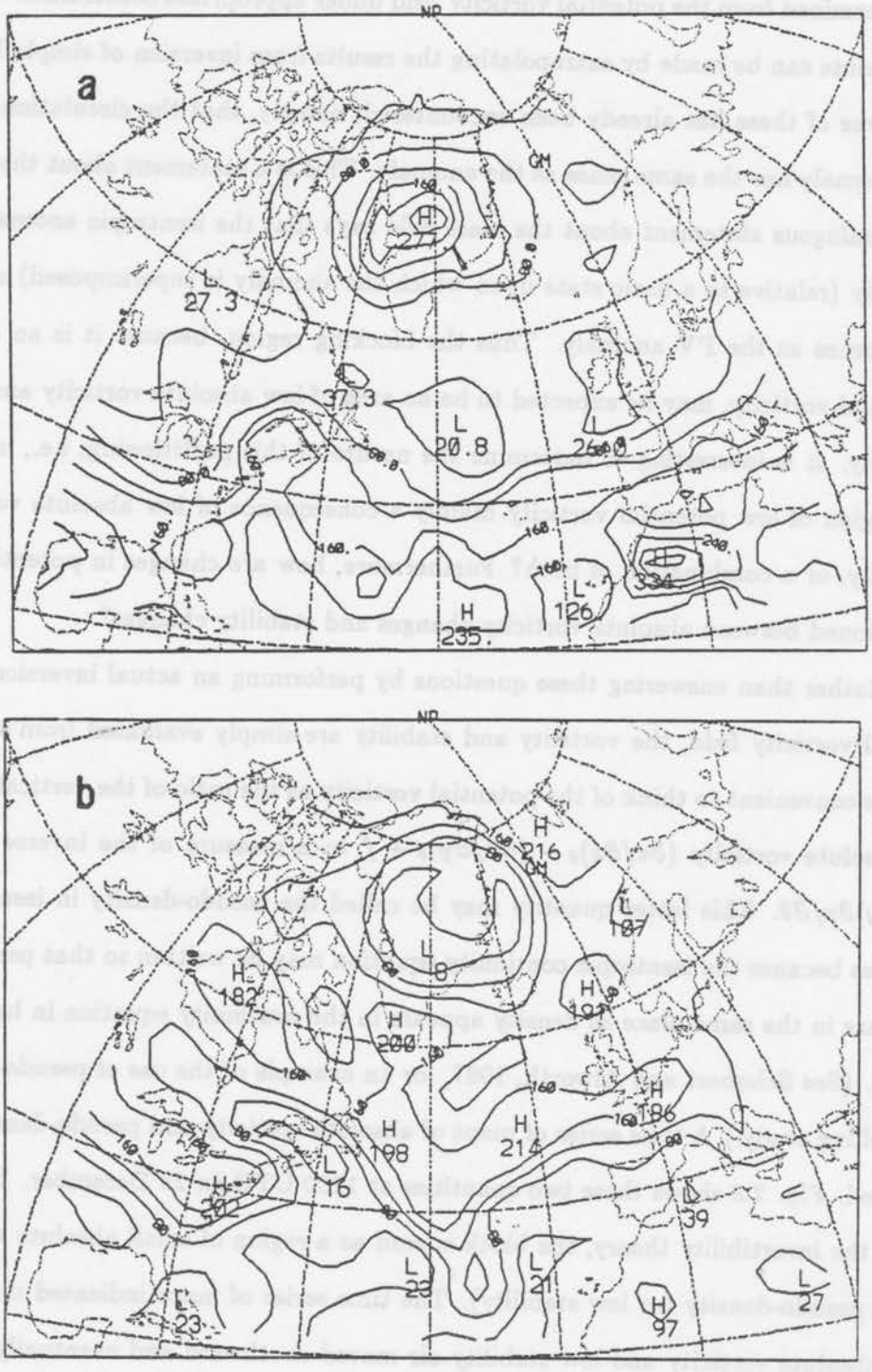

Figure 2.8: (a) The pseudo-density in units of $kgm^{-2}K^{-1}$, and (b) the absolute vorticity in units of $10^{-6}s^{-1}$ at 1200 UTC on 25 December.

in the blocking region centered on the point (70N, 40W). To avoid problems with a later calculation, any points where the data analysis yielded zero or negative values of ς_a or P were not included in the average. The time evolution of these quantities is shown in Fig. 2.9. The potential vorticity in the blocking region rapidly becomes smaller as the block develops in accordance with a decrease in absolute vorticity and an increase in pseudo-density. Therefore, the block can be readily identified from the evolution of absolute vorticity or pseudo-density. If the potential vorticity is small the absolute vorticity (in the numerator) tends to be small and the pseudo-density (in the denomimator) tends to be large. The reverse is true if the potential vorticity is large.

Defining the pseudo-density by $r = -(1/g)\partial p/\partial\theta$ and the absolute vorticity by $\varsigma_a = (\partial v/\partial x)_\theta - (\partial u/\partial y)_\theta + f$, the potential vorticity P may be written

$$P = \varsigma_a / r \ . \tag{4.1}$$

Further defining an overbar to refer to the spatial average over the nine point region mentioned above and angle brackets to refer to a time average over a given time interval, (4.1) may be manipulated to read

$$\Delta\langle\overline{\ln P}\rangle = \Delta\langle\overline{\ln \varsigma_a}\rangle - \Delta\langle\overline{\ln r}\rangle \ , \tag{4.2}$$

where Δ is the difference between two distinct time averages. If the data analysis yielded points where ς_a, and consequently, P, were zero or negative these points were not included in the spatial average because $\ln x$ is not defined for negative x. Two time averages were considered, the first from 0000 UTC, 16 December to 0000 UTC, 19 December, and the second from 1200 UTC, 19 December to 0000 UTC, 28 December. The first period is representative of the flow prior to the block and the second representative of the mature blocking stage. Thus, evaluation of (4.2) for these two periods yields a measure of the relative effects of absolute vorticity changes and pseudo-density changes on the change in the potential vorticity from the relatively high values of the pre-blocking flow to the relatively low values characteristic of the mature block. The terms in (4.2) and their magnitudes at 315K are listed below:

$$\Delta\langle\overline{\ln P}\rangle = -2.68$$

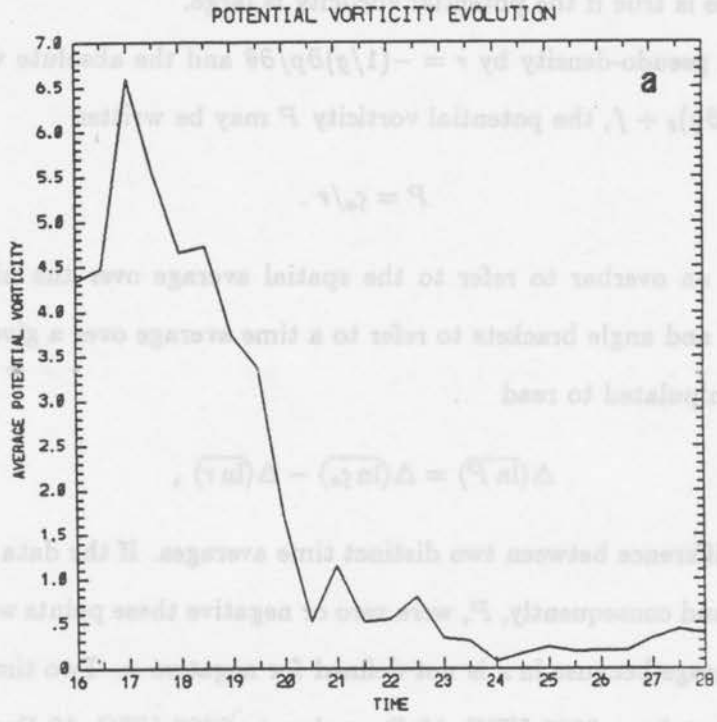

Figure 2.9: Time series of (a) the potential vorticity, (b) the absolute vorticty and (c) the pseudo-density averaged over the nine points centered on the point (70N, 40W). The potential vorticity has been non-dimensionalized as in Fig. 2.6. The absolute vorticity has been non-dimensionalized by $10^{-6}s^{-1}$. Values on the abscissa refer to the day of the month at 0000 UTC.

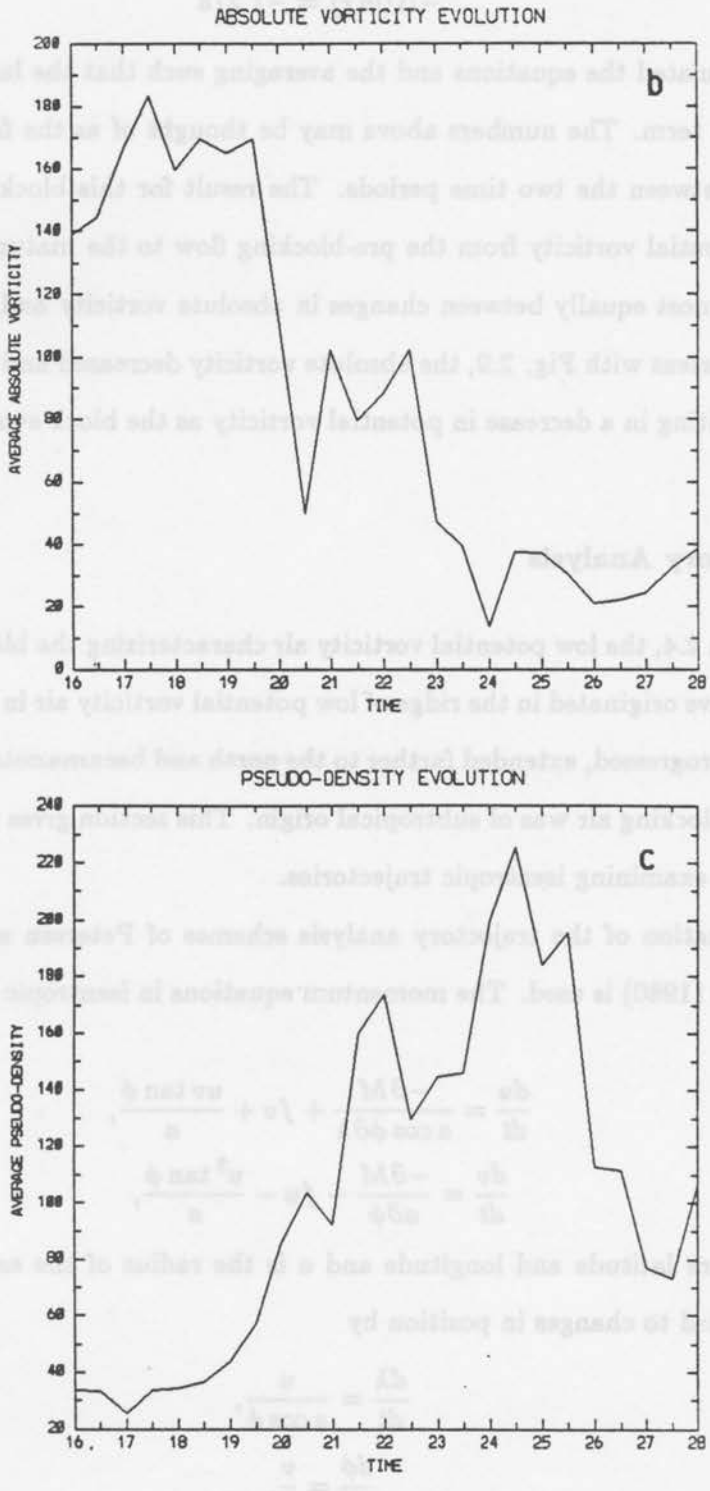

Figure 2.9: continued.

$$\Delta\langle\overline{\ln \varsigma_a}\rangle = -1.401$$

$$-\Delta\langle\overline{\ln r}\rangle = -1.278$$

We have formulated the equations and the averaging such that the last two terms add to equal the first term. The numbers above may be thought of as the fractional changes in P, ς_a and r between the two time periods. The result for this blocking case is that the change in potential vorticity from the pre-blocking flow to the mature blocking flow was partitioned almost equally between changes in absolute vorticity and changes in pseudo-density. Consistent with Fig. 2.9, the absolute vorticity decreased and the pseudo- density increased resulting in a decrease in potential vorticity as the block evolved into its mature stage.

2.5 Trajectory Analysis

In Section 2.4, the low potential vorticity air characterizing the block was subjectively observed to have originated in the ridge of low potential vorticity air in the central Atlantic that, as time progressed, extended farther to the north and became cutoff. The implication was that the blocking air was of subtropical origin. This section gives further evidence for that origin by examining isentropic trajectories.

A modification of the trajectory analysis schemes of Petersen and Uccellini (1979) and Tremback (1980) is used. The momentum equations in isentropic coordinates may be written

$$\frac{du}{dt} = \frac{-\partial M}{a\cos\phi\partial\lambda} + fv + \frac{uv\tan\phi}{a}, \tag{5.1a}$$

$$\frac{dv}{dt} = \frac{-\partial M}{a\partial\phi} - fu - \frac{u^2\tan\phi}{a}, \tag{5.1b}$$

where (λ, ϕ) are latitude and longitude and a is the radius of the earth. The velocities (u, v) are related to changes in position by

$$\frac{d\lambda}{dt} = \frac{u}{a\cos\phi}, \tag{5.2a}$$

$$\frac{d\phi}{dt} = \frac{v}{a}. \tag{5.2b}$$

The integration scheme essentially involves calculating accelerations from the right hand side of (5.1) and then computing new positions from (5.2). The actual steps are as follows:

(i) Specify an initial position and time for the parcel. (All trajectories calculated here begin at either 0000 UTC or 1200 UTC.) Calculate the gradient of M. Initialize u and v from NMC winds.

(ii) Using a fourth order Runge-Kutta scheme, integrate (5.1) and (5.2) as a coupled set of four first order ordinary differential equations to obtain the position and velocity of the parcel at time $t = t_0 + \delta t$ where t_0 is the present time and δt is the time step. Integration can be forward or backward in time; i.e., δt can be positive or negative.

(iii) Interpolate linearly in time between the 12 hour intervals at which data is available to obtain M at time $t_0 + \delta t$. Calculate the gradient of M and use a bi-cubic spline to interpolate the gradient to the new position.

(iv) Evaluate the right hand side of (5.1) and (5.2).

(v) If the trajectory has been integrated for less than the time desired, go to step (ii); otherwise, end the trajectory calculation.

Tremback (1980) modified Petersen and Uccellini's (1979) original scheme by incorporating a time integration method that was more accurate and did not involve special formulas for the first time step. The additional modification here is the consideration of (5.1) and (5.2) as a coupled set of ordinary differential equations which can be efficiently and accurately integrated by a Runge-Kutta technique. This type of trajectory analysis was shown by Petersen and Uccellini (1979) and Tremback (1980) to be better than earlier iterative methods such as Petterssen (1956) and Danielson (1961). It also has the advantage of conceptual simplicity without loss of the essential physics—velocities and positions are simply calculated from knowledge of the forces acting on an air parcel. There are, however, limitations on the accuracy of the trajectory results. Linear interpolation of the streamfunction field in time [see step (iii) above] is unrealistic as the pattern may evolve slowly for part of a 12 hour period and rapidly for a different part. Merrill, et.al. (1986) show that this need not degrade the trajectories too much, provided the trajectories do not encounter explosively deepening systems. There are also errors associated with spatial interpolation, time differencing, additional forces in the momentum equations that

have been neglected, and observational errors. Finally, there are errors that occur if the trajectories are assumed to be completely adiabatic; diabatic heating would move an air parcel to a different θ surface where a different streamfunction pattern would result in a different trajectory path.

These last errors can be partially overcome by application of Tremback's (1980) moist trajectory scheme. At the end of each time step, the parcel's saturation mixing ratio $q_s(p,T)$ is calculated. If the saturation mixing ratio is less than the mixing ratio q that the parcel had at the beginning of the time step, condensation occurred during that time step. An iterative process is then employed to find the change in θ due to the latent heating. First, an initial change in θ is calculated using

$$\Delta\theta = \left(\frac{L}{c_p}\right)\left(\frac{p_{00}}{p}\right)(q - q_s)\,, \tag{5.3}$$

where L is the latent heat of condensation. A new value of $q_s(p,T)$ is calculated at the new θ level and (5.3) is applied again to find a second value of $\Delta\theta$. The process is repeated until the change in $\Delta\theta$ is less than some specified value. In agreement with Tremback, the number of iterations was usually less than eight. The end result of the entire process is new parcel values of p, temperature T, θ, q and q_s which have taken into account condensation. Several assumptions are implicit in this technique: (1) condensation causes only changes in the vertical position of the parcel at the end of the time step; i.e., the parcel's (λ,ϕ) are not changed regardless of whether condensation occurred, (2) M and p vary linearly with θ, and (3) complicated microphysics are ignored [see Tremback (1980) for details].

A continuing problem with trajectory analysis is the lack of a direct way to determine the accuracy of the trajectories. Perhaps the best indirect way (Reiter, 1972) is to see how well the energy equation

$$\int_{t_0}^{t_0+\delta t} \frac{d}{dt}\left(\frac{u^2+v^2}{2} + M + Lq\right) dt = \int_{t_0}^{t_0+\delta t} \frac{\partial M}{\partial t} dt \tag{5.4}$$

is satisfied. (For a derivation, see Dutton, 1976.) The energy error is the difference between the two terms. For the trajectories discussed below, the accumulated absolute energy error over the length of the trajectories was a factor of three or more smaller than either the

accumulated absolute energy change [the sum over all time steps of the left hand side of (5.4)] or the accumulated absolute average local change [the sum over all time steps of the right hand side of (5.4)]. Even when the error was less than an order of magnitude smaller than the two terms that created it, the trajectories still seemed reasonable when compared with the time evolution of the streamfunction fields. Furthermore, equivalent potential temperature θ_e should be conserved for moist trajectories. Because of the numerical and physical approximations introduced, exact conservation is not achieved; however, the ratio of changes in θ_e to changes in θ during condensation was always much less than one in magnitude. Despite its limitations, this trajectory scheme is among the best available and is accepted as a useful tool for understanding many phenomena.

The origin of the low potential vorticity air comprising the block is now considered. Several 36 hour adiabatic trajectories on the 315K surface ending at 1200 UTC on 20 December are shown in Fig. 2.10. The time period was chosen to correspond to the initial development of the high latitude blocking ridge. Starting positions were estimated from the endpoints of backward integrated trajectories. The time step used was 300s for the first hour and 900s thereafter. Table 2.1 lists the position, pressure and potential vorticity at the beginning and end points of these trajectories. Fig. 2.10 shows that the blocking air at 315K originated well to the south of the block in the central Atlantic. With one exception, the trajectories ascended more than 100mb in the 36 hour period. Comparison with the streamfunction maps indicates that the trajectories are a reflection of the flow on the east side of a strong trough off the North American coast and hence are related to the strong storm associated with that trough. This is additional evidence that strong storms may play an important role in the development of blocks.

The effect of latent heat release on these trajectories is illustrated in Fig. 2.11 and in Table 2.2 for one particular trajectory. The qualitative results from the adiabatic trajectories are unchanged; however, latent heat release can effect noticeable changes in the trajectory path as well as in the parcel's pressure and potential temperature. Over its lifetime the adiabatic trajectory moved upward approximately 175mb from the mid-troposphere to the upper troposphere. Because of condensation, the moist trajectory experienced a larger pressure change, nearly 200mb. The maximum change in θ was slightly

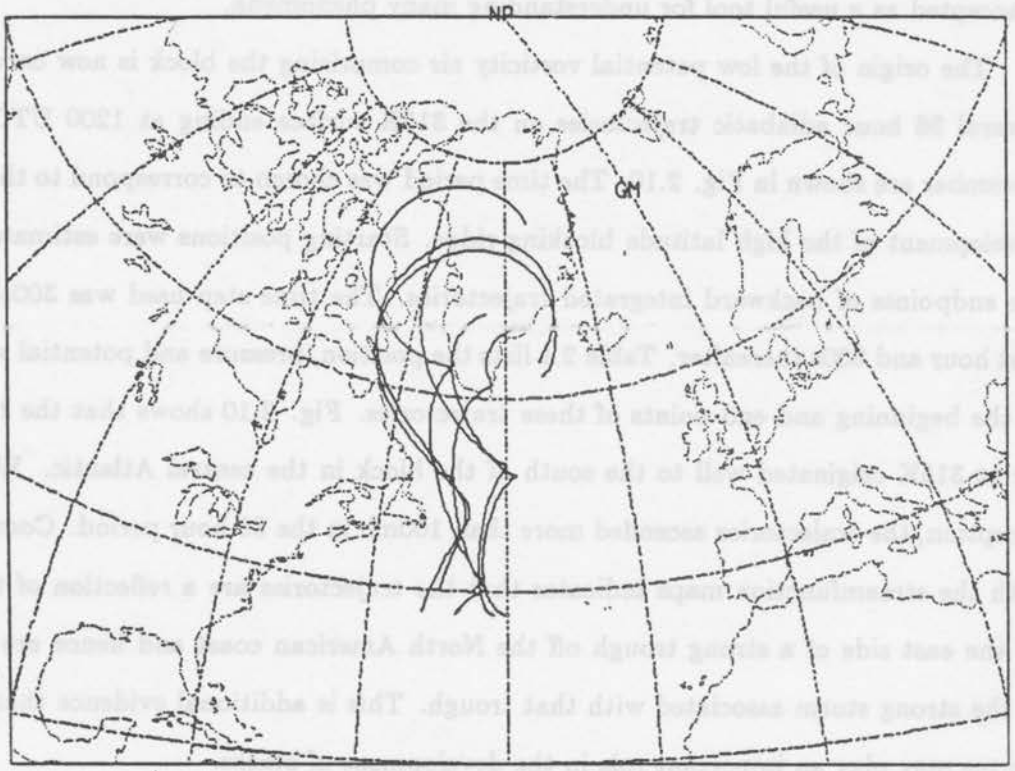

Figure 2.10: A group of 36 hour adiabatic trajectories on the 315K surface ending at 1200 UTC, 20 December.

Table 2.1: The latitude and longitude, pressure, and potential vorticity (scaled by $10^{-6} m^2 K kg^{-1} s^{-1}$) at the beginning (top row) and end (bottom row) of the trajectories shown in Fig. 2.10.

Latitude	Longitude	Pressure	Potential Vorticity
37.5 N	42.5 W	452 mb	0.56
71.8 N	57.5 W	275 mb	0.23
37.5 N	40.0 W	437 mb	0.74
67.6 N	44.3 W	310 mb	0.30
40.0 N	45.0 W	473 mb	0.40
75.2 N	33.2 W	308 mb	1.6
40.0 N	50.0 W	447 mb	0.25
63.3 N	32. 7 W	331 mb	0.24
37.5 N	47.5 W	471 mb	0.12
66.5 N	34.2 W	329 mb	0.34
37.5 N	52.5 W	364 mb	0.87
62.0 N	32.6 W	333 mb	0.21

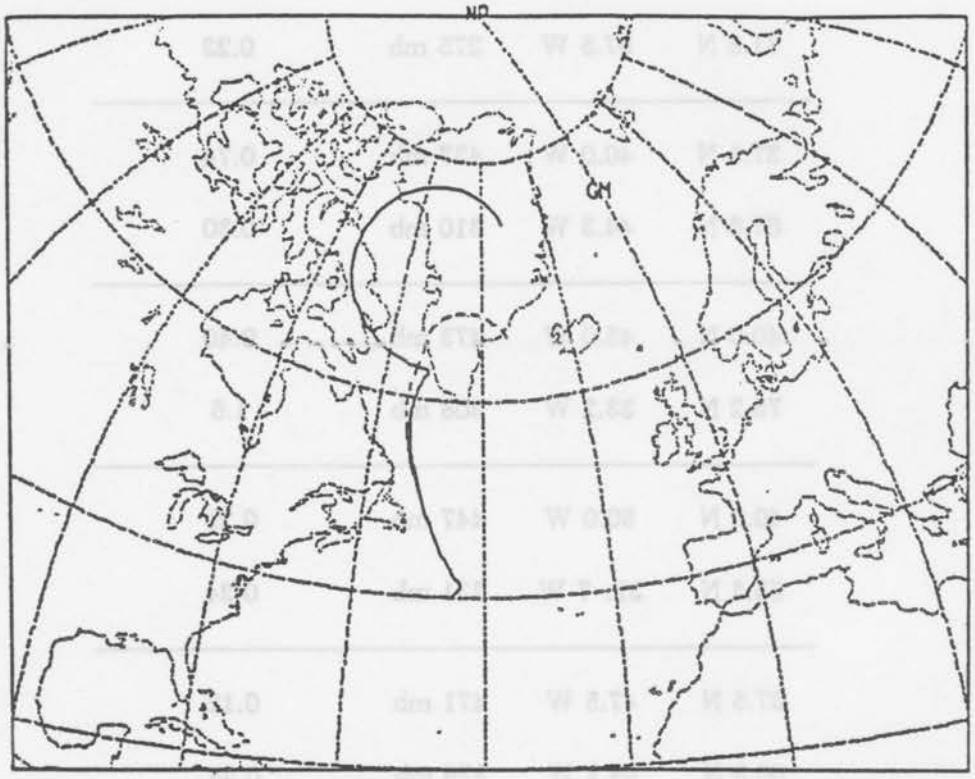

Figure 2.11: Adiabatic (solid line) and moist adiabatic (dashed line) 36 hour trajectories originating on the 315K surface and ending at 1200 UTC, 20 December. The moist trajectory was initialized with a relative humidity of 100%, corresponding to a worst case scenario.

Table 2.2: The latitude and longitude, pressure, and potential temperature at 12 hour intervals for the adiabatic and moist adiabatic trajectories shown in Fig. 2.11. The top row in each time block is for the adiabatic trajectory while the bottom row is for the moist adiabatic trajectory. The potential vorticity (scaled by $10^{-6} m^2 K kg^{-1} s^{-1}$) at the beginning and end of the trajectories is also listed.

Time	Latitude	Longitude	Pressure	Potential Temperature	Potential Vorticity
0000 UTC	40.0 N	45.0 W	473 mb	315.0 K	0.40
19 December	40.0 N	45.0 W	473 mb	315.0 K	0.40
1200 UTC	50.4 N	50.7 W	353 mb	315.0 K	
19 December	50.5 N	51.0 W	317 mb	319.9 K	
0000 UTC	62.8 N	53.4 W	405 mb	315.0 K	
20 December	65.1 N	52.6 W	341 mb	319.9 K	
1200 UTC	75.2 N	33.2 W	308 mb	315.0 K	1.6
20 December	65.8 N	34.2 W	266 mb	320.6 K	0.55

over 5K. Larger changes in θ would not be expected because the parcel is consistently located in the middle and upper troposphere where moisture content is low and where, on a thermodynamic diagram, the slope of dry adiabats approaches the slope of moist adiabats. Trajectories beginning on lower θ surfaces would presumably be more affected by condensation.

Although the blocking high is well established by 21 December, the dipole pattern common to North Atlantic blocks does not appear until a few days later. Trajectory analysis was also used to determine the origin of the high potential vorticity air located in the southern half of the dipole. The endpoints of backward integrated trajectories were used to define the starting points at 0000 UTC, 23 December for the group of adiabatic trajectories shown in Fig. 2.12. The position, pressure, and potential vorticity at the starting and ending points of each of these trajectories is given in Table 2.3.

The trajectories indicate the the air in the southern half of the dipole originated almost due west near the Great Lakes region at nearly the same pressure level. This is in agreement with the streamfunction maps for the period which show very consistent westerly flow. The inclusion of latent heat release in these trajectories (not shown) has little noticeable effect—none of these parcels experience a great enough change in pressure to make condensation important.

The trajectory scheme outlined above is not formulated to explicitly conserve potential vorticity. Therefore, there is no guarantee that the potential vorticities at the beginning and end of each trajectory are equal. Tables 2.1-2.3 have listed the starting and ending potential vorticities for all the trajectories in Figures 2.10-2.12 and indicate that the potential vorticity is indeed not conserved. How serious is the non-conservation? One measure of the conservation error is the ratio of the change in potential vorticity for a given trajectory, denoted by ΔP_t, to the change in potential vorticity from a characteristic high value to a characteristic low value, denoted by ΔP_{max}. From Fig. 2.6 the non-dimensional potential vorticity in low potential vorticity areas is typically less than unity while in high potential vorticity areas the value ranges between 5 and 7. Thus $\Delta P_{max} \approx 6$. Examination of Tables 2.1-2.3 then indicate that $\Delta P_t / \Delta P_{max}$ is always less than one and in many

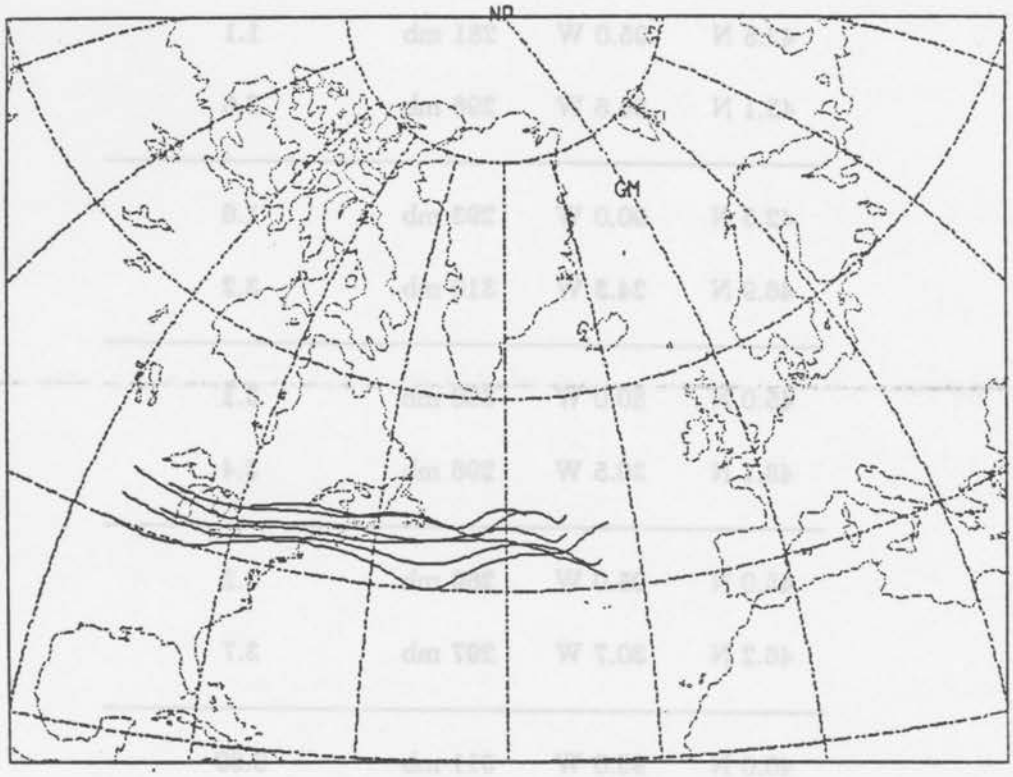

Figure 2.12: A group of 36 hour adiabatic trajectories on the 315K surface ending at 1200 UTC, 24 December.

Table 2.3: The latitude and longitude, pressure, and potential vorticity (scaled by $10^{-6} m^2 K kg^{-1} s^{-1}$) at the beginning (top row) and end (bottom row) of the trajectories shown in Fig. 2.12.

Latitude	Longitude	Pressure	Potential Vorticity
42.5 N	95.0 W	281 mb	1.1
43.1 N	25.6 W	298 mb	2.6
42.5 N	90.0 W	293 mb	1.6
46.9 N	24.3 W	310 mb	3.2
45.0 N	80.0 W	300 mb	3.1
48.1 N	30.5 W	296 mb	3.4
45.0 N	95.0 W	269 mb	3.2
46.2 N	30.7 W	297 mb	3.7
40.0 N	95.0 W	311 mb	0.89
41.2 N	25.3 W	313 mb	1.7
45.0 N	90.0 W	282 mb	5.1
48.4 N	36.8 W	293 mb	4.6

cases $\Delta P_t/\Delta P_{max} \sim O(0.1)$. This result indicates that the degree of non-conservation is not serious.

Nevertheless, the potential vorticity is not conserved. There are several reasons. As noted above, the trajectory scheme does not explicitly guarantee conservation. There are inherent errors in calculating the potential vorticty field itself using a finite difference approximation. Finally, potential vorticity is not conserved when frictional and diabatic effects are present as they undoubtedly are in some degree. Table 2.2 indicates, for one trajectory, that conservation was more nearly achieved when condensation was taken into account in the trajectory calculation. Interesting future work would include a more complete analysis of the sources of non-conservation of potential vorticity.

2.6 Summary, Conclusions and Speculations

Blocking events are important because they restrict the passage of cyclonic storms and their associated fronts through a given region for a period of a week to ten days, or more, and hence have an impact on medium range weather forecasts.

A single episode of blocking during December 1978 was investigated from NMC gridpoint data using the technique of isentropic analysis. A primary advantage of this viewpoint is that air parcels stay on isentropic surfaces in the absence of diabatic effects. Furthermore, isentropic analysis is the best way to examine the potential vorticity—a conserved quantity under the two constraints above. The following results were obtained. An analysis of the Montgomery streamfunction on the 315K isentropic surface was found to be preferable to the more traditional analysis of geopotential height on the 300mb surface for describing the evolution of of the block. The evolution of the surface pressure pattern showed several intense cyclonic storms upstream of the block prior to its development. The vertical structure of the block showed little tilt with a warm core throughout most of the troposphere and a high tropopause. The block was also shown to have significantly affected the passage of fronts through the blocking region.

Analysis of isentropic potential vorticity indicated that the block was a broad, uniform area of low potential vorticity. An EOF analysis added confirmation to this while

illustrating well the development of the block. The evolution of the two components of potential vorticity, namely, the absolute vorticity and the pseudo-density (a measure of the inverse of stability), was also shown to evolve in the same way as the potential vorticity itself. If the potential vorticity became smaller, typically the absolute vorticity became smaller and the pseudo-density became larger.

Subjective interpretation of the potential vorticity maps indicated that the low potential vorticity air characterizing the block originated from well south of the block. Isentropic trajectories verified this and noted the relationship between the trajectories and the advection ahead of an intense cyclonic storm. Advection of warmer air from well south of the block may explain in part the high tropopause over the blocking region.

This study appears to be one of the first examples of isentropic analysis applied to blocking. Excepting the familiarity of the conventional isobaric analysis, nothing is lost by taking this viewpoint. Much of what is gained is gleaned from the analysis of potential vorticity, which, as noted, is most conveniently and informatively analyzed on isentropic surfaces. The analysis of potential vorticity on isentropic surfaces showed the block to be a broad area of uniformly low potential vorticity, provided a theoretical framework for relating this to a high pressure area with clockwise circulation and low stability (relative to the air around it on the same isentropic surface), and subjectively indicated the origin of the low potential vorticity air (later confirmed by isentropic trajectories). These points could have been extracted from a more traditional analysis; however, isentropic analysis highlighted them more efficiently and clearly. One might argue, following Hoskins, *et al.* (1985) that the potential vorticity maps themselves are a complete picture of the block, both synoptically and dynamically. The value of the study, therefore, lies not so much in the discovery of new information, but rather in the application of a better framework in which to present known information.

One specific way in which the isentropic framework illustrated its suitability was in the determination of the origin of the blocking air and the possible role of intense cyclones in blocking development. Consider the following observations. Mature blocks (at least in the North Atlantic) almost always have a cutoff high at upper levels. (A cutoff high may

be defined as the region inside a closed contour on the streamfunction map.) Frequently, there is also a cutoff low to the south. These seem to form a stable dipole structure that may account for most of the persistence of these blocks. Accepting this possibility, the question of blocking development then reduces to the question of how this structure is formed. More specifically, how does low potential vorticity air find its way into the northern half of the dipole and high potential vorticity air into the southern half? The potential vorticity maps and trajectory analyses for this particular block indicate that the low potential vorticity air in the cutoff high was advected northward ahead of the trough associated with an intense cyclone while the high potential vorticity air came directly from the west. The sequence of events was the northward advection of low potential vorticity air, the formation of a cutoff area of low potential vorticity air, and then the advection of high potential vorticity air from the west into a region south of the blocking high and the formation of the dipole structure. Both halves of the dipole did not develop simultaneously; rather, the northern half developed first, then the southern half. The nature of the southern half of the dipole is more speculative as it is never as well defined or as consistently present on the maps as the northern half. For example, the maps sometimes show a tight, very well defined region of high potential vorticity air south of the block as in Fig. 2.6e, at other times the high potential vorticity air is more diffuse. The same fluctuating nature may be seen in the streamfunction patterns. This aspect may be attributed to the continuous propagation of cyclones into and through that region. These ideas may have some bearing on Frederiksen's (1982) dipole mode instabilities. In any case, intense cyclones appear to play some role in this development and isentropic analysis has helped to elucidate that role.

REFERENCES

Colucci, Stephen J., Arthur Z. Loesch and Lance F. Bosart, 1981: Spectral evolution of a blocking episode and comparison with wave-interaction theory. *J. Atmos. Sci.*, **38**, 2092-2111.

Colucci, Stephen J., 1985: Explosive cyclogenesis and large-scale circulation changes: implications for atmospheric blocking. *J. Atmos. Sci.*, **42**, 2701-2717.

Conte, S.D. and Carl deBoor, 1986: *Elementary Numerical Analysis. An Algorithmic Approach*, 3rd edition, McGraw-Hill, 432pp.

Danielsen, E.F., 1959: The laminar structure of the atmosphere and its relation to the concept of a tropopause. *Arch. Meteorol. Geophys. Bioklimatol., Ser. A*, **11**(3), 293-332.

Danielsen, E.F., 1961: Trajectories: Isobaric, isentropic and actual. *J. Meteor.*, **18**, 479-486.

Dole, Randall M., 1986: Persistent anomalies of the extratropical northern hemisphere wintertime circulation: structure. *Mon. Wea. Rev.*, **114**, 178-207.

Dutton, John A., 1976: *The Ceaseless Wind*, McGraw-Hill, 579pp.

Ertel, H., 1942: Ein Neuer hydrodynamischer Wirbelsatz. *Met. Z.*, **59**, 271-281.

Frederiksen, J.S., 1982: A unified three dimensional instability theory of the onset of blocking and cyclogenesis. *J. Atmos. Sci.*, **39**, 969- 982.

Hanson, Anthony R. and T-S. Chen, 1982: A spectral energetics analysis of atmospheric blocking. *Mon. Wea. Rev.*, **110**, 1146-1165.

Hoskins, B.J., M.E. McIntyre and A.W. Robertson, 1985: On the use and significance of isentropic potential vorticity maps. *Quart. J. Roy. Meteor. Soc.*, **111**, 877-946.

Illari, Lodovica, 1984: A diagnostic study of the potential vorticity in a warm blocking anitcyclone. *J. Atmos. Sci.*, **41**, 3518-3526.

Ji, L.R. and S. Tibaldi, 1983: Numerical simulations of a case of blocking: the effects of orography and land-sea contrast. *Mon. Wea. Rev.*, **111**, 2068-2086.

McIntyre, M.E. and T.N. Palmer, 1984: The "surf zone" in the stratosphere. *J. Atmos. Terres. Phys.*, **46**, 825-849.

Merrill, John T., Rainer Bleck, and Douglas Boudra, 1986: Techniques of Langragian trajectory analysis in isentropic coordinates. *Mon. Wea. Rev.*, **114**, 571-581.

Namias, J., 1938: Thunderstorm forecasting with the aid of isentropic charts. *Bull. Amer. Met. Soc.*, **19**, 1-14.

Petersen, R.A. and L. Uccellini, 1979: The computation of isentropic atmospheric trajectories using a "discrete model" formulation. *Mon. Wea. Rev.*, **107**, 566-574.

Petterssen, S., 1956: *Weather Analysis and Forecasting*, Volume I, McGraw-Hill, 428pp.

Reiter, Elmar R., 1972: *Atmospheric Transport Processes. Part 3: Hydrodynamic Tracers*, AEC Critical Review Series, 212pp.

Rex, Daniel F., 1950: Blocking action in the middle troposphere and its effect upon regional climate. I. An aerological study of blocking action. *Tellus*, **2**, 196-211.

Rossby, C.G., 1937: Aerological evidence of large-scale mixing in the atmosphere. *American Geophysical Union*, Transactions, 18th Annual Meeting, 8p.

Sanders, F. and J.R. Gyakum, 1980: Synoptic-dynamic climatology of the "bomb." *Mon. Wea. Rev.*, **108**, 1589-1606.

Schubert, Wayne H. and Brian T. Alworth, 1987: Evolution of potential vorticity in tropical cyclones. *Quart. J. Roy. Meteor. Soc.*, **113**, 147-162.

Tremback, C., 1980: A moist adiabatic trajectory computation technique based on a modified "discrete model" formulation. M.S. Thesis, Northern Illinois University. Available upon request from the author at the Department of Atmospheric Science, Colorado State University, Fort Collins, CO, 80523.

Uccellini, L. 1976: Operational diagnostic applications of isentropic analysis. *Nat. Wea. Dig.*, **1**, 4-12.

White, W.B. and N.E. Clark, 1975: On the development of blocking activity over the central north Pacific. *J. Atmos. Sci.* , **32**, 489-502.

Chapter 3

BAROTROPIC INSTABILITY WITH DOWNSTREAM AND ASYMMETRIC CROSS-STREAM VARIATIONS: IDEALIZED CALCULATIONS

3.1 Introduction

Studies of dynamic instabilities–those instabilities that depend inherently on the motion of the flow relative to the earth–have played a central role in the history of theoretical meteorology. The pioneering work by Kuo (1949), Charney (1947) and others on barotropic and baroclinic instabilities have elucidated many fundamental aspects of geophysical fluid dynamics as well as offered possible explanations of observed atmospheric phenomena such as mid-latitude synoptic storms. Similar advances for other dynamic instabilities have also taken place. These lines of research continue to be fruitful at the present time as the original approaches are enhanced, modified and applied to a variety of new situations.

The classical approach to the study of dynamic instabilities for geophysical fluid dynamics problems has been to consider the structure, growth and propagation of linearized perturbations superimposed on a specified flow, typically called the basic state flow. Depending on the problem under consideration, this basic flow is assumed to vary in the north-south direction (y), the vertical direction (z), or both, but not, at least in the classical treatment, in the east-west direction (x). This assumption allows for the representation of the x structure by a single wave. The propagation speed, and growth rate of this wave as well as its structure in y and z are then determined by analytical or numerical means, the latter being necessary for all but the simplest, most idealistic cases. The calculation can be repeated for different wavelengths until the most unstable wavelength is determined.

Each of the unstable (or stable or neutral, as the case may be) waves is referred to as a normal mode of the system. It is argued that if the fluid system under consideration is perturbed from its basic state flow by infinitesimal perturbations of all wavelengths, the characteristics of the most unstable normal mode will eventually dominate. Such is the classical instability approach which has proved to be so useful.

However, the classical approach is not without its limitations such as the requirement of a basic state with no variation in x. This is unrealistic. For example, if we identify our basic state with the time averaged January flow, this flow exhibits considerable longitudinal variation with two major jet regions, and planetary wave components of significant amplitude. This limitation can be overcome. One of the first attempts in this direction was made by Lorenz (1972) who studied the barotropic stability of a basic state consisting of zonal flow plus a Rossby wave. Such flow was found to be unstable if the Rossby wave was strong enough or of short enough wavelength. Hoskins and Hollingsworth (1973) re-examined the Lorenz system and found a simple necessary and sufficient condition for instability. The extension to include inertia gravity waves was done by Duffy (1975) while the extension to the stability of Rossby Haurwitz waves on the sphere is due to Hoskins (1973). Additional noteworthy literature in this area is the long series of papers by Frederikson (e.g. Frederikson, 1978a,b; 1979a,b; 1982; 1983a,b) who has primarily studied the baroclinic instability of three dimensional (meaning variation in all three spatial directions) flows on the sphere. He has considered both idealized basic states consisting of planetary waves superimposed on zonal jets (Frederikson, 1979a,b) and basic states defined by time averaged flow in the real atmosphere (Frederikson, 1982). A main focus of his work has been the identification of those instabilities which may be related to observed large scale phenomena such as blocks or teleconnection patterns. Niehaus (1980) studies a similar problem. Grotjahn (1984) presents a very useful review of all the relevant articles up to that time. Also noteworthy are the two analytical papers by Peng and Williams (1986,1987) on barotropic and baroclinic instabilities of streamwise varying easterly flows in a beta- channel. These build upon the earlier numerical work of Tupaz *et al.* (1978) and Williams *et al.* (1984). The focus of these studies is the application of the concept of spatial growth rate in order to understand the behavior of the instabilities.

There appear to be several distinct approaches for these types of instability problems. *The time integration method* (e.g. Brown, 1969) proceeds by initializing a linearized time dependent model with random perturbations and integrating forward in time, monitoring appropriate quantities until normal mode form is achieved. The growth rate, phase speed and structure of the disturbance can then be noted. The *eigenvalue method* (e.g. Frederikson, 1978a) proceeds by discretizing the linearized governing equations in space (most commonly by applying a Galerkin spectral method using orthogonal functions appropriate to the geometry) and then assuming that the time variation is proportional to a complex exponential. This reduces the calculation to a matrix eigenvalue problem where the eigenvalue is the complex frequency and the eigenvector determines the unknown perturbation variables. A set of stable and unstable modes is found, contrary to the time integration method which gives only the most unstable mode (but see Simmons and Hoskins, 1976). In theory, the time integration method requires little computer storage, but a lot of execution time and so may be considered computationally intensive. In contrast, the eigenvalue approach requires much more storage, but less execution time and so is not computationally intensive, although storage requirements may demand a large computer system. In fact, these storage requirements limit the resolution of the eigenvalue method (Grotjahn, 1987). Given enough computer time, the time integration method can be employed with very high resolution. However, the eigenvalue method is superior in that it can distinguish between two modes with similar growth rate–a potential problem in a time integration. See Frederikson (1978b) for additional discussion. A thorough analysis of these instability problems should probably critically compare results from both approaches.

The previously noted work by Peng and Williams (1986, 1987) suggests yet a different way of thinking about these instabilities, based on the concept of spatial growth rate rather than temporal growth rate. The latter is associated with one or more real wavenumbers and a complex frequency while the former has a real frequency and a complex wavenumber. In their analytical treatment, the frequency is specified and a *complex* wavenumber is calculated as the eigenvalue of a problem which is simplified by assuming that the basic state varies more slowly in x than in y . The equivalent numerical calculation is to force a

wave of fixed frequency and let it propagate downstream, noting the changes in amplitude as it passes through regions of unstable flow. This, in fact, is what Tupaz, *et al.* (1978) have done. Thus the concept of a spatial growth rate can be discussed in an analytical or numerical framework. An advantage of this method is that any x variation in the scale of the instability is easily determined.

Although barotropic instability inherently involves a basic state which varies in the north-south direction, previous theoretical studies have concentrated on symmetric variations, i.e., those zonal wind profiles that vary symmetrically about some central latitude. The Bickley jet (e.g. Haltiner and Williams, 1980) is the classical case. More complicated structures, such as double jets, have also been studied (Haltiner and Song, 1963). Certainly the observed flows used by Frederikson (1982) are asymmetric in this sense. However, little has been done on a fundamental level to document the effects of such asymmetries on the instabilities.

This paper reports the results of a study of *barotropic* instability for basic states which vary in the east-west direction and have zonal wind profiles that vary asymmetrically about a central latitude. We will use the terminology that such basic states have *downstream* and *asymmetric cross-stream* variation. Undoubtedly, there are a large number of plausible, meaningful experiments that can be made under this scenario. To focus our study, we will concentrate on a rather idealized basic state described by a single functional form. One parameter in this functional form controls the degree of downstream variation which ranges from no variation (i.e., parallel flow) to a configuration where, to the east and west of a strong jet centered at a particular longitude, there is diffluence leading to weak, almost constant and almost parallel flow. Such a flow facilitates a different analysis of the effect of downstream variation than flows consisting of a planetary wave superimposed on a zonal jet. Another parameter controls the degree of asymmetric cross-stream variation. We design this affect to simply skew the jet profile. Section 3.2 provides additional detail on the basic state. We then focus primarily on a comparison of the eigenvalue and time integration approaches described above, although we comment on the applicability of the spatial growth rate concept. Furthermore, we document the sensitivity of the results to changes in

the basic state, concentrating on cases of fundamental geophysical fluid dynamics interest. Our results show that one of the main results of Peng and Williams (1986); namely, that the maximum amplitude of the unstable perturbation occurs *downstream* from the region with maximum shear, can be reproduced without directly invoking the techniques common to the spatial growth rate approach. The eigenvalue and time integration approaches compare favorably. Both indicate that as downstream variation is increased, i.e., as the region containing a strong jet becomes smaller and more localized, the growth rate decreases, but the frequency remains approximately the same. At the same time the scale of the instability decreases. As increasing asymmetric cross-stream variation is introduced into parallel flow, the growth rate and frequency are relatively unaffected but the structure changes significantly with larger amplitude and stronger tilt on the side of the jet with the strongest shear. Cases with both downstream and asymmetric cross- stream variation yield instabilities that can be understood as a combination of the results arising from considering each individual type of variation by itself. A preliminary non–linear calculation illustrates a splitting of the disturbances with the high centers moving to the north and the low centers to the south. The disturbances also increase in scale and stabilize the mean flow without removing the x–variation. We see these results as a stepping stone to help us understand more complicated cases in the real atmosphere.

Following Frederikson, we believe that these instability calculations have some bearing on the problem of blocking. We hypothesize that blocking is a manifestation of instability of the large scale flow. Whether a block forms may depend crucially on whether the basic state flow is favorable for instabilities with blocking characteristics. This study reports on preliminary work documenting the sensitivity of barotropic instabilities to basic state structure. Suggestions for additional work relating instabilities to blocking is given in the final section.

In Section 3.2 the model and basic state are described and a prototype calculation is made in the spirit of Tupaz et.al. (1978) and Peng and Williams (1986). Sections 3.3 and 3.4 employ the eigenvalue and time integration approaches respectively, to the case of downstream variation. The asymmetric cross-stream variation is introduced in Section

3.5. The preliminary non– linear calculation is described in Section 3.6. Finally, Section 3.7 contains the summary and discussion.

3.2 Model Development and a Prototype Calculation

3.2.1 Description of model

We approach the problem using the simplest possible system that can describe barotropic instability: the non-divergent barotropic vorticity equation. This may be written on a beta-plane as

$$\varsigma_t + J(\psi, \varsigma) + \beta\psi_x = F \tag{2.1a}$$

$$\nabla^2\psi = \varsigma \tag{2.1b}$$

where ψ is a streamfunction for the non-divergent flow (i.e., $u = -\psi_y, v = \psi_x$), ς is the relative vorticity, β is the (constant) northward derivative of the coriolis parameter and F is a forcing term. We assume the flow takes place in the domain $0 \le x \le L_x,\ 0 \le y \le L_y$ and put walls $y = 0, L_y$ so that we have a beta-channel. Periodicity is required in x. At the north and south walls, the normal velocity $v = \psi_x$ vanishes, implying

$$\psi(x, 0, t) = \psi_S(t)\ , \tag{2.2a}$$

$$\psi(x, L_y, t) = \psi_N(t)\ . \tag{2.2b}$$

Now we separate the streamfunction, vorticity and forcing by writing

$$\psi(x, y, t) = \bar{\psi}(x, y) + \psi'(x, y, t), \tag{2.3a}$$

$$\varsigma(x, y, t) = \bar{\varsigma}(x, y) + \varsigma'(x, y, t), \tag{2.3b}$$

$$F(x, y, t) = \bar{F}(x, y) + F'(x, y, t), \tag{2.3c}$$

where $\bar{\psi}(x,y)$ and $\bar{\varsigma}(x,y)$ are specified functions independent of time. Substituting into (2.1a) yields

$$\varsigma'_t + J(\psi',\bar{\varsigma}) + J(\bar{\psi},\varsigma') + J(\bar{\psi},\bar{\varsigma}) \tag{2.4}$$

$$+J(\psi',\varsigma') + \beta\psi'_x + \beta\bar{\psi}_x = \bar{F} + F'$$

Following Pedlosky (1979) and Frederikson(1978a, 1979b) we assume that, in the absence of perturbations, the basic flow $\bar{\psi}$ satisfies the governing equation. Thus $\bar{F}$ is just the forcing needed so that

$$J(\bar{\psi},\bar{\varsigma}) + \beta\bar{\psi}_x = \bar{F}. \tag{2.5}$$

In certain special cases, such as purely zonal flow $\bar{\psi} = -\bar{u}y$, or if $\bar{\psi}$ is the streamfunction corresponding to a stationary Rossby wave, $\bar{F}$ will be zero; in general, $\bar{F}$ is non-zero. This forcing can be thought of as the topographical and land-sea contrasts which help maintain the time-averaged flow. Of course, this is a simplification: in the real atmosphere the time-averaged flow is maintained not only by topography and land-sea contrasts but by the eddies as well–an effect neglected here.

Applying (2.5) to (2.4) and linearizing the result gives

$$\varsigma'_t + J(\psi',\bar{\varsigma}) + J(\bar{\psi},\varsigma') + \beta\psi'_x = F', \tag{2.6a}$$

$$\nabla^2\psi' = \varsigma'. \tag{2.6b}$$

We require $\psi_S(t)$ and $\psi_N(t)$ to be zero for the perturbation flow (but not for the basic state) so that the boundary conditions are

$$\psi'(x,0,t) = 0, \tag{2.7a}$$

$$\psi'(x,L_y,t) = 0. \tag{2.7b}$$

Eqs (2.6) and (2.7) define the basic model from which all our calculations are made.

3.2.2 The basic state

Our philosophy in specifying a basic state is to define *one functional form* for $\bar{\psi}$ that can produce simple downstream *and* asymmetric cross-stream variations by allowing certain parameters to change their values. In this way the number of seemingly plausible experiments is reduced and all the experiments become connected by their relationship to a single expression for the basic state. This makes sensitivity studies more meaningful and helps in the interpretation of results. For example, in Section 3.5 an experiment containing both downstream and asymmetric cross-stream variation is discussed. The instability growing on that basic state has a particular structure. That both types of basic state variations arise from parameter changes in a single expression for $\bar{\psi}$ enables us to say with more confidence that some characteristics of the structure may be explained by the downstream variation while others are explained by the asymmetric cross-stream variation.

We define our basic state by the modified Bickley jet

$$\bar{\psi}(x,y) = -y_{00}u_{00}r\,A(x)\int_0^y \operatorname{sech}^2\left(\frac{y'+\alpha(y')-y_c}{y_0(x)}\right)dy' - \hat{u}y \tag{2.8}$$

where

$$r = \int_0^{L_y} \operatorname{sech}^2\left(\frac{y+\alpha(y)-y_c}{y_{00}}\right)dy \Bigg/ \int_0^{L_y} \operatorname{sech}^2\left(\frac{y-y_c}{y_{00}}\right)dy\ , \tag{2.9}$$

$$A(x) = 2\tanh(y_c/y_{00}) \Bigg/ \int_0^{L_y} \operatorname{sech}^2\left(\frac{y+\alpha(y)-y_c}{y_0(x)}\right)dy\ , \tag{2.10}$$

$y_c = L_y/2$, $\hat{u}$, y_{00}, u_{00} are constants, and $y_0(x)$ and $\alpha(y)$ are specified functions. This is an adaptation of the expression used by Tupaz *et al.* (1978). Note first that the boundary conditions requiring $\bar{\psi}$ to be independent of x at $y = 0$ and $y = L_y$ are satisfied.

The "half-width" y_0 varies with x according to

$$y_0(x) = y_{00}\left[\frac{1+a\cos 2\pi x/L_x}{1-a}\right]. \tag{2.11}$$

Thus the downstream variation is effected by changes in the non-dimensional parameter a. When $a = 0$, the half-width takes the constant value y_{00} and there is no downstream variation: the flow is parallel. For non-zero a, the half-width still takes the value y_{00} at the center of the channel ($x = L_x/2$), but decreases to the east and west, producing a simple form of downstream variation. A contour plot of $\bar{\psi}$ for $a = 0.3$ is shown in Fig. 3.1. Three profiles of $\bar{u}$ at different values of x corresponding to this value of a are shown in Fig. 3.2. This basic state is intended to be a crude representation of the observed wintertime flow which exhibits similar patterns of confluence and diffluence to the west and east of jet regions occurring off the east coast of the continents (Fig. 3.3). Experiment has shown that a in the range $0 \leq a \leq 1/2$ allows for reasonable sensitivity studies.

The arbitrary function $\alpha(y)$, which we define as

$$\alpha(y) = y_c(y/y_c - 1)^2 e^{-\left(\frac{y-y_c}{by_c}\right)^2} \tag{2.12}$$

allows for asymmetric cross-stream variation. The non-dimensional parameter b determines the degree of variation. When b is very small, $\alpha(y)$ approaches zero and the flow is symmetric about $y = y_c$. For larger $b's$ the flow becomes asymmetric. Several profiles of $\bar{u}$ for different values of b are shown in Fig. 3.4. Experiment has shown that b in the range $0 < b \leq 1.25$ allows for reasonable sensitivity studies.

The parameters u_{00} and r are best understood by looking at the expression for $\bar{u}(x, y)$ given by

$$\bar{u}(x, y) = -\bar{\psi}_y = y_{00}u_{00}rA(x)\text{sech}^2\left(\frac{y + \alpha(y) - y_c}{y_0(x)}\right) + \hat{u} \tag{2.13}$$

From this it is evident that u_{00} is the maximum velocity (not including the constant flow $\hat{u}$) in the channel. This maximum occurs at $x = L_x/2, y = y_c$. The parameter r is introduced so that regardless of whether asymmetric variation about y_c is present, u_{00} remains the maximum eastward velocity.

In the experiments reported on in this paper, we adopt the following physically reasonable values: $y_{00} = 800km, u_{00} = 60ms^{-1}, \hat{u} = 10ms^{-1}$.

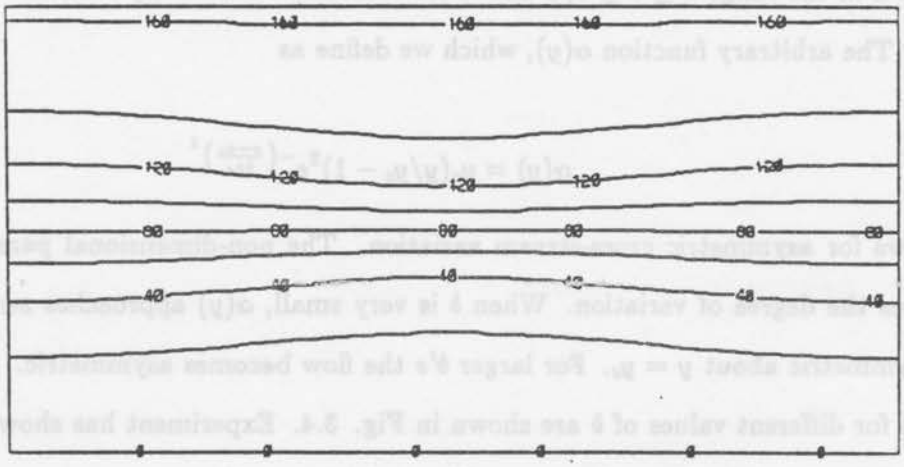

Figure 3.1: Contours of the basic state streamfunction for $a = 0.3$.

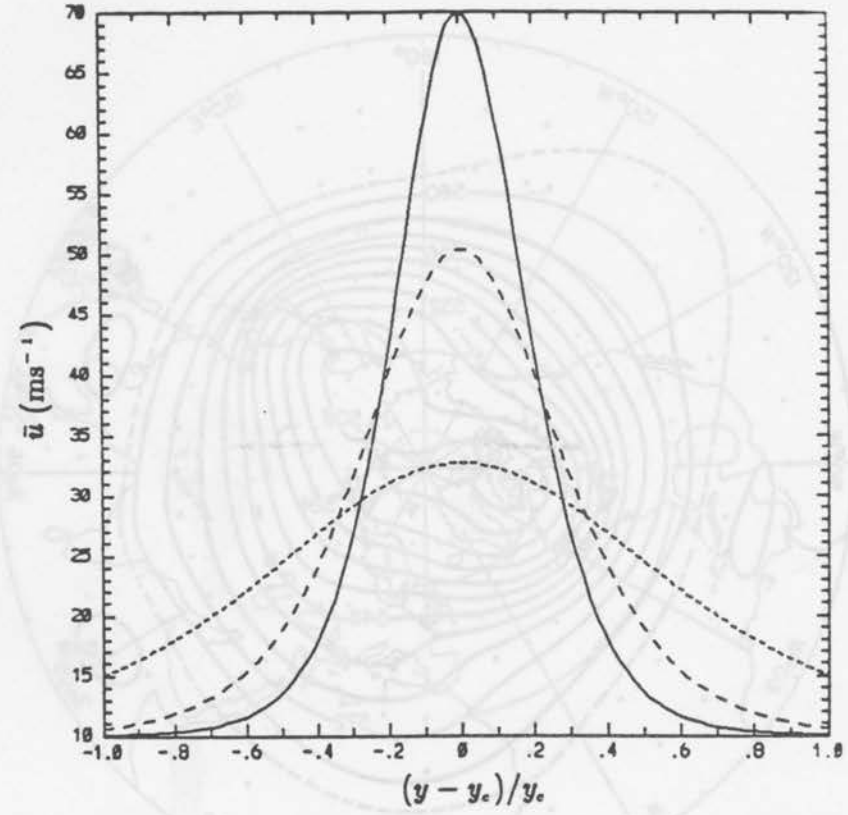

Figure 3.2: Profiles of $\bar{u}$ as a function of $(y - y_c)/y_c$ for the basic state of Fig. 3.1 at $x = L_x/2$ (solid line), $x = 2L_x/3$ (long–dashed line) and $x = L_x$ (short–dashed line).

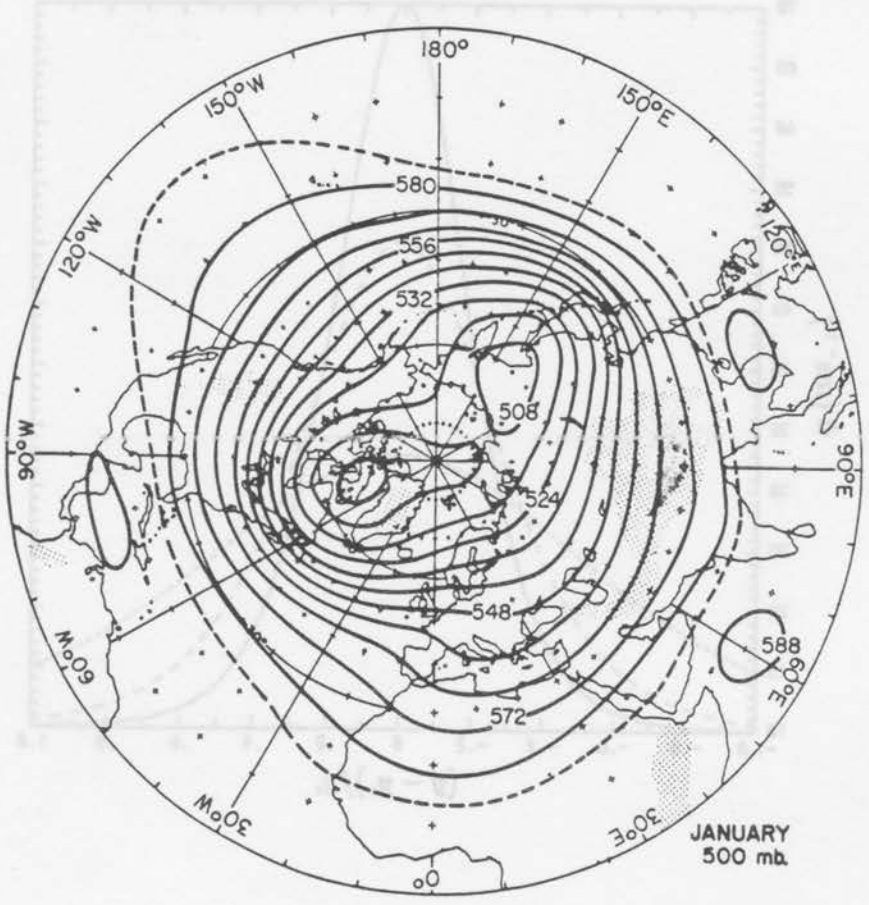

Figure 3.3: Time mean 500 mb contours in January. Heights are shown in tens of meters. (From Palmén and Newton, 1969).

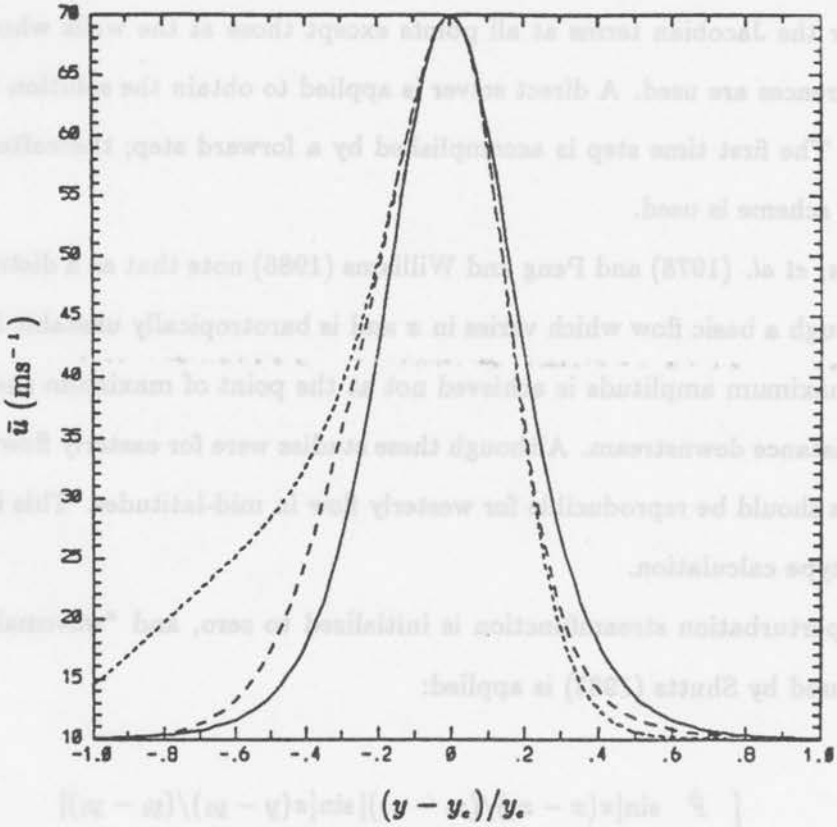

Figure 3.4: The basic state zonal wind $\bar{u}$ as a function of $(y - y_c)/y_c$ for values of the cross–stream asymmetry parameter b of $b = 0$ (solid line), $b = 0.5$ (long–dashed line), and $b = 1.25$ (short–dashed line).

3.2.3 A prototype calculation

Here we describe a simple, time dependent calculation along the lines of Tupaz, *et al.* (1978)–the numerical study that preceded Peng and Williams' (1986) analytical work. The purpose of this prototype calculation is to elucidate, with an easily understood simulation, some fundamental instability characteristics of flows with x variation. Later sections will determine and describe the instabilities more rigorously; the idea here is to obtain an intuitive feel for the results using a rather naive approach.

The basic model is discretized in space with finite differences using Arakawa's (1966) scheme for the Jacobian terms at all points except those at the walls where simple one-sided differences are used. A direct solver is applied to obtain the solution to the Poisson equation. The first time step is accomplished by a forward step; thereafter, the Adams-Bashforth scheme is used.

Tupaz, *et al.* (1978) and Peng and Williams (1986) note that as a disturbance propagates through a basic flow which varies in x and is barotropically unstable for some range of x, its maximum amplitude is achieved not at the point of maximum shear, but rather at some distance downstream. Although these studies were for easterly flow in the tropics, the results should be reproducible for westerly flow in mid-latitudes. This is the object of our prototype calculation.

The perturbation streamfunction is initialized to zero, and "wavemaker" forcing of the kind used by Shutts (1983) is applied:

$$F'(x,y,t) = \begin{cases} \hat{F} \quad \sin[\pi(x-x_\ell)/(x_r-x_\ell)]\sin[\pi(y-y_b)/(y_t-y_b)] & \\ \times \quad \cos[3\pi(x-x_\ell-\bar{u}t)/(x_r-x_\ell)], & x_\ell \le x \le x_r \\ & y_b \le y \le y_t \\ 0, & otherwise \end{cases} \tag{2.14}$$

The values x_ℓ, x_r, y_b and y_t define the spatial extent of the forcing region, while $\hat{F}$ determines the forcing amplitude. We allow one wave to emerge from the wavemaker and

follow it as it propagates through a mean flow defined by (2.8). We use a grid spacing of 290km and a time step of 1200s.

The instantaneous structure of ψ' at several different times during the integration is shown in Fig. 3.5. Contours of the basic state are also shown. The parameter a is chosen so that the necessary condition for barotropic instability, applied locally rather than to the zonally averaged flow, is satisfied in the center of the channel but not at the eastern and western ends. Profiles of $\beta - \bar{u}_{yy}$ at various values of x are depicted in Fig. 3.6. At $x = L_x/2$ (the center of the channel), $\beta - \bar{u}_{yy}$ changes sign and so satisfies the necessary condition for instability. East of the center, at $x = 2L_x/3$, the profile just satisfies the condition and there is no change of sign at the ends of the channel. We are not suggesting that there is any rigorous theoretical support for a local application of the classical condition. We have not developed such a theory nor are we aware of one; we use the theory simply as a guide for our explanation of the results. The wave emanating from the wavemaker propagates through the mean flow, increasing its amplitude as it encounters the barotropically unstable part of the flow. A trajectory of the maximum amplitude of ψ' along the line $y = y_c$ versus the value of x where that maximum occurs is shown in Fig. 3.7. It is clearly seen that the streamfunction reaches its maximum amplitude well downstream from the point of maximum shear – a result qualitatively reproduced for different wavelengths emanating from the wavemaker. This result has a plausible explanation. When the wave encounters the barotropically unstable part of the jet, it begins to grow, tilting opposite to the shear as shown in Fig. 3.5. (Before that time, the tilt of the wave is in the same sense as the shear.) As it moves past the point of maximum shear, it may still be encountering flow that is barotropically unstable and hence its amplitude may still be increasing. When it eventually moves out of the unstable region, it is no longer growing by extracting energy from the mean flow and may disperse, decay, or both, depending on the physics in the problem. At this point it begins once more to tilt in the same sense as the shear and its amplitude begins to decrease. The maximum amplitude occurs east of the point of maximum shear. This essentially happens because the wave propagates.

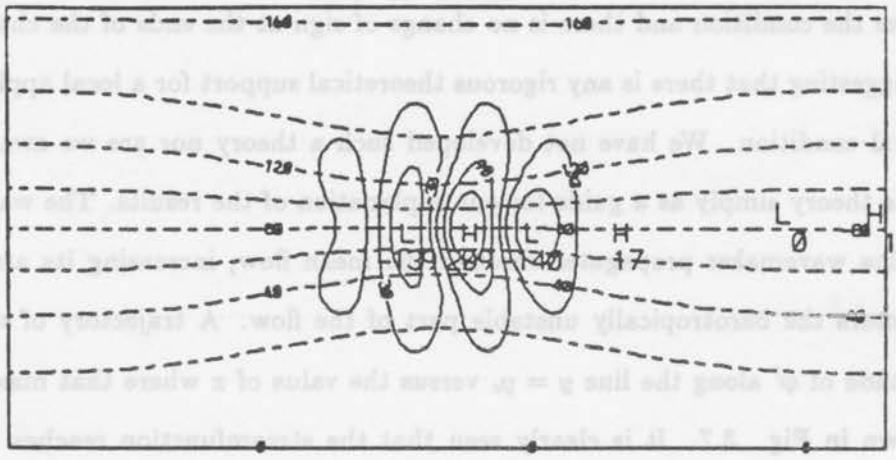

Figure 3.5: Contour plots of the instantaneous structure of ψ' (solid lines) from the prototype calculation at (a) 66.7 hours, (b) 100 hours and (c) 133.3 hours. Dashed lines are contours of the basic state.

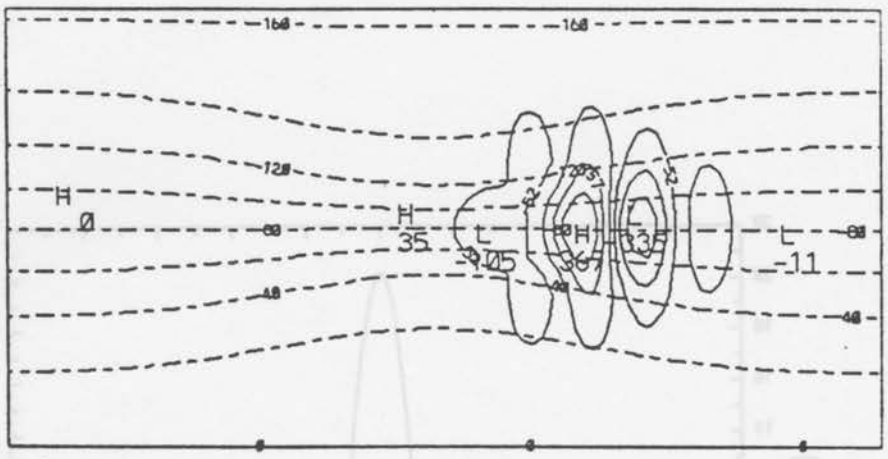

(b)

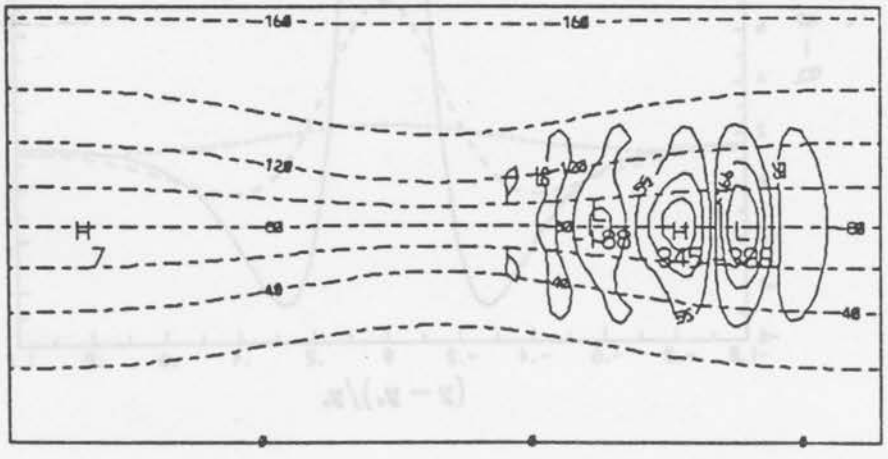

(c)

Figure 3.5: continued.

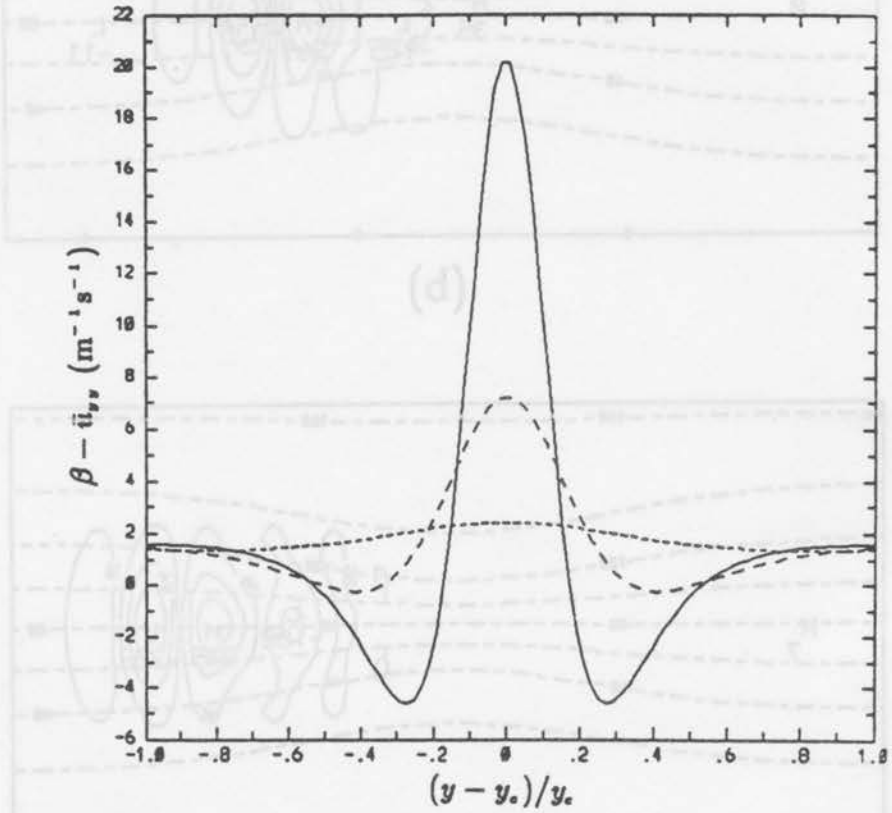

Figure 3.6: Profiles of $\beta - \bar{u}_{yy}$ as a function of $(y - y_c)/y_c$ for the basic state in Fig. 3.5 at $x = L_x/2$ (solid line), $x = 2L_x/3$ (long–dashed line) and $x = L_x$ (short–dashed line). Values of the ordinate are scaled by 10^{11}.

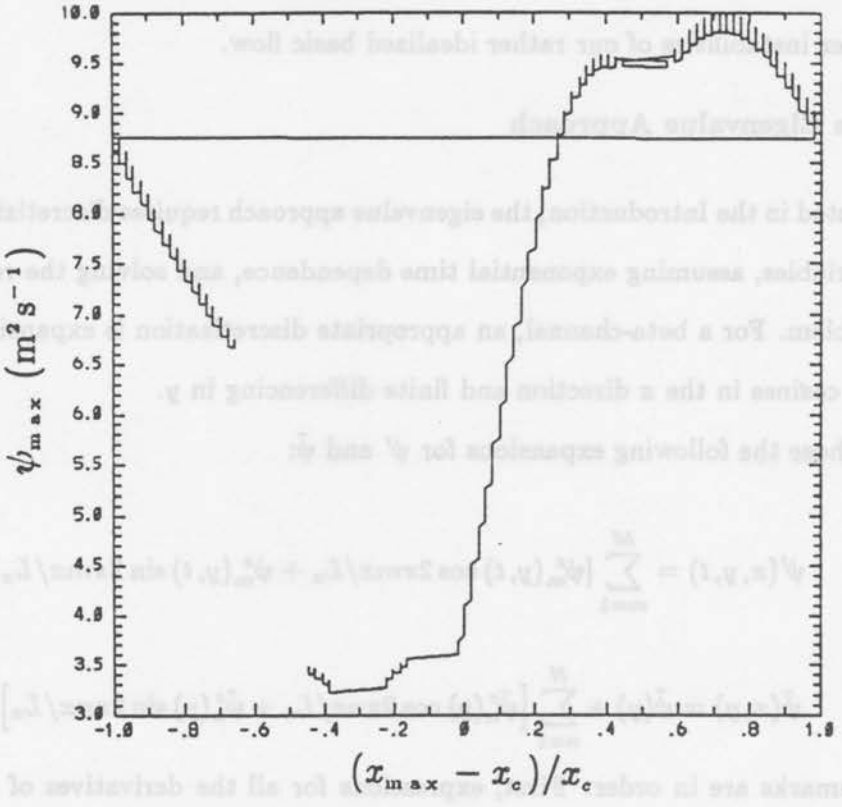

Figure 3.7: Trajectory of the maximum amplitude of ψ' along the line $y = y_c$ versus the value of x where that maximum occurred. The scale on the ordinate is relative; $x_c = L_x/2$. Wavemaker parameters are $x_1 = 8d, x_r = 25d, y_b = y_c - 8d, y_t = y_c + 8d$ where d is the grid spacing. The forcing amplitude $\hat{F}$ is 1.0×10^{-9}.

We have reproduced in a simple calculation one of the results of Tupaz, *et al.* (1978) and Peng and Williams (1986); namely, that a disturbance propagating through a flow with downstream variation that is barotropically unstable for some longitudinal band, achieves its maximum amplitude downstream from the region of maximum shear. Admittedly, this calculation is not very rigorous. It is intended only to give a feel for the behaviour of unstable disturbances propagating through basic states which vary in x. In the following sections we will use more general instability techniques to verify this result as well as to study other instabilities of our rather idealized basic flow.

3.3 The Eigenvalue Approach

As noted in the Introduction, the eigenvalue approach requires discretizing the perturbation variables, assuming exponential time dependence, and solving the resulting eigenvalue problem. For a beta-channel, an appropriate discretization is expansion in terms of sines and cosines in the x direction and finite differencing in y.

We chose the following expansions for ψ' and $\bar{\psi}$:

$$\psi'(x,y,t) = \sum_{m=1}^{M} \left[\psi_m^c(y,t)\cos 2\pi m x/L_x + \psi_m^s(y,t)\sin 2\pi m x/L_x\right], \qquad (3.1a)$$

$$\bar{\psi}(x,y) = \hat{\psi}(y) + \sum_{n=1}^{N} \left[\bar{\psi}_n^c(y)\cos 2\pi n x/L_x + \bar{\psi}_n^s(y)\sin 2\pi n x/L_x\right]. \qquad (3.1b)$$

Several remarks are in order. First, expressions for all the derivatives of and ψ' and $\bar{\psi}$ are obtained by differentiating these expressions. Derivatives in y are represented with finite differences. Second, the boundary conditions are enforced by the way in which the matrices for the eigenvalue problem are formed. Third, the expansion for ψ' does not contain any terms that are independent of x i.e., $m = 0$ terms. It is not clear, a *priori*, that neglecting such terms is correct when the basic state varies in x. We choose to use (3.1a) as it stands and justify it by noting that we are looking only for those solutions that have no part independent of x. There may indeed be other solutions, but we have not investigated them here. The solutions obtained in this way are physically reasonable

and interpretable and thus provide an a *posteriori* check on the appropriateness of the assumption.

The eigenvalue problem is obtained by substituting (3.1a,b) into (2.6) and applying the orthogonality conditions appropriate to Fourier series. The result may be formally written

$$\mathbf{A}\frac{d\mathbf{w}}{dt} = \mathbf{B}\mathbf{w}, \tag{3.2}$$

where $\mathbf{w}$ is an unknown vector function of time consisting of $\psi_m^c(y,t)$ and $\psi_m^s(y,t)$ for all values of m and for discrete values of y, and $\mathbf{A}$ and $\mathbf{B}$ are matrices whose elements depend on the coefficients of the basic state expansion (3.1b). More detail is provided in the Appendix . Systems like (3.2) have solutions of the form $e^{-i\sigma t}$ so we let $\mathbf{w} = \hat{\mathbf{w}}e^{-i\sigma t}$ yielding

$$-i\sigma\mathbf{A}\hat{\mathbf{w}} = \mathbf{B}\hat{\mathbf{w}}, \tag{3.3}$$

a generalized matrix eigenvalue problem. The eigenvalues σ and the eigenvectors $\hat{\mathbf{w}}$ are generally complex. The formulation described in the Appendix shows that the size of $\mathbf{A}$ and $\mathbf{B}$ is $2M(J-2)$ where J is the number of discrete y points in the channel. It is obvious that M and J do not have to become too large before significant storage is required. For example, if $M = J =$16, 401408 words are needed to store the matrices. Most eigenvalue routines require at least one additional work space of the same size. This pushes the memory requirements close to the limit of the CRAY-1 machine at NCAR (The National Center for Atmospheric Research). Fortunately, the CRAY X-MP has significantly larger memory capacity. But the point is made: resolution in the eigenvalue approach may be limited by computing technology. We solve (3.3) with a routine from the IMSL library. Once σ and $\hat{\mathbf{w}}$ are obtained, the coefficients as functions of time are known and the Fourier series (3.1a) can be summed to arrive at the perturbation streamfunction corresponding to a given eigenpair. The frequency and growth rate of the disturbance, given by the real and imaginary parts of the eigenvalue, respectively, can be tabulated, and the streamfunction plotted at any given time.

We have made several calculations using the eigenvalue approach with the basic state defined by (2.8). In this section we concentrate on symmetric basic state flows with downstream variation. Asymmetric flows with and without downstream variation are treated in Section 3.5. The Fourier expansion (3.1a) is truncated at $M = 12$ and 24 points are used in y. The expansion for the basic state is truncated at $N = 20$ with 24 points in y. Figure 3.8 shows the most unstable eigenfunction, superimposed on contours of the basic state, when $a = 0.3$. The highs and lows in the disturbance exchange with one another every half period, but the pattern of amplitude remains fixed in space so that one can think of waves propagating through a stationary envelope of amplitude. The eigenvalue associated with this eigenfunction is $(\sigma_r, \sigma_i) = (2.74 \times 10^{-5}, 1.67 \times 10^{-6})$, corresponding to an e-folding time of 6.9d and a period of 2.6d. The point of most interest to this study is that the maximum amplitude of the perturbation again occurs downstream from the region of maximum shear. Thus, one of the main results of Tupaz *et al.* (1978) and Peng and Williams (1986) has been reproduced from a different perspective. In fact, the eigenvalue approach is a clear example of the use of temporal growth rates, to use Peng and Williams' terminology, rather than spatial growth rate. Yet the result is the same and can be understood using their argument that the structure of the unstable disturbance lags in adjusting to the local instability characteristics. As for the prototype calculation, this essentially happens because the disturbance is propagating.

It would seem of fundamental geophysical fluid dynamics interest to document the sensitivity of the eigensolution to changes in the basic state, specifically, changes in the degree of downstream variation. Fig. 3.9 shows the eigenfunctions for four other values of a. Several observations can be made. When a is large and there is strong downstream variation, significant streamfunction amplitude is concentrated in a relatively small area in the eastern half of the channel. For smaller a, corresponding to more nearly parallel flow, the area of significant streamfunction amplitude broadens and is distributed more equally throughout the length of the channel. In each case with $a > 0$, the maximum amplitude is again located downstream from the point of maximum shear. Only when $a = 0$ is the amplitude equally distributed. Subjectively, the scale of the instability is less

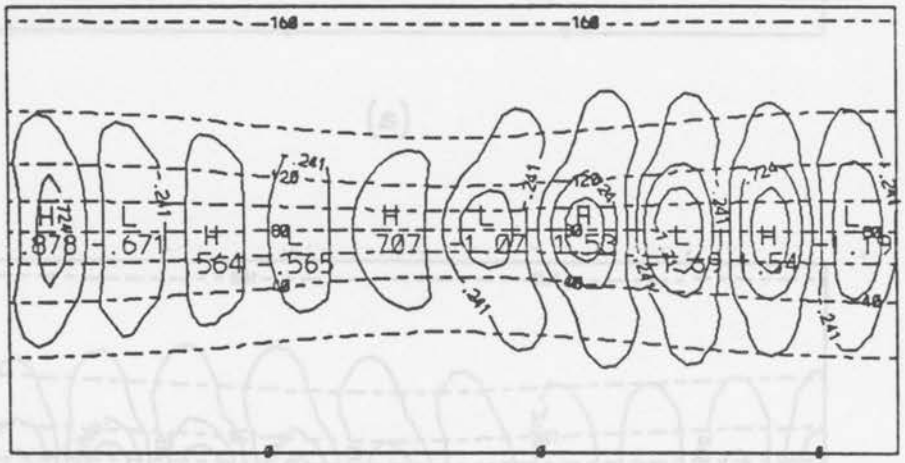

Figure 3.8: Streamfunction contours of the most unstable mode at $t = 0$ (solid lines) using the eigenvalue method when $a = 0.3$. Dashed lines are contours of the basic state.

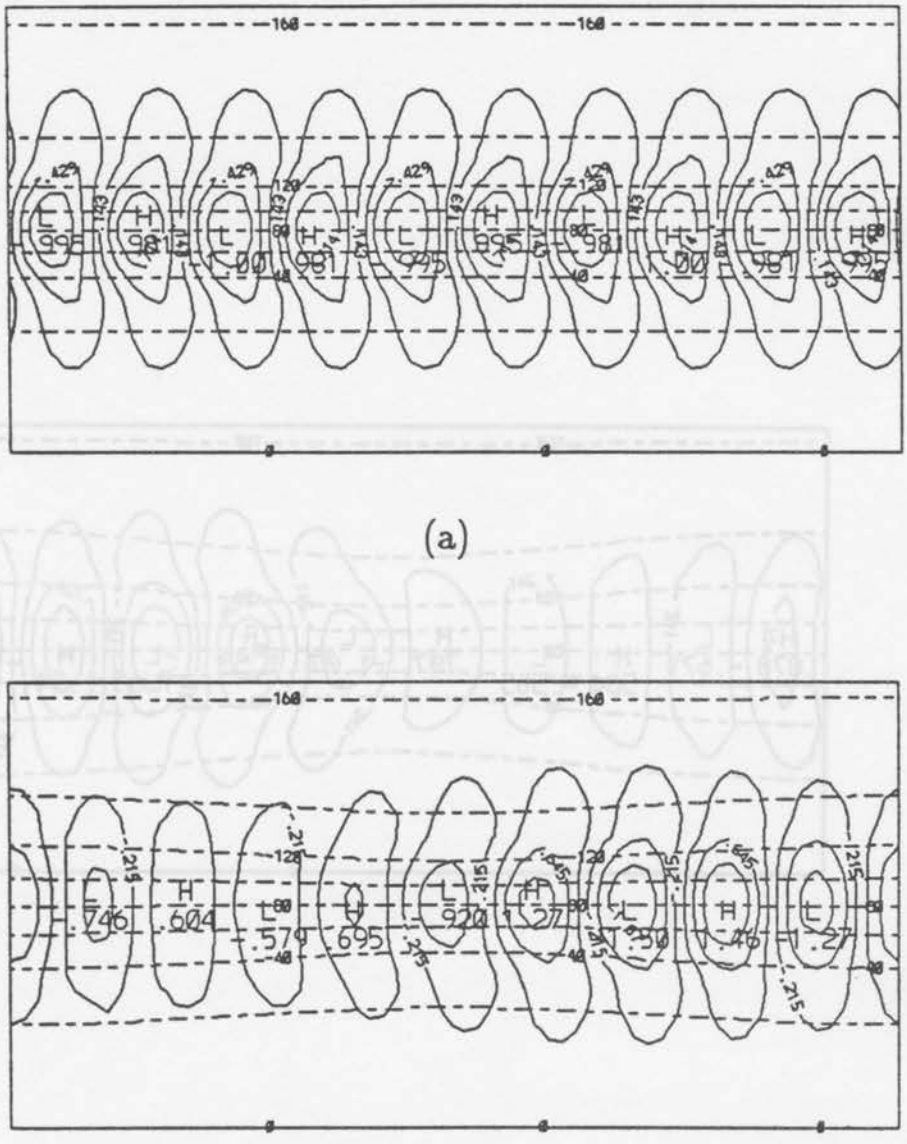

Figure 3.9: Streamfunction contours of the most unstable mode at $t = 0$ (solid lines) using the eigenvalue method when (a) $a = 0$, (b) $a = 0.2$, (c) $a = 0.4$, (d) $a = 0.5$. Dashed lines are contours of the basic state.

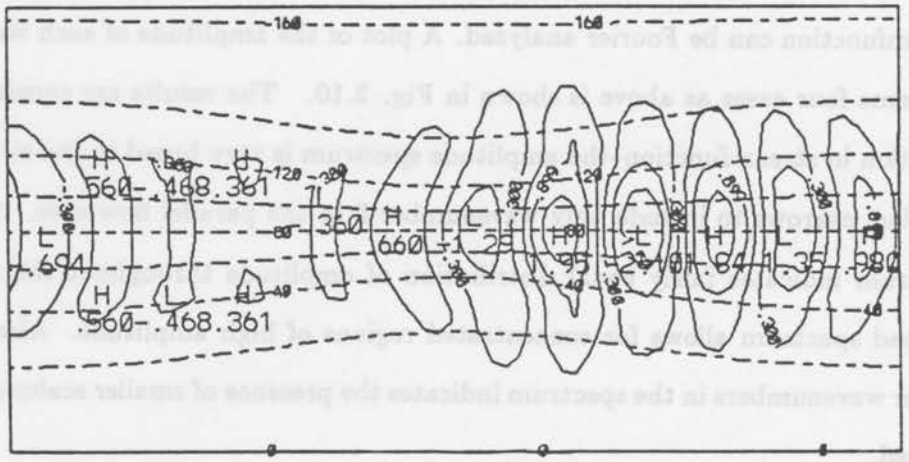

(c)

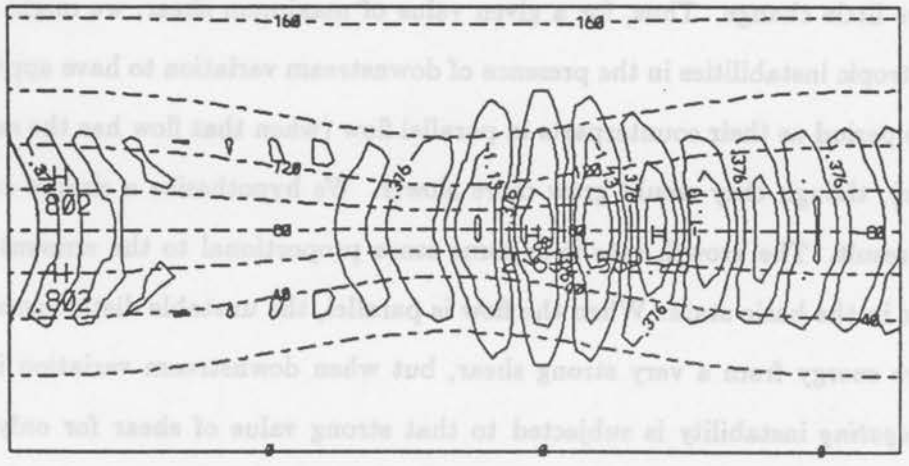

(d)

Figure 3.9: continued.

for stronger variation than for more nearly parallel flow. Finally, all the streamfunctions exhibit the correct tilt with y for barotropic instability in the unstable regions, but show little or no tilt outside those regions.

Along the line $y = y_c$ passing through the center of the channel, the disturbance streamfunction can be Fourier analyzed. A plot of the amplitude of each wavenumber for the same four cases as above is shown in Fig. 3.10. The results are consistent with the variation in streamfunction–the amplitude spectrum is very broad in the strongly varying case but narrows to include only wavenumber 5 in the parallel flow case. A very narrow spectrum indicates fairly equal distribution of amplitude throughout the channel while a broad spectrum allows for concentrated regions of high amplitude. Also, inclusion of higher wavenumbers in the spectrum indicates the presence of smaller scales as subjectively noticed.

Figure 3.11 depicts σ_r and σ_i as a function of a for the two most unstable modes. The growth rates corresponding to parallel flow are an order of magnitude faster than the growth rates corresponding to the most strongly varying case. However, the frequency shows little change. Thus, for a given value of maximum shear, we might expect actual barotropic instabilities in the presence of downstream variation to have approximately the same period as their counterparts in parallel flow (when that flow has the same maximum shear), though they would grow more slowly. We hypothesize a simple explanation for this result. The growth rate is in some sense proportional to the amount of latitudinal shear in the basic state. When the flow is parallel, the unstable disturbance continuously draws energy from a very strong shear, but when downstream variation is present, the *propagating* instability is subjected to that strong value of shear for only a finite time before moving into regions of lesser shear and hence into regions where it cannot grow as fast. Therefore, its growth rate is smaller. From Fig. 3.11 it seems as though the frequencies of the first two unstable modes are switched for $a = 0.5$. The frequencies would more naturally be opposite from what is plotted so that the most unstable mode always has the smaller value of σ_r. The growth rates for the first two modes are very similar, suggesting that some sort of numerical inaccuracy lead to the switching. To help

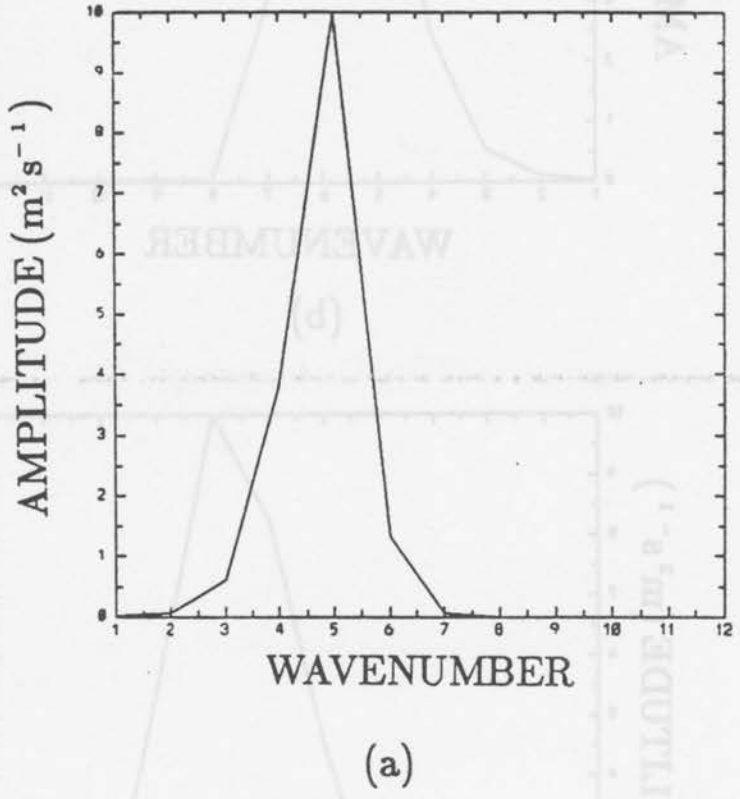

Figure 3.10: The amplitude of ψ' as a function of wavenumber for the unstable modes of Fig. 3.9; (a) $a = 0.2$, (b) $a = 0.4$, (c) $a = 0.5$. The scale of the ordinate is arbitrary.

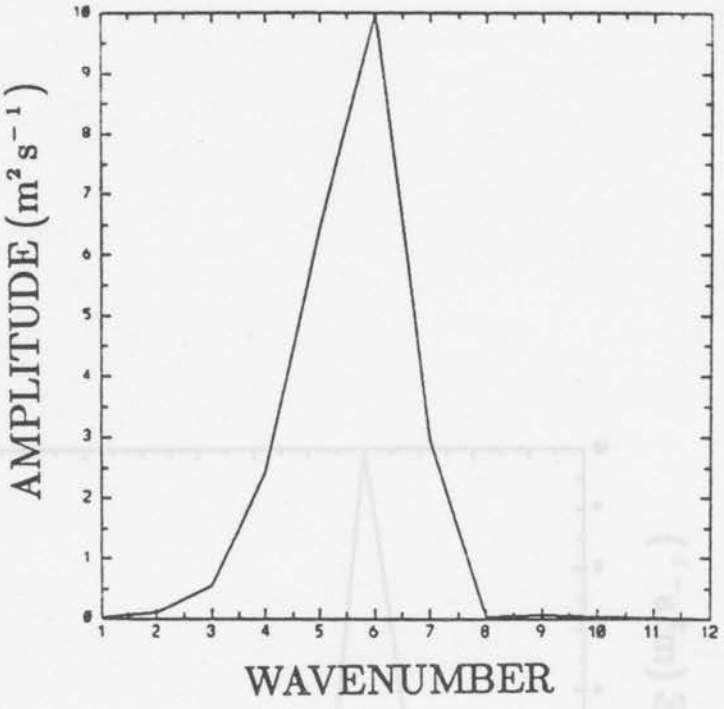

(b)

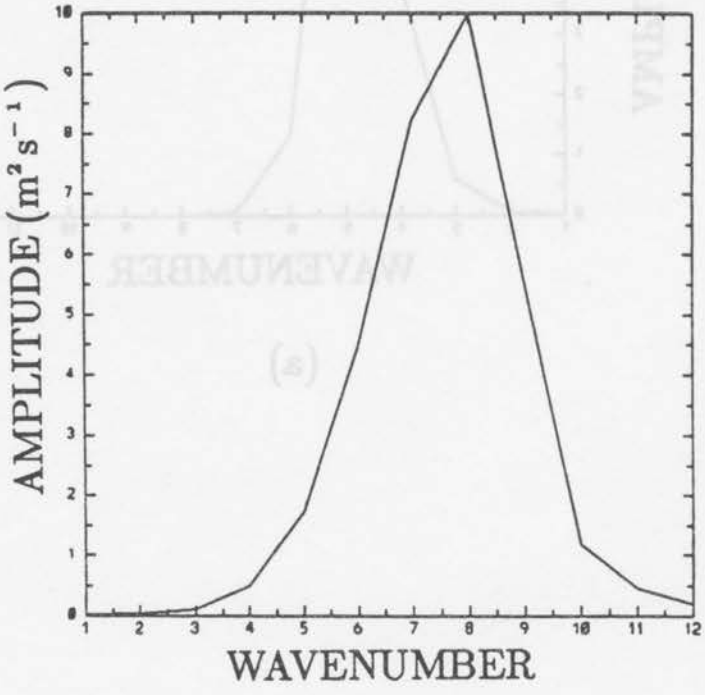

(c)

Figure 3.10: continued.

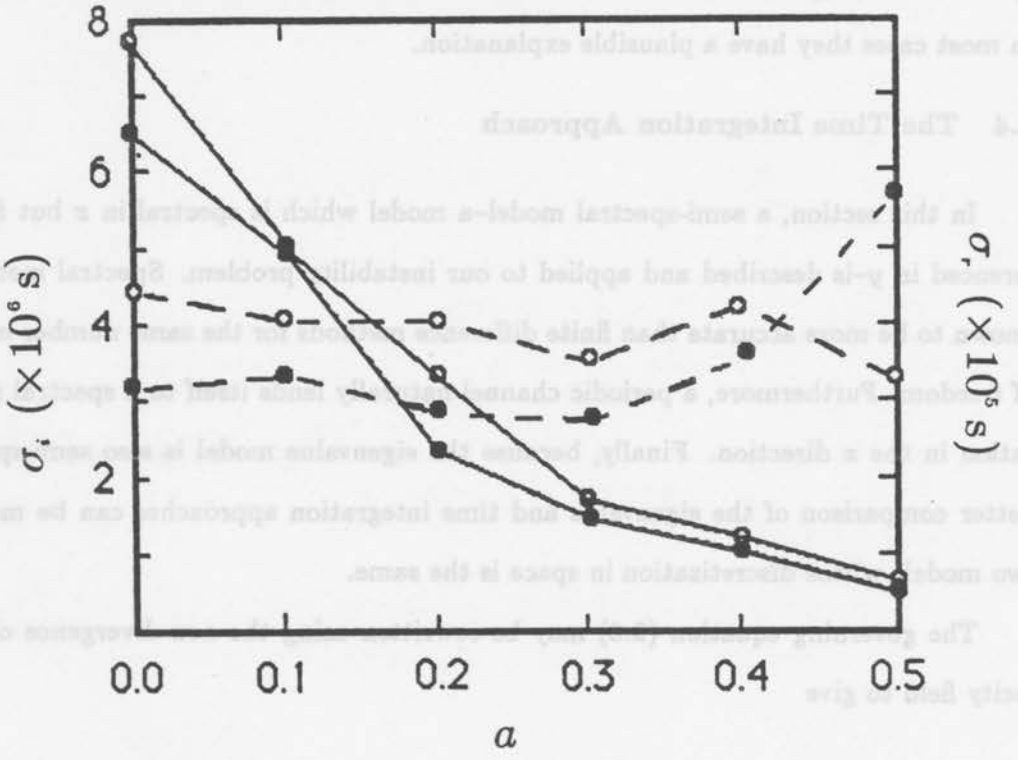

Figure 3.11: The growth rate σ_i (solid line) and frequency σ_r (dashed line) as a function of a for the eigenvalue method. Solid circles refer to the most unstable mode while open circles refer to the second most unstable mode. Note the different multiplicative factors for the growth rate and frequency scales.

understand this inconsistency, we show the second most unstable eigenfunction in Fig. 3.12 and its amplitude spectrum in Fig. 3.13. The structure also would more naturally be switched to get smoother changes as a function of a. Similar inconsistencies occur in other applications of both the eigenvalue and time integration methods. These problems may result from the geometry of our fluid system–a periodic beta-plane channel imposes a certain discreteness on the possible solutions that would not necessarily occur on the sphere. Annoying inconsistencies like these do not change the results we feel are important. In most cases they have a plausible explanation.

3.4 The Time Integration Approach

In this section, a semi-spectral model–a model which is spectral in x but finite differenced in y–is described and applied to our instability problem. Spectral methods are known to be more accurate than finite difference methods for the same number of degrees of freedom. Furthermore, a periodic channel naturally lends itself to a spectral representation in the x direction. Finally, because the eigenvalue model is also semi-spectral, a better comparison of the eigenvalue and time integration approaches can be made with two models whose discretization in space is the same.

The governing equation (2.6) may be rewritten using the non-divergence of the velocity field to give

$$\frac{\partial \varsigma'}{\partial t} = -\frac{\partial}{\partial x}(\bar{u}\varsigma') - \frac{\partial}{\partial x}(u'\bar{\varsigma}) - \frac{\partial}{\partial y}(\bar{v}\varsigma') - \frac{\partial}{\partial y}(v'\bar{\varsigma}) - \beta v'. \tag{4.1}$$

Now the basic state depends on x so that each Fourier mode can not be evaluated independently of the others as is the case for basic states that are functions of y only. Rather, the terms on the right hand side lead to coupling between Fourier modes. There are two ways to handle such interactions. The first is to follow the development of the eigenvalue approach: expand both the perturbation and the basic state variables in a Fourier series in x. The result is essentially an interaction coefficient model (Haltiner and Williams, 1980) and it has the major problem inherent in those models; namely, the need to evaluate interaction coefficients at each time step. This is known to be computationally

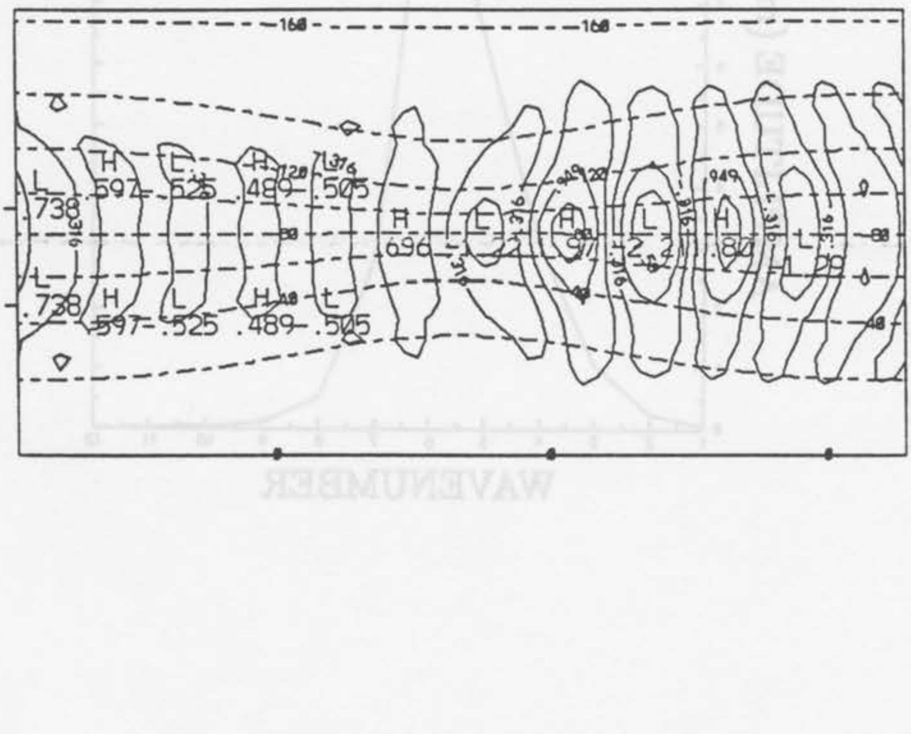

Figure 3.12: Streamfunction contours of the second most unstable mode at $t = 0$ (solid lines) for the eigenvalue method when $a = 0.5$. Dashed lines are contours of the basic state.

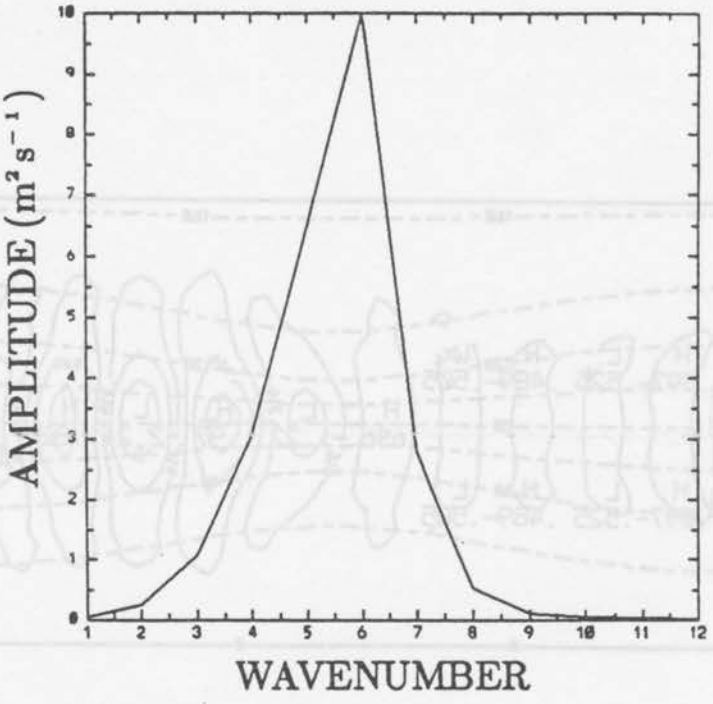

Figure 3.13: The amplitude of ψ' as a function of wavenumber for the unstable mode of Fig. 3.12.

prohibitive when the number of coefficients is large or the integration period is long. (Note that although the eigenvalue model is, and in fact needs to be, an interaction coefficient model, the usual problem does not appear because there is no integration in time.) The second way to handle terms that involve coupling is to apply the transform method (e.g., Orszag 1970). Instead of evaluating interaction coefficients at each time step, the terms in parenthesis on the right hand side are calculated on a grid in physical space and then transformed to spectral space where the derivatives are taken. Increased computational efficiency is made possible by the use of fast Fourier transforms. To determine instabilities using the time integration method, long integration times are often needed; therefore, we will use the transform method. More detail on the specific application of the method is provided below.

We define $A = \bar{u}\varsigma', B = \bar{v}\varsigma', C = u'\bar{\varsigma}, D = v'\bar{\varsigma}$ and then write

$$\begin{pmatrix} \psi'(x,y,t) \\ u'(x,y,t) \\ v'(x,y,t) \\ \varsigma'(x,y,t) \\ A(x,y,t) \end{pmatrix} = \sum_{m=1}^{M} \left[\begin{pmatrix} \psi_m^c(y,t) \\ u_m^c(y,t) \\ v_m^c(y,t) \\ \varsigma_m^c(y,t) \\ A_m^c(y,t) \end{pmatrix} \cos k_m x + \begin{pmatrix} \psi_m^s(y,t) \\ u_m^s(y,t) \\ v_m^s(y,t) \\ \varsigma_m^s(y,t) \\ A_m^s(y,t) \end{pmatrix} \sin k_m x \right], \tag{4.2}$$

where $k_m = 2\pi m/L_x$. Similar expansions are used for B, C and D. The coefficients in the u', v' and ς' expansions are obtained by differentiating the expansion for ψ'; e.g. $u_m^c = -\partial\psi_m^c/\partial y$ and $v_m^c = k_m\psi_m^s$. If the expansions are substituted into the governing equation (4.1) and the orthogonality of sines and cosines employed the result is

$$\frac{\partial \varsigma_m^c}{\partial t} = -k_m(A_m^s + C_m^s) - \frac{\partial B_m^c}{\partial y} - \frac{\partial D_m^c}{\partial y} - \beta v_m^c, \tag{4.3a}$$

$$\frac{\partial \varsigma_m^s}{\partial t} = k_m(A_m^c + C_m^c) - \frac{\partial B_m^s}{\partial y} - \frac{\partial D_m^s}{\partial y} - \beta v_m^s. \tag{4.3b}$$

The following computational procedure is then used to integrate the equations forward in time:

(i) assuming ψ_m^c and ψ_m^s are known at some time, determine $u_m^c, u_m^s, v_m^c, v_m^s, \varsigma_m^c, \varsigma_m^s$

(ii) transform to physical space to obtain u', v' and ζ'

(iii) multiply to determine A, B, C and D in physical space

(iv) transform to spectral space to obtain $A_m^c, A_m^s, B_m^c, B_m^s, C_m^c, C_m^s, D_m^c, D_m^s$

(v) evaluate the right hand side of (4.3)

(vi) predict new values of ζ_m^c and ζ_m^s using an Adam's Bashforth scheme (except for the first time step where a forward step is used)

(vii) determine new values of ψ_m^c and ζ_m^s from $(\partial^2/\partial y^2 - k_m^2)\psi_m^c = \zeta_m^c$ and $(\partial^2/\partial y^2 - k_m^2)\psi_m^s = \zeta_m^s$ subject to the boundary conditions $\psi_m^c = \psi_m^s = 0$ on the channel walls.

The initialization depends on the basic state. When downstream variation is present, the model is initialized with random perturbations of all wavenumbers and random structure in y. When the basic state flow is parallel, the model in initialized with one wavenumber having random structure in y. In the latter case, the most unstable mode is found by running the model several times, each time with a different initial wavenumber. The frequency and growth rate are extracted in the following way. At the beginning of the last 10 days of integration, the point where the perturbation streamfunction amplitude is maximum is calculated and the streamfunction at that point is saved at every time step for the remainder of the integration. The period, and hence the frequency, is then found by numerically finding the time between zero values of this discrete function. The average enstrophy in the channel is calculated at each time step. This quantity should grow exponentially once normal mode form is reached; the growth rate is found from the slope of the curve of the natural logarithm of average enstrophy vs. time using the last 10 days of data. The length of integration is determined on a trial and error basis: if normal mode form with exponential growth and constant frequency are not yet achieved for a given integration time, the calculation is repeated using a longer time. If in doubt, longer simulations are made. The length of time depended on the basic state. Sometimes 75 days was more than sufficient; in other cases more than 1000 days was needed. Additional comments on the method follow in the context of individual examples.

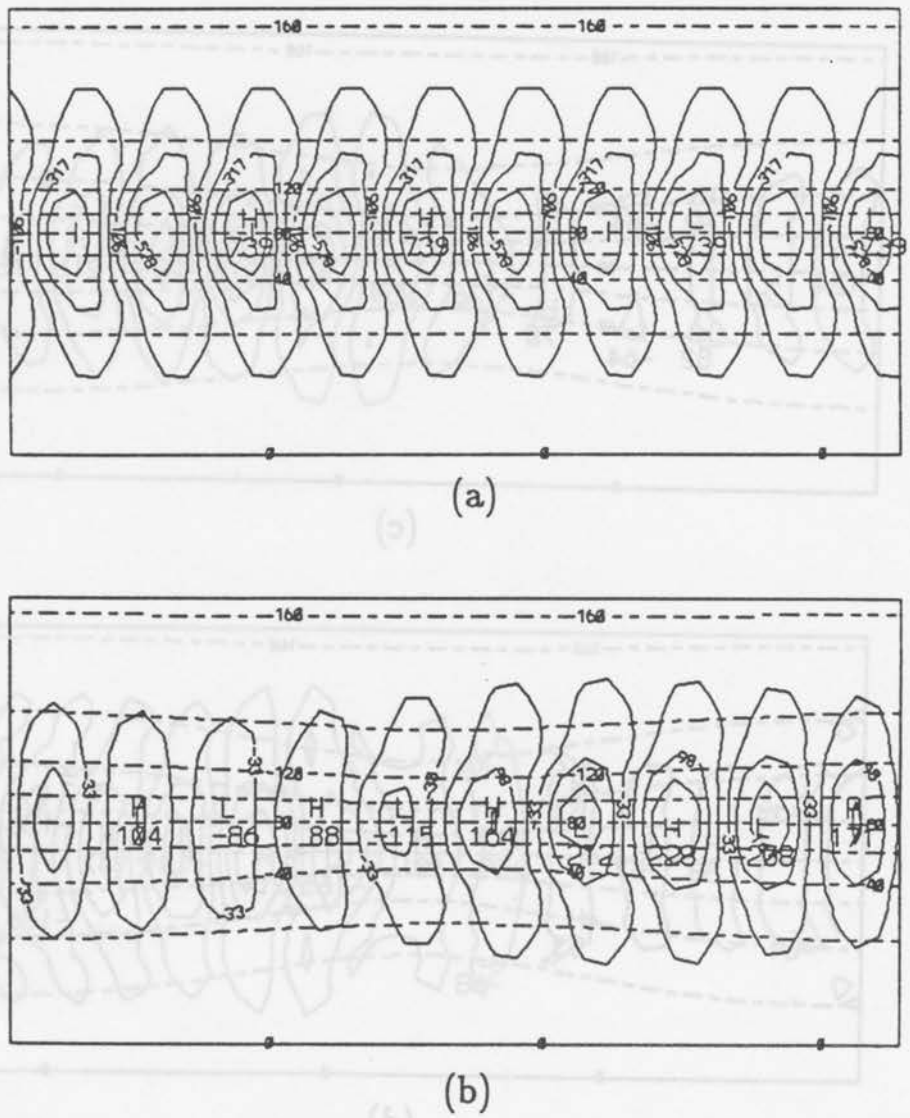

Figure 3.14: Streamfunction contours of the most unstable mode (solid lines) using the time integration method when (a) $a = 0$, (b) $a = 0.2$, (c) $a = 0.4$, (d) $a = 0.5$. Dashed lines are contours of the basic state.

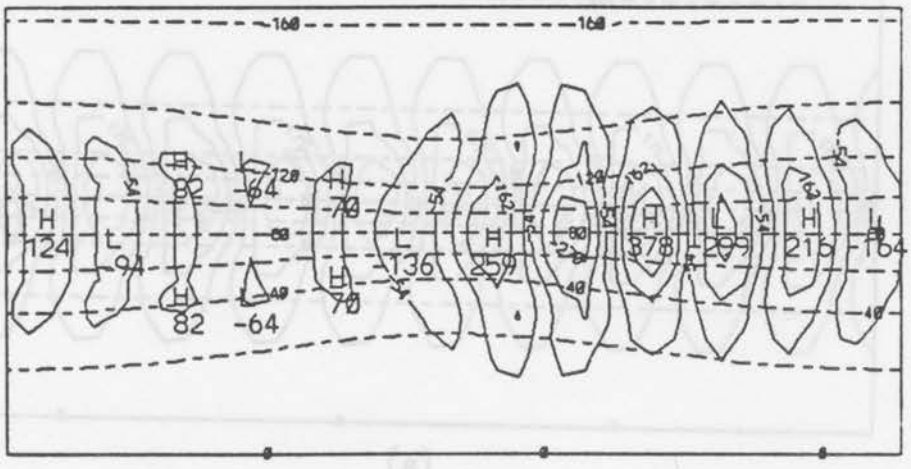

(c)

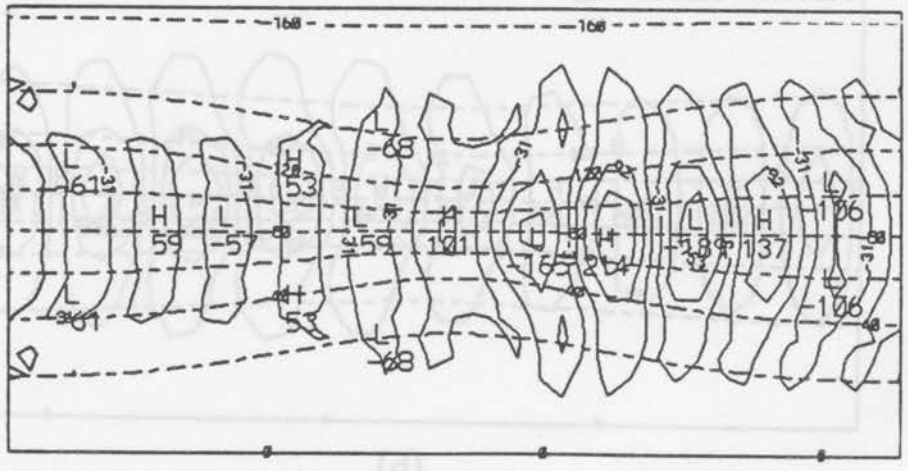

(d)

Figure 3.14: continued.

Figure 3.14 shows the structure of the most unstable mode for several values of a. The plots compare favorably with those obtained with the eigenvalue method. The same characteristics are exhibited; namely, the concentration of streamfunction amplitude downstream from the point of maximum shear, the decrease in the scale of the disturbance as the downstream variation is increased, and the tilt appropriate to barotropic instability. The wavenumber spectra corresponding to these structures are shown in Fig. 3.15. These also compare favorably with their counterparts in Fig. 3.10: the spectrum broadens as the degree of downstream variation is increased.

In the previous section, we mentioned that these instabilities may be thought of as waves propagating through a stationary envelope of amplitude. This is illustrated in Fig. 3.16, a Hovmöller diagram with time along the ordinate and x along the abscissa. Contours of ψ' at $y = y_c$ are plotted and the exponential growth rate has been taken out. The diagram clearly shows eastward propagating waves moving through an amplitude envelope that has a maximum downstream from the center of the channel. It provides a particularly clear picture of the propagating, oscillatory behavior of the instability.

The frequency and growth rate as a function of a are shown in Fig. 3.17 for the time integration method. Again, the values compare favorably with those obtained with the eigenvalue method: the growth rate is an order of magnitude larger for parallel flow than for strongly varying flow while the frequency remains approximately unchanged.

We need to comment one final time on the case $a = 0.5$. The time integration approach has picked out a frequency that closely matches that associated with the second most unstable mode of the eigenvalue method. The structure matches the second most unstable mode as well. Aside from the fact that the frequency curve as a function of a looks smoother in Fig. 3.17 than in Fig. 3.11, it is difficult to say which method is in error. It is worth noting that for this particular case we needed an integration time of 2000 days to obtain the normal mode solution while 800 days or less was sufficient for other cases. A long integration time was necessary for two reasons. First, the growth rate itself is slow, and second, the eigenvalue method indicates that there are two modes that are growing at very nearly the same rate. Consider two normal modes ψ_1 and ψ_2 with

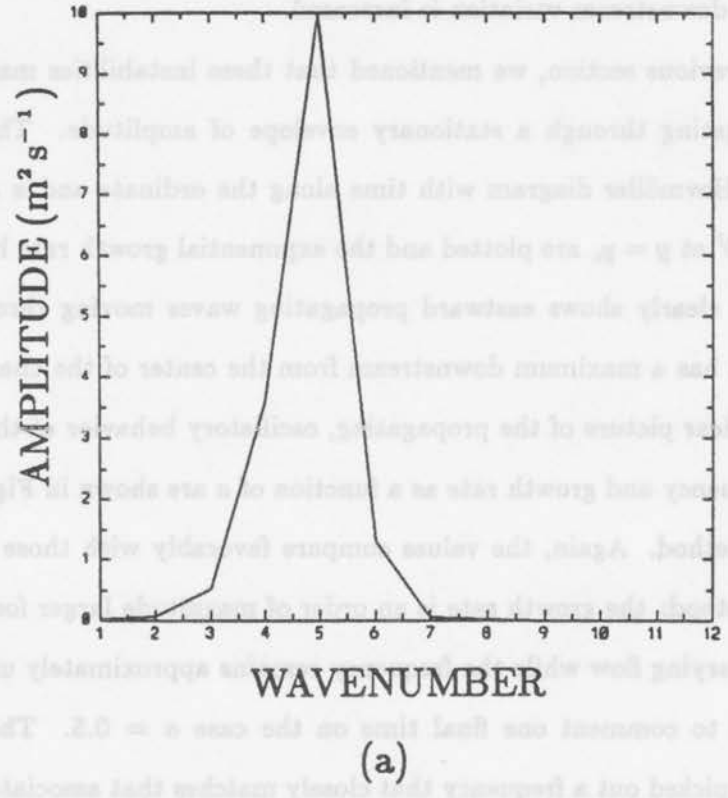

Figure 3.15: The amplitude of ψ' as a function of wavenumber for the unstable modes of Fig. 3.14; (a) $a = 0.2$, (b) $a = 0.4$, (c) $a = 0.5$.

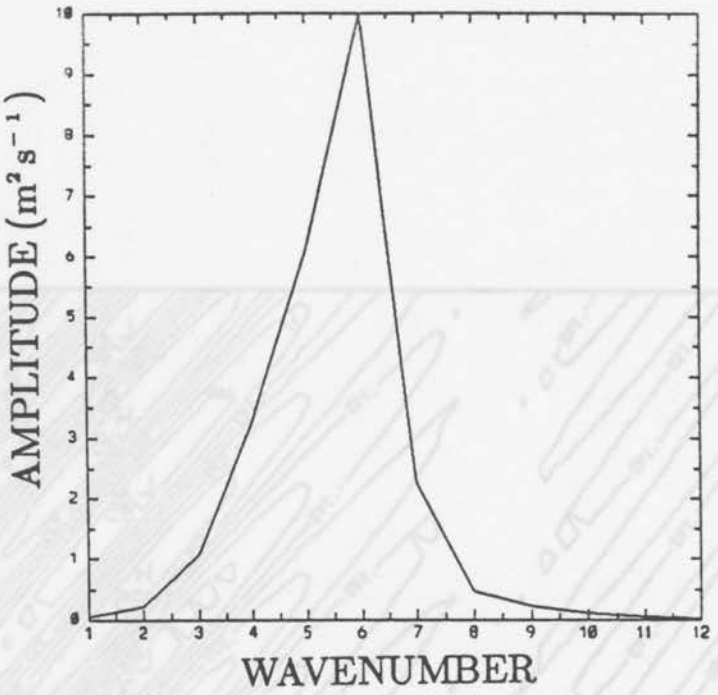

(b)

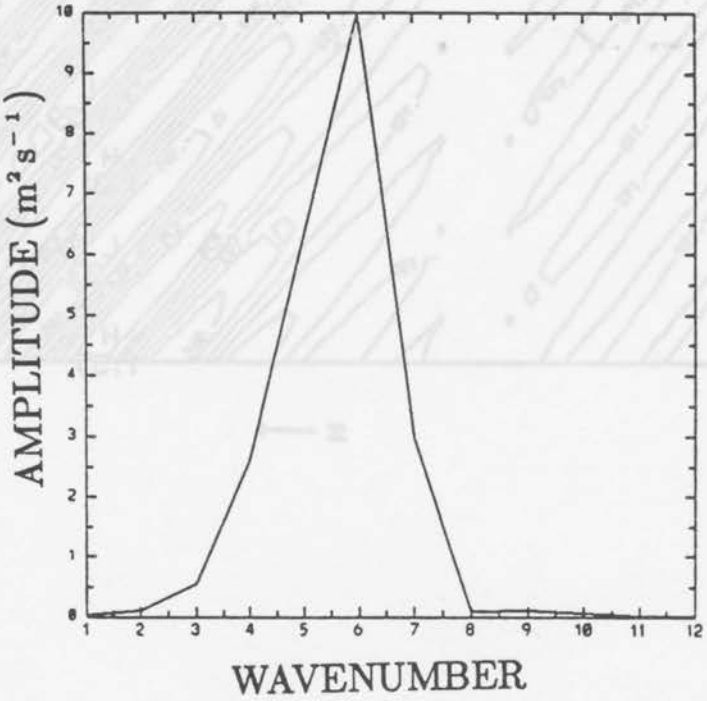

(c)

Figure 3.15: continued.

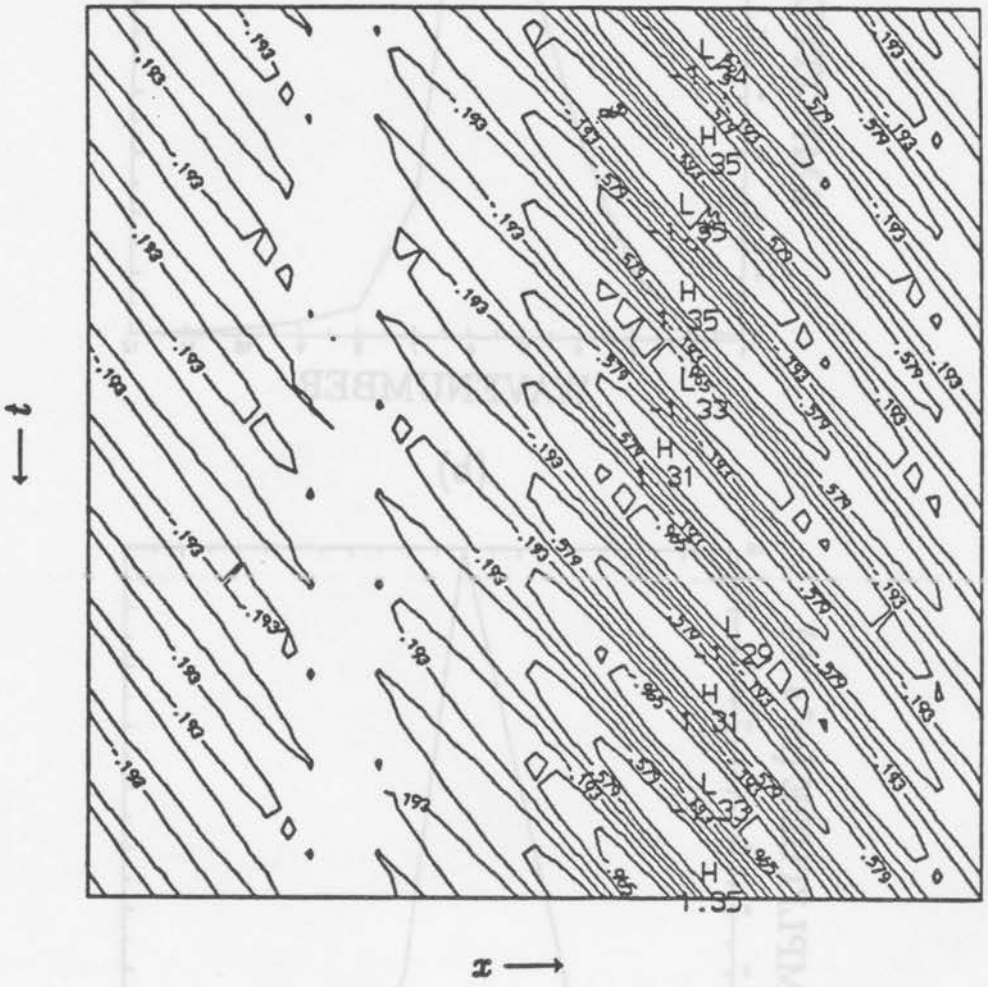

Figure 3.16: Contours in the (x,t) plane of streamfunction values along the line $y = y_c$ for the most unstable mode with $a = 0.4$ using the time integration method. The ordinate covers a span of 10 days, increasing downward. The exponential growth of the streamfunction has been taken out in order to more clearly see the oscillatory nature.

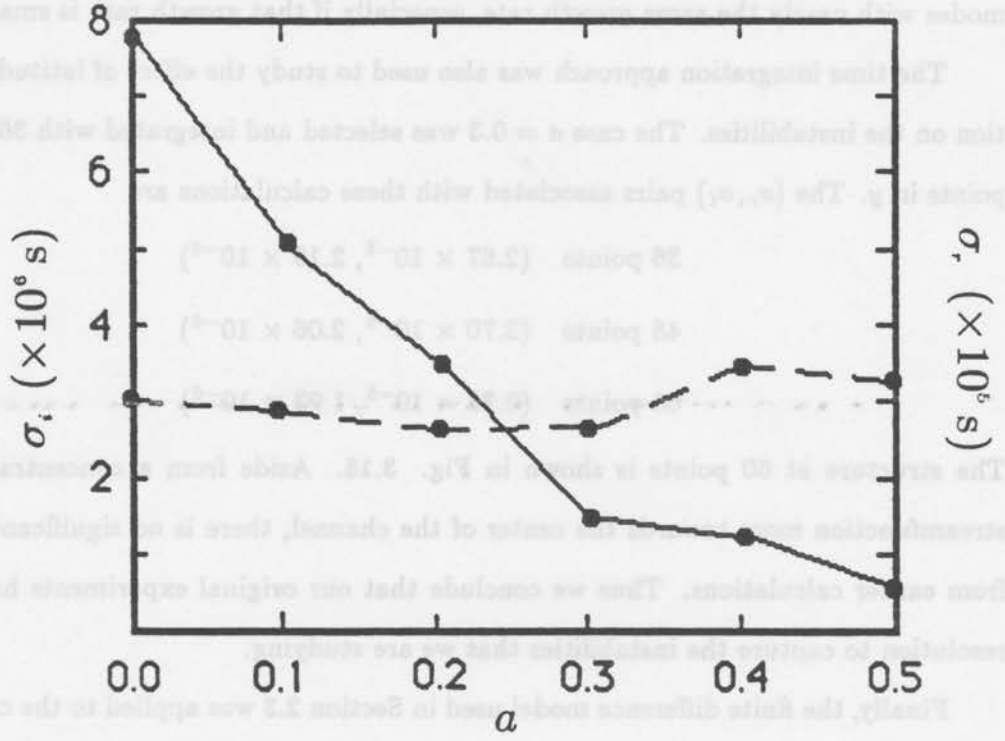

Figure 3.17: The growth rate σ_i (solid line) and the frequency σ_r (dashed line) of the most unstable mode as a function of a for the time integration method. Note the different multiplicative factors for the growth rate and frequency scales.

growth rates σ_1 and $\sigma_2(\sigma_1 > \sigma_2)$, respectively. Then the time t^* that it takes for ψ_1 to grow to a value 10 times larger than ψ_2 is

$$t^* = \frac{\ln 10}{\sigma_1 - \sigma_2}. \tag{4.4}$$

Using the values of σ from the eigenvalue method yields $t^* = 980$ days. This is certainly an example of one of the problems with the time integration method mentioned in the Introduction: the method may have difficulty converging when there are two or more modes with nearly the same growth rate, especially if that growth rate is small.

The time integration approach was also used to study the effect of latitudinal resolution on the instabilities. The case $a = 0.3$ was selected and integrated with 36, 48 and 60 points in y. The (σ_r, σ_i) pairs associated with these calculations are

$$\begin{aligned} &36 \text{ points} \quad (2.67 \times 10^{-5}, 2.13 \times 10^{-6}) \\ &48 \text{ points} \quad (2.70 \times 10^{-5}, 2.06 \times 10^{-6}) \\ &60 \text{ points} \quad (2.73 \times 10^{-5}, 1.93 \times 10^{-6}) \end{aligned}$$

The structure at 60 points is shown in Fig. 3.18. Aside from a concentration of the streamfunction more towards the center of the channel, there is no significant difference from earlier calculations. Thus we conclude that our original experiments have enough resolution to capture the instabilities that we are studying.

Finally, the finite difference model used in Section 2.3 was applied to the case $a = 0.3$ using a grid spacing of 290km. Dissipation in the form of a term $\nu\nabla^2\zeta$ was needed to keep the 400 day integration stable. The coefficient ν was chosen to damp $2\Delta x$ waves in 12 hours. The frequency and growth rate obtained were $\sigma_r = 2.56 \times 10^{-5}, \sigma_i = 2.60 \times 10^{-6}$. The frequency closely matches the previous results, but the growth rate is significantly larger–a perplexing result given that the model includes dissipation. The structure (Fig. 3.19), as well as the wavenumber distribution, compares very favorably with the earlier results.

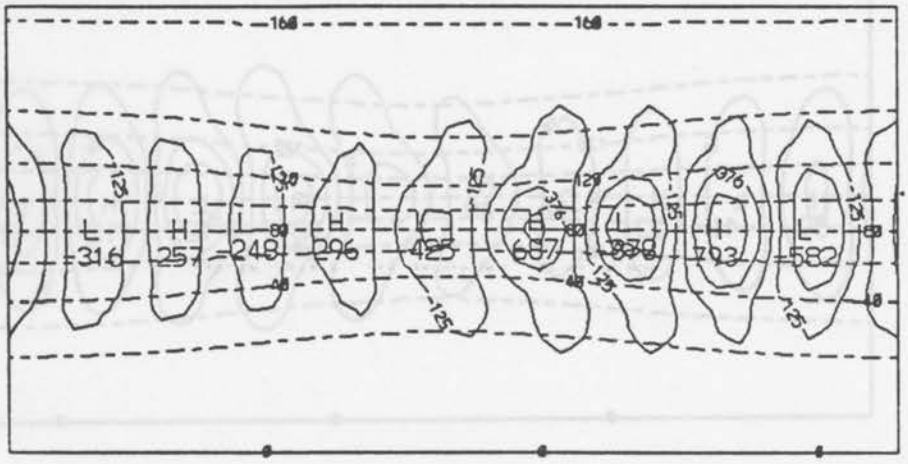

Figure 3.18: Streamfunction contours for the most unstable mode (solid lines) at $t = 0$ for the time integration method with $a = 0.3$ and $b = 0.0$ using 60 points in the y direction. Dashed lines are contours of the basic state.

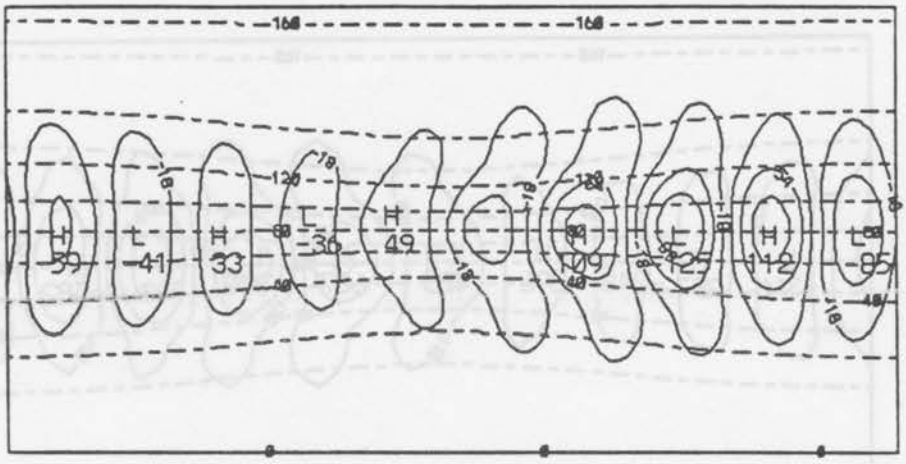

Figure 3.19: As in Fig. 3.18 except for the finite difference model with a grid spacing of 290 km.

3.5 Instabilities of Asymmetric Flows

We have applied a variety of techniques to obtaining instabilities of flows which have downstream variation but are symmetric about a line of constant y passing through the center of the channel. We now relax the latter assumption, which in practice means altering the value of b in (2.12). For the first simulations, downstream variation is inhibited by setting $a = 0$ in (2.11); thus we are studying the classical instability problem with symmetric cross-stream variation replaced by asymmetric cross-stream variation. We apply both the eigenvalue method and the time integration method.

As Fig. 3.4 indicates, increasing b increases the shear on the northern side of the jet and decreases it on the southern side. The location of the maximum jet speed remains in the center of the channel and the maximum speed itself remains the same.

The growth rate and frequency of unstable modes growing on this jet structure are listed as a function of b in Table 3.1 for the eigenvalue method. The degree of asymmetric variation does not seem to have much effect on these quantities. The structure of the instabilities, however, does exhibit some noticeable and significant changes as illustrated in Fig. 3.20 by a contour plot of the streamfunction for $b = 1.25$. Qualitatively, one can see an asymmetric distribution of the amplitude and tilt of the unstable disturbance. This may be examined more carefully by looking at the variation in amplitude and phase (Fig. 3.21). Of course, when b is very small, both the amplitude and phase are symmetrically distributed about $y = y_c$. As b increases, the amplitude maximum remains in the center of the channel but otherwise becomes asymmetrically distributed with larger amplitude on the northern, or more strongly sheared, side of the jet. For symmetric flow, the phase is symmetric and indicative of a tilt opposite to the shear. As the flow becomes more asymmetric, the phase follows suit, showing very strong eastward tilt to the north of the jet maximum and weak westward tilt to the south. In summary, when parallel flow becomes asymmetric in y, the barotropic instability which grows upon it is also asymmetric with larger amplitude and more pronounced tilt on the side of the jet with strongest shear.

This result can be understood from a simple energetics argument. The conversion term between the mean and eddy kinetic energies is given by

Table 3.1: The growth rate, frequency and wavenumber of the three most unstable modes as a function of the asymmetry parameter b using the eigenvalue method

b	Growth rate $(\times 10^{-6} s^{-1})$	Frequency $(\times 10^{-5} s^{-1})$	wavenumber
	7.73	3.34	5
1.25	7.41	4.58	6
	7.40	2.24	4
	7.49	3.32	5
1.0	7.25	4.56	6
	7.07	2.21	4
	7.21	3.25	5
0.75	6.95	4.55	6
	6.65	2.16	4
	7.19	3.17	5
0.5	6.51	2.06	4
	6.33	4.51	6
	7.69	3.16	5
0.0	6.56	4.25	6
	6.46	2.02	4

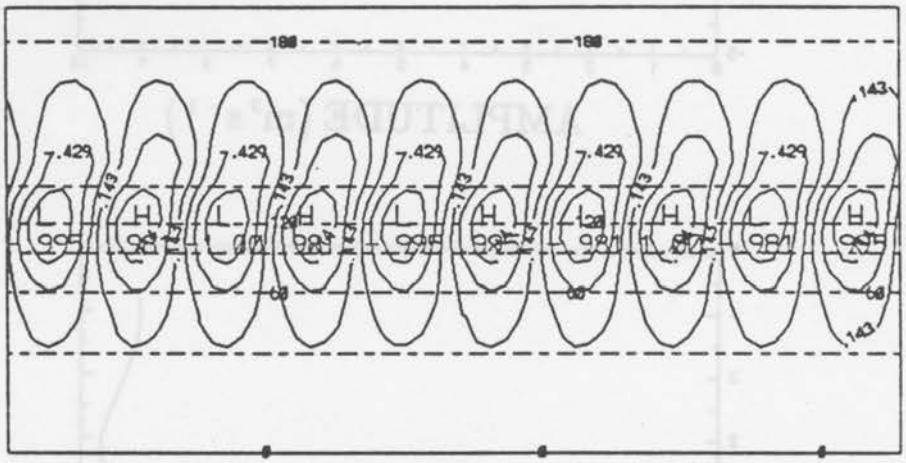

Figure 3.20: Streamfunction contours of the most unstable mode at $t = 0$ (solid lines) with $a = 0$ and $b = 1.25$ using the eigenvalue method. Dashed lines are contours of the basic state.

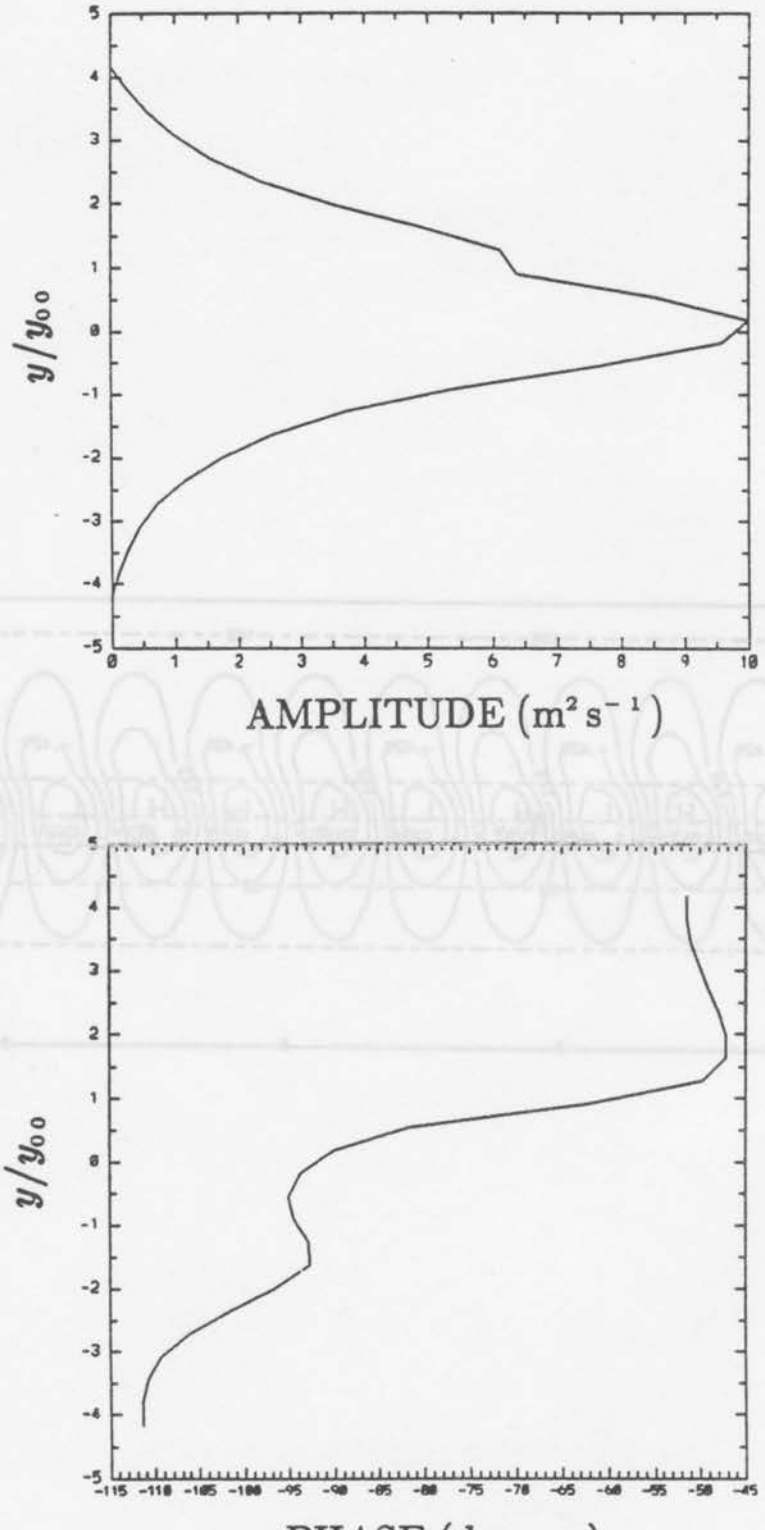

Figure 3.21: The amplitude and phase corresponding to the structure in Fig. 3.20.

$$C_K = \int_0^{L_y} \overline{u'v'} \frac{d\bar{u}}{dy} dy. \tag{5.1}$$

where the overbar refers to an x average over the domain. The conversion term physically means that a disturbance grows if it tilts opposite to the shear. The amplitude and phase plotted in the figures has been determined from

$$\psi'(x, y, t) = A_m(y) \cos(2\pi m x / L_x - \sigma_r t - \theta(y)), \tag{5.2}$$

where A_m is the amplitude and θ the phase. From this we can show that

$$C_K = \frac{\pi m}{L_x} \int_o^{L_y} A_m^2(y) \frac{d\theta}{dy} \frac{d\bar{u}}{dy} dy \tag{5.3}$$

Now for a given mean wind structure, the most unstable disturbance will have a structure that allows for the maximum energy conversion. This means maximizing the value of the integral C_K. The easiest way to do this is to make the amplitude and phase change large where the shear is large. As we change the mean wind profile, the amplitude of the shear becomes larger on the north side and smaller on the south side. In order to maximize the energy conversion, the tilt and amplitude of the disturbance should become larger on the north side and smaller on the south side. This is exactly what we see in Fig. 3.21 indicating that the structure of the barotropic instability of an asymmetrically sheared flow can be understood from simple theory.

To obtain results using the time integration method we initialize the spectral model with a single wavenumber in x and integrate forward in time. The growth rate and frequency are determined as in Section 3.4. For most cases, 75 days was a more than sufficient length of integration. Table 3.2 lists the growth rates and frequencies for several wavenumbers as a function of b . At first, the results seem disturbing as they are consistently different from the eigenvalue method results. For the latter method, wavenumber five is consistently the most unstable wavenumber while the time integration method yields wavenumber four as the most unstable for every asymmetric case. The frequencies of the most unstable modes are correspondingly different and there are often differences in the

Table 3.2: The growth rate, frequency and wavenumber of the three most unstable modes as a function of the asymmetry parameter b using the time integration method

b	Growth rate ($\times 10^{-6} s^{-1}$)	Frequency ($\times 10^{-5} s^{-1}$)	wavenumber
	7.24	2.09	4
1.25	6.60	4.51	6
	6.41	3.23	5
	7.01	2.05	4
1.0	6.43	4.51	6
	6.20	3.19	5
	6.79	2.00	4
0.75	6.17	3.12	5
	6.12	4.51	6
	6.85	1.92	4
0.5	6.75	3.01	5
	5.42	4.43	6
	7.80	3.01	5
0.0	6.76	1.92	4
	6.49	4.03	6

second and third most unstable modes as well. Doubling the integration time to 150 days causes almost no change in the growth rate and so does not alleviate the problem.

Fortunately, there is a plausible explanation. As mentioned on several previous occasions, a problem with the time integration method is that it may have difficulty distinguishing between two or more modes with very similar growth rates. Examination of the growth rates for the asymmetric cases shows that for wavenumbers 4-6, the growth rates are all within 15% of each other. The percentage is smaller when only wavenumbers 4-5 are taken into account. Thus it seems that we have a case where several modes have very close growth rates. The time integration method is simply finding a different most unstable mode from the eigenvalue method. Note that the growth rates have the widest spread in the symmetric case, where both methods agree on the most unstable mode, lending support to our argument.

The blame should not be put entirely on the time integration method. This method may indeed have trouble distinguishing between two or more modes with nearly the same growth rates; in fact, we have seen an example of this in Section 3.4. However, the eigenvalue method is not without possible problems. Specifically, we want to briefly note that the order of the eigenvalue problem in these calculations is 528. Given the number of operations associated with each element in the matrices (see the Appendix) it is conceivable that numerical problems could lead to differences in eigenvalues of the same order which we are seeing in the Tables.

In any case, although there may be some differences, examination of the streamfunction reveals that the essential dynamical result is the same: asymmetrically sheared flow leads to an asymmetric instability with larger amplitude and more pronounced tilt on the more strongly sheared side of the jet (Fig. 3.22).

Finally, we investigate the sensitivity of the instability to changes in the latitudinal resolution. For the parameter value $b = 1.25$, calculations were made for 36, 48, and 60 points in the y direction, the latter representing 150% more resolution than the original 24 points. At 60 points, the (σ_r, σ_i) pairs are

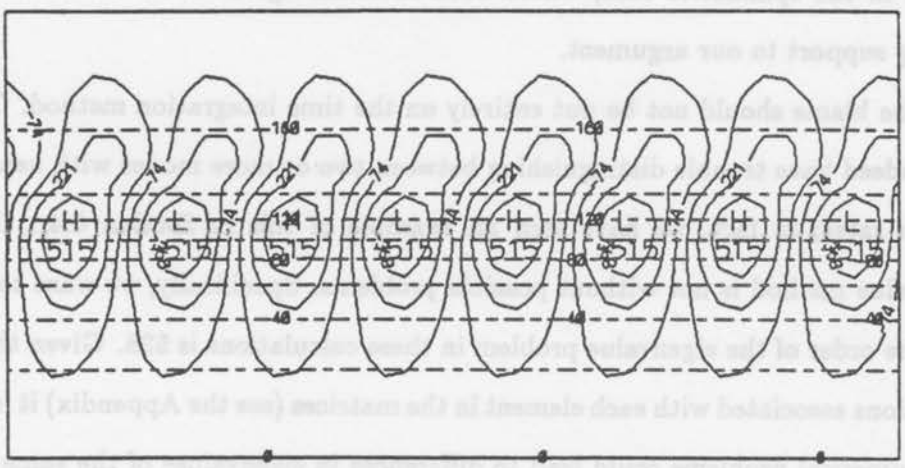

Figure 3.22: Streamfunction contours of the most unstable mode (solid lines) for the time integration method when $a = 0, b = 1.0$. Dashed lines are contours of the basic state.

wavenumber 6 $(4.67 \times 10^{-5}, 1.09 \times 10^{-5})$

wavenumber 5 $(3.49 \times 10^{-5}, 1.02 \times 10^{-5})$

wavenumber 4 $(2.33 \times 10^{-5}, 7.75 \times 10^{-6})$.

The maximum change in the amplitude $|\sigma| = \sqrt{\sigma_r^2 + \sigma_i^2}$ between 24 and 60 points is only about 10%. Note that wavenumber 6 is now the most unstable wave. (The selection of this wavenumber over the others is, in part, a function of the numerical method as discussed above. No strong physical basis for this scale selection is suggested.) The structure of the wavenumber 4 instability (chosen for comparison with the 24 point case) is shown in Fig. 3.23.

The amplitude is slightly more concentrated in the center of the channel, otherwise, there is no significant difference from the earlier experiment. We conclude that the calculations made with the eigenvalue and time integration methods using 24 points have captured, both qualitatively and quantitatively, the physical instability.

We now add downstream variation to the asymmetric flow by letting the parameter a take on non-zero values. A large number of cases could be considered here; we focus on a few selected examples that are typical of the results when both types of basic state variation are present. First consider the case where $a = 0.4$ and $b = 1.0$. The frequency and growth rate of the most unstable mode obtained with the eigenvalue method are $\sigma_r = 2.58 \times 10^{-5}$ and $\sigma_i = 2.06 \times 10^{-6}$. The structure is shown in Fig. 3.24. The characteristics of the instability appear to be a combination of the individual effects of the downstream variation and cross-stream asymmetry. The growth rate is significantly smaller than in the parallel flow case while the frequency is slightly smaller. This is in accord with the previous results where downstream variation was associated with smaller growth rates and relatively unchanged frequencies and cross-stream asymmetry had little effect on either the growth rate or frequency. In the same way, the structure is a combination of a shifting of the streamfunction maximum downstream from the point of maximum shear and a greater amplitude and stronger tilt on the more strongly sheared side of the jet. Note also that the location of the high and low centers do not lie along a straight line but instead lie

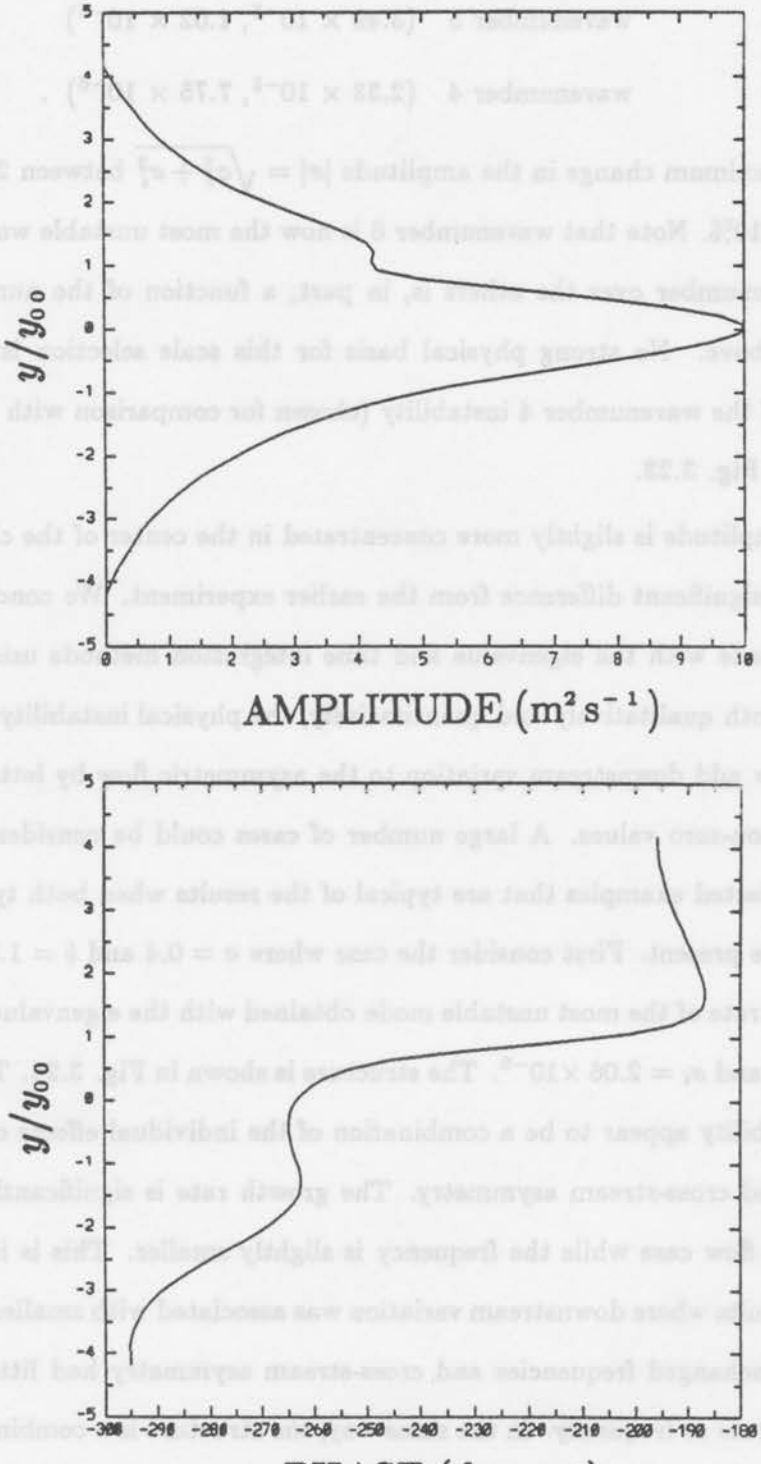

Figure 3.23: Amplitude and phase of the unstable mode with wavenumber 4 when $a = 0, b = 1.25$ for the time integration method using 60 points in y.

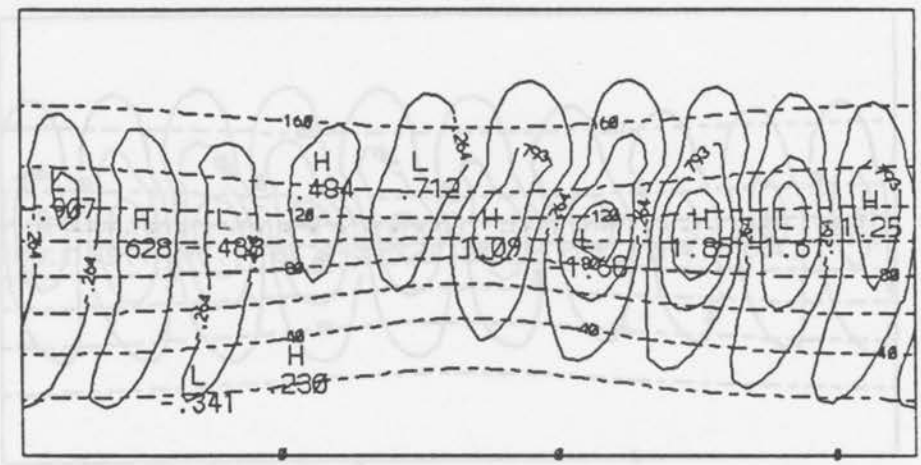

Figure 3.24: As in Fig. 3.8 but for $a = 0.4$ and $b = 1.0$.

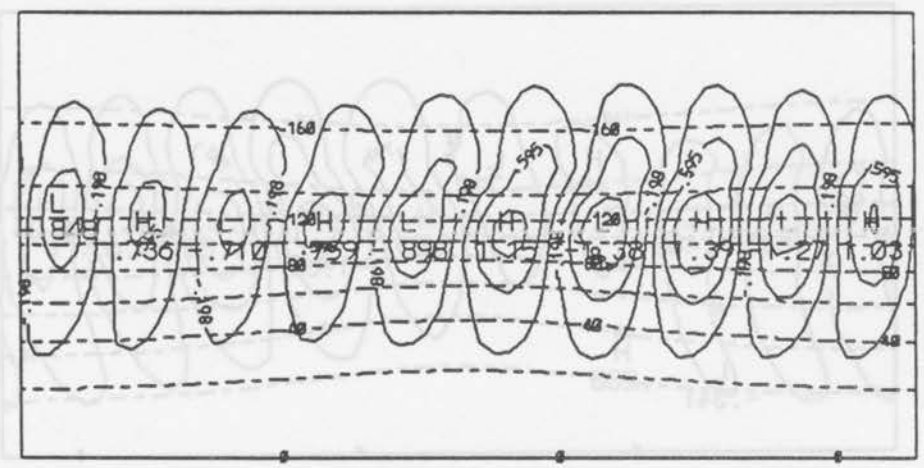

Figure 3.25: As in Fig. 3.24 but for $a = 0.2$ and $b = 1.0$.

along a slightly wavy line. Other cases, such as $a = 0.2, b = 1.0$ (Fig. 3.25) have similar characteristics.

The time integration method was also applied to this problem using both the semi-spectral and finite differenced models. The results (not shown) compare favorably with those just discussed.

The cases with both downstream and asymmetric cross-stream variation are the most realistic simulations that we have made. Their results are the most difficult to understand (although we have suggested that they can be understood as a combination of each of the other cases), but probably have the most relevance to the real atmosphere where downstream and asymmetric cross- stream variations are always present.

3.6 A Non–Linear Calculation

Linear instability theory is useful in postulating basic explanations of observed phenomena, for example, the formation of synoptic scale storms. In this study, the theory has given us an idea of what to expect from an unstable basic state with downstream variation. However, linear instabilities, by definition, are not observable, because the linear assumption is valid only when the instability has small amplitude relative to the basic state upon which it is growing. When the amplitude is large enough to be observed, it is also large enough to permit non–linear interactions with the basic state. These interactions have been shown, in the case of growing baroclinic disturbances, to significantly effect the character of the disturbance (e.g., Gall *et al.*, 1976; Simmons and Hoskins, 1978). In this section, a typical linear instability in the presence of downstream variation is allowed to evolve into the non–linear regime in order to gain a preliminary understanding of how non–linearity effects the previous calculations.

In accordance with Williams *et al* (1984) and Frederikson and Puri (1985), our methodology consists of the following steps. First, a basic state is prescribed and the most unstable linear instability growing upon it is calculated. For simplicity we chose a basic state given by (2.8) with a = 0.3 and b = 1.0, i.e., one with downstream variation but no cross–stream asymmetry. The most unstable mode corresponding to this basic state

has been documented in previous sections. Second, we explicitly determine the forcing F that satisfies

$$J(\bar{\psi},\bar{\zeta}) + \beta\bar{\psi}_x = F + \nu\nabla^2\bar{\zeta} \tag{6.1}$$

This is the same as (2.5) except for the inclusion of the dissipation term. Finally, the fully non–linear barotropic vorticity equation given by

$$\zeta_t + J(\psi,\zeta) + \beta\psi_x = F + \nu\nabla^2\zeta \tag{6.2}$$

is integrated forward in time from an initial condition consisting of the specified basic state plus a perturbation with the same structure as the most unstable normal mode. The perturbation is given a small enough amplitude so that both the linear and non–linear stages of the instability can be studied. If the perturbation is zero, the total flow is given by the basic state part and the forcing prevents any time evolution (apart from discretization errors). However, if the perturbation is non–zero, instability will develop. The disturbance will extract energy from the mean flow eventually reaching a large enough amplitude so that it can interact non–linearly to change that mean flow. As mentioned in Section 3.2, F represents the external forces which maintain the time averaged flow. By including F in the non–linear calculation, we are assuming that such forces continue to act even though the basic state is being altered by interactions with the instability. This treatment of the forcing is employed by Williams, *et al.* (1984) and Frederikson and Puri (1985).

In our results, we emphasize the time evolution of the disturbance streamfunction structure and the total velocity field. By disturbance streamfunction we mean the difference between the total streamfunction and the prescribed basic state streamfunction. The model defined by (6.2) is integrated for 30 days. The average kinetic energy of the disturbance as a function of time is shown in Fig. 3.26. There is an initial period of rapid growth lasting about one week followed by a small amplitude vacillation which persists for the rest of the integration. Figure 3.27 shows the structure of the disturbance at several times during the integration. The initial structure is the same as in Fig. 3.19. By day 2, the

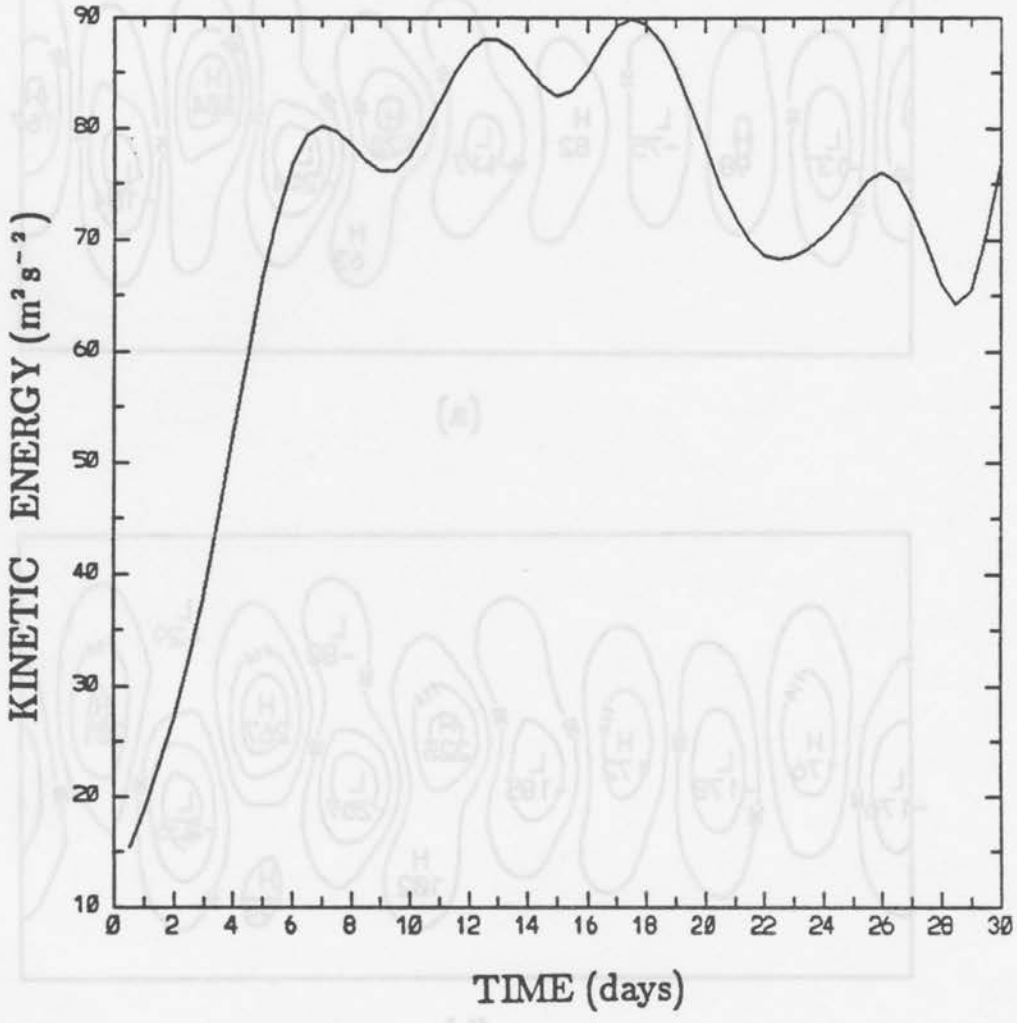

Figure 3.26: The average kinetic energy as a function of time for the non–linear disturbance growing upon the basic state defined by (2.8) with $a = 0.3$ and $b = 0$.

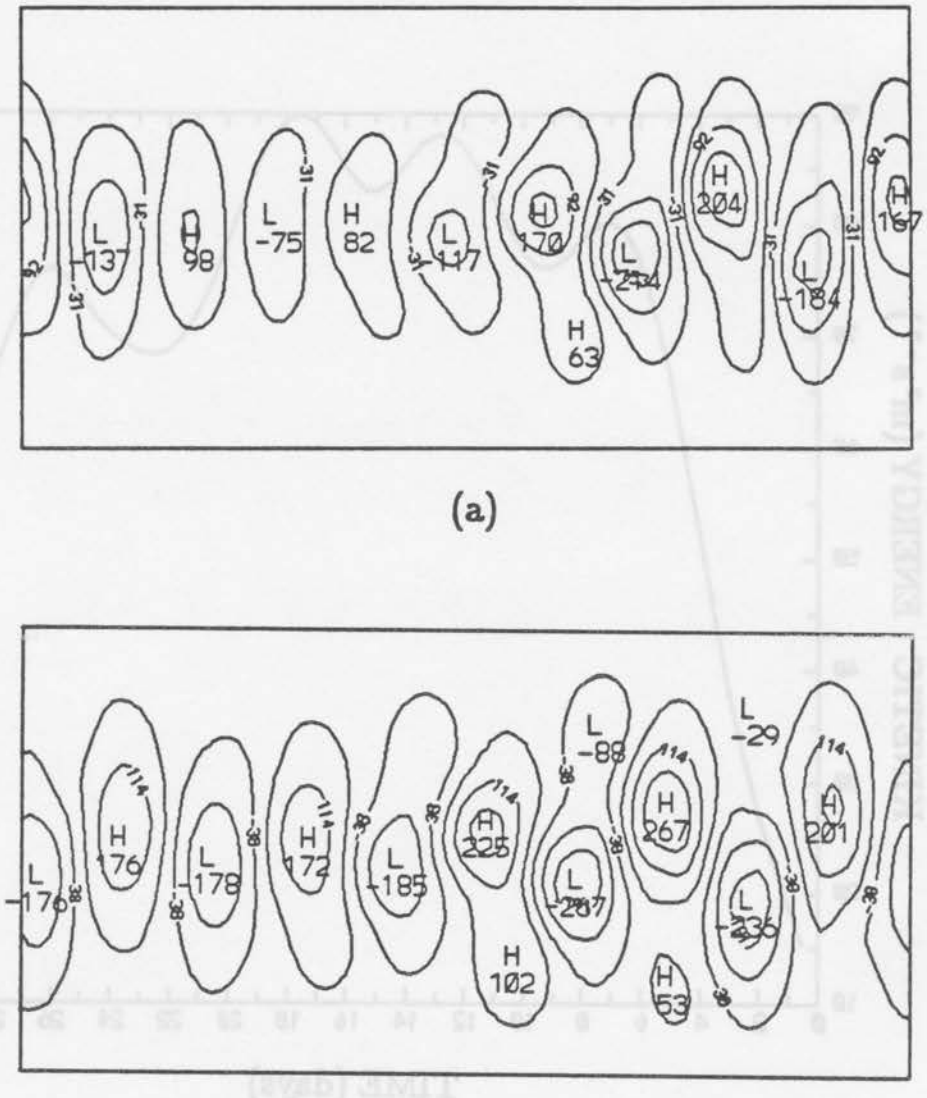

Figure 3.27: The structure of the unstable non–linear disturbance for the same basic state as Fig. 3.26 at (a) day 2 (b) day 4 (c) day 8 (d) day 24.

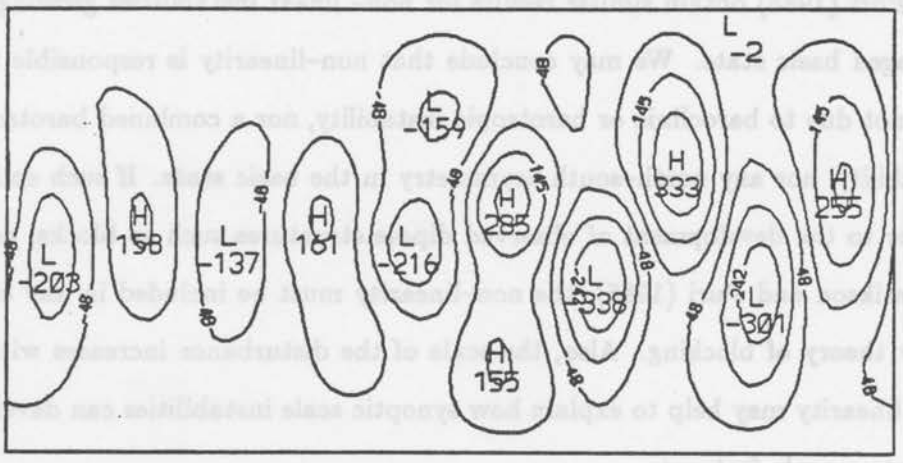

(c)

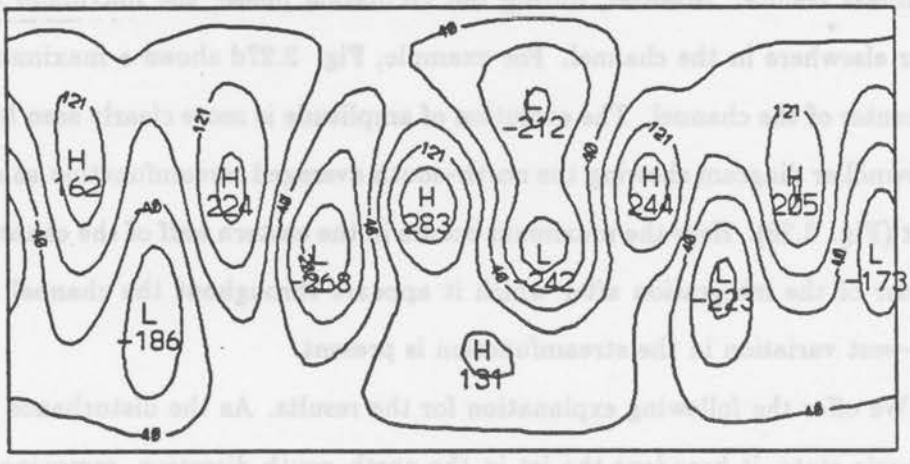

(d)

Figure 3.27: continued.

initial structure has become distorted, with the high centers located slightly north of the center of the channel and the low centers slightly south. This is enhanced as the integration proceeds, so that by day 8 there is significant north–south displacement. Frederikson and Puri (1985) obtain similar results for non– linear instabilities growing on a January averaged basic state. We may conclude that non–linearity is responsible for this result; it is not due to baroclinic or barotropic instability, nor a combined barotropic/baroclinic instability, nor any north–south asymmetry in the basic state. If such splitting is a precursor to the development of observed dipole structures such as blocks, as suggested by Frederikson and Puri (1985), the non–linearity must be included in any complete instability theory of blocking. Also, the scale of the disturbance increases with time. Thus, non–linearity may help to explain how synoptic scale instabilities can develop into nearly planetary scale features.

Throughout the first week of the integration, the maximum disturbance amplitude occurs downstream from the point of maximum shear in the basic state, consistent with the linear results. However, during the vacillation phase, the maximum amplitude can occur elsewhere in the channel. For example, Fig. 3.27d shows a maximum just west of the center of the channel. The evolution of amplitude is more clearly seen by constructing a Hovmöller diagram showing the north–south averaged streamfunction as a function of x and t (Fig. 3.28). Here the maximum occurs in the eastern half of the channel for the first quarter of the integration after which it appears throughout the channel. At all times, east–west variation in the streamfunction is present.

We offer the following explanation for the results. As the disturbance interacts with the basic state, it broadens the jet in the north–south direction, removing the source of instability, without, however, removing all the downstream variation. Once the basic state is stabilized, what is left is a sort of finite amplitude, neutral mode propagating through a downstream varying flow. With the source of instability removed, the mechanism for the downstream maximum as discussed in previous sections no longer exists with the consequence that the maximum amplitude can occur anywhere in the channel.

Some confirmation of this explanation comes from examination of the total velocity fields. Figure 3.29 shows the zonal velocity profiles for three different values of x at the

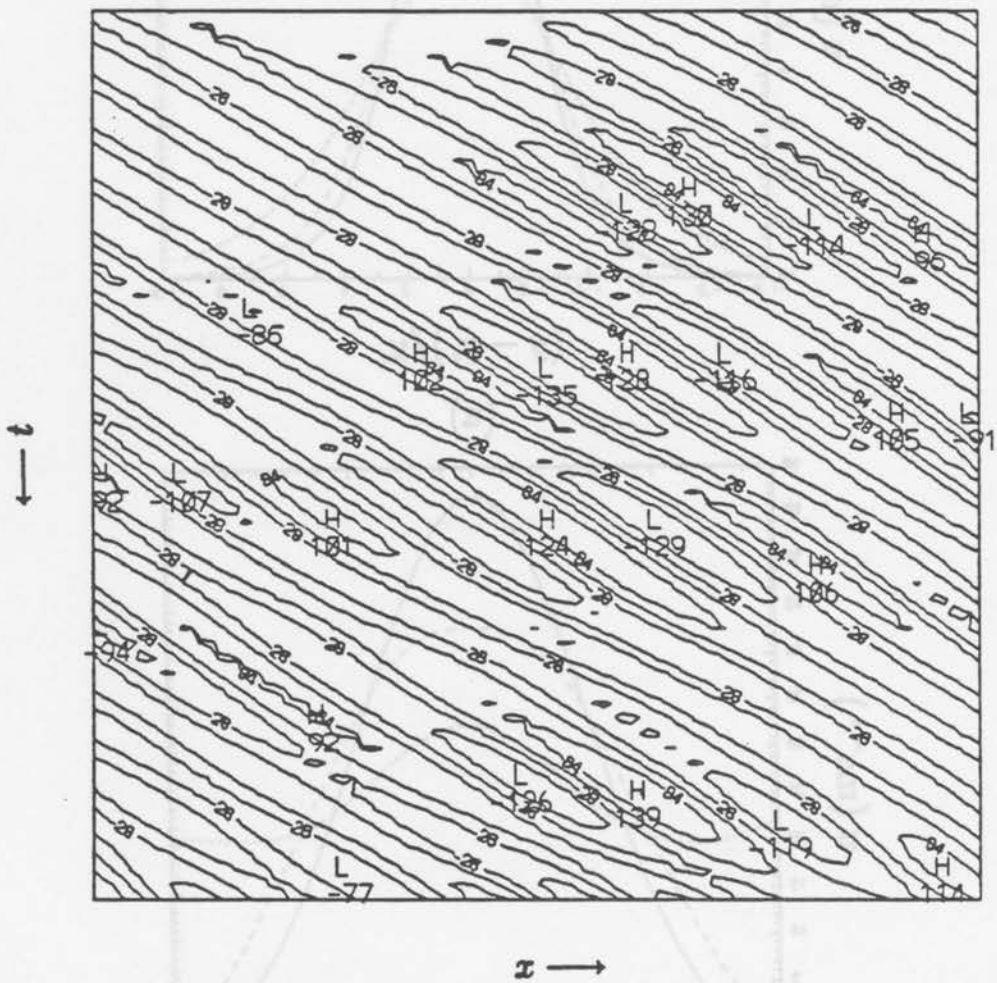

Figure 3.28: The disturbance streamfunction for the instability of Fig. 3.27 averaged in the north-south direction as a function of x and t. Time increases downward and covers all the 30 days of integration.

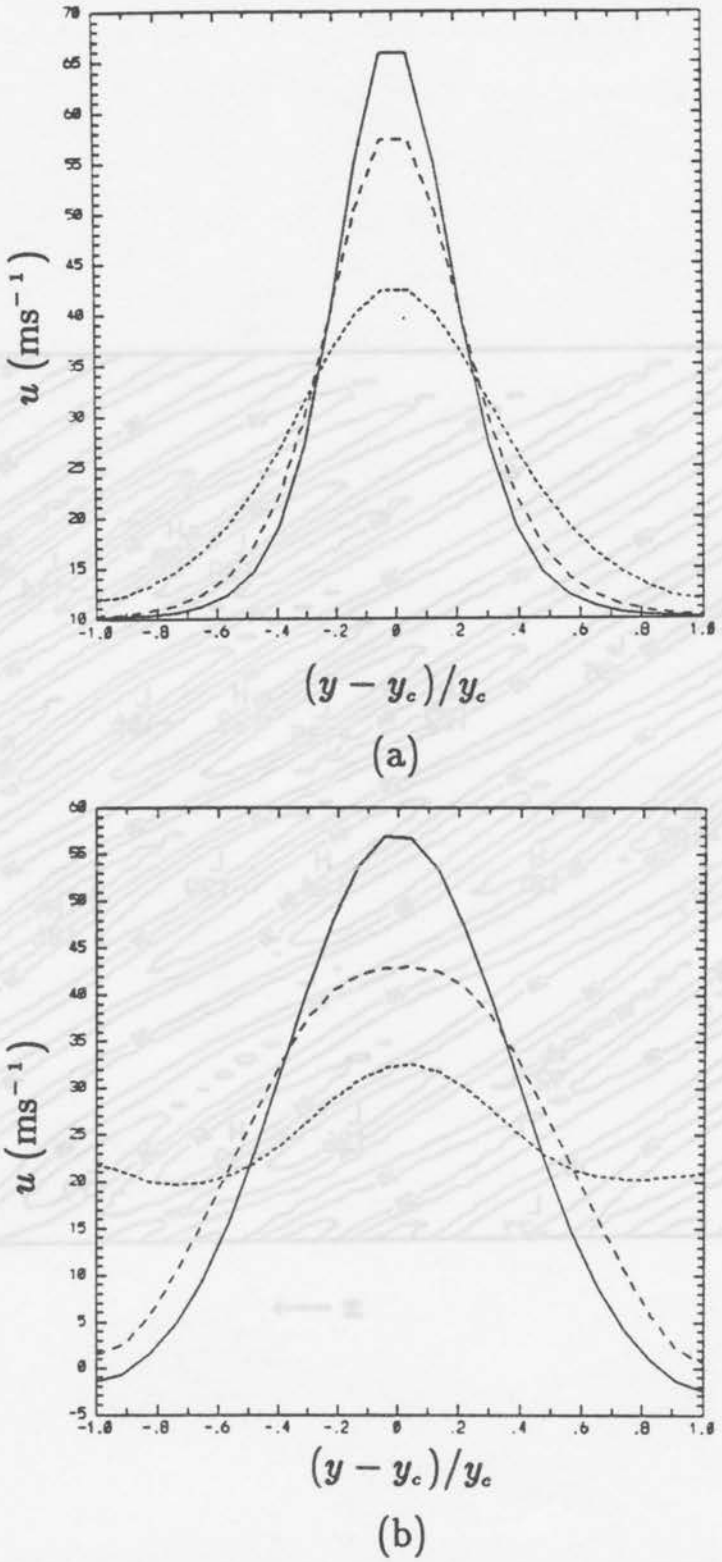

Figure 3.29: Zonal velocity profiles in ms^{-1} for the integration of Fig. 3.26 at $x = L_x/2$ (solid line), $x = 2L_x/3$ (long dashed line), and $x = L_x$ (short dashed line) for (a) $t = 0$ and (b) the average of day 8 through day 30.

beginning of the integration and for the time average of the last 23 days. The latter corresponds to an average over the vacillation phase. The maximum jet speeds are reduced and the jet itself is broadened without eliminating the downstream variation. As a consequence of the broadening, the instability characteristics are changed. Figure 3.30 shows profiles of $\beta - u_{yy}$ at $x = L_x/2$ for the same times as Fig. 3.29. Initially, the necessary condition for barotropic instability is satisfied, but the time averaged flow during the vacillation phase seems to satisfy the condition only marginally. Given the rather limited number of points in $y(24)$, little weight should be attached to the meager non–zero values of $\beta - u_{yy}$ in Fig. 3.30b. Therefore, the total flow field confirms some necessary aspects of our explanation.

3.7 Summary and Discussion

We have investigated the barotropic instability of basic states with downstream and asymmetric cross-stream variations. The simplest model that can describe the instability is applied: the non-divergent, barotropic vorticity equation formulated in a periodic beta-channel. The basic state is defined by a single expression for the streamfunction. Two parameters control the degree of downstream and asymmetric cross-stream variation. The downstream variation is given by a configuration where, to the east and west of a jet centered at a particular longitude, there is diffluence to weak, almost constant and almost parallel flow. Such a basic state allows for a different form of downstream variation than that obtained by superimposing a planetary wave on a zonal jet. Specifically, it highlights the effects of areas of diffluence, rather than the steering effects of superimposed waves. Such diffluent areas are common downstream from storm tracks. Both an eigenvalue method and a time integration method are employed to obtain the instabilities.

The results are summarized in two categories: comments on the physics and comments on the methods. We began with a prototype calculation that allowed a single wave pulse to propagate through a basic state with downstream variation. The wave achieved its maximum amplitude downstream from the point where the latitudinal shear was maximum, in agreement with the results of Tupaz, *et al.* (1978) and Peng and Williams (1986). This behavior arises from the growth of the disturbance over the *entire* region of

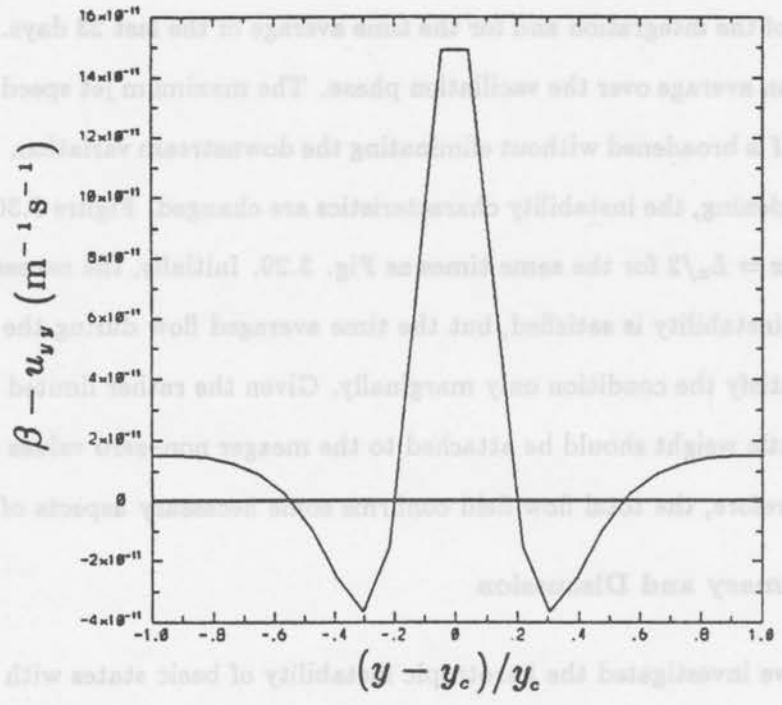

(a)

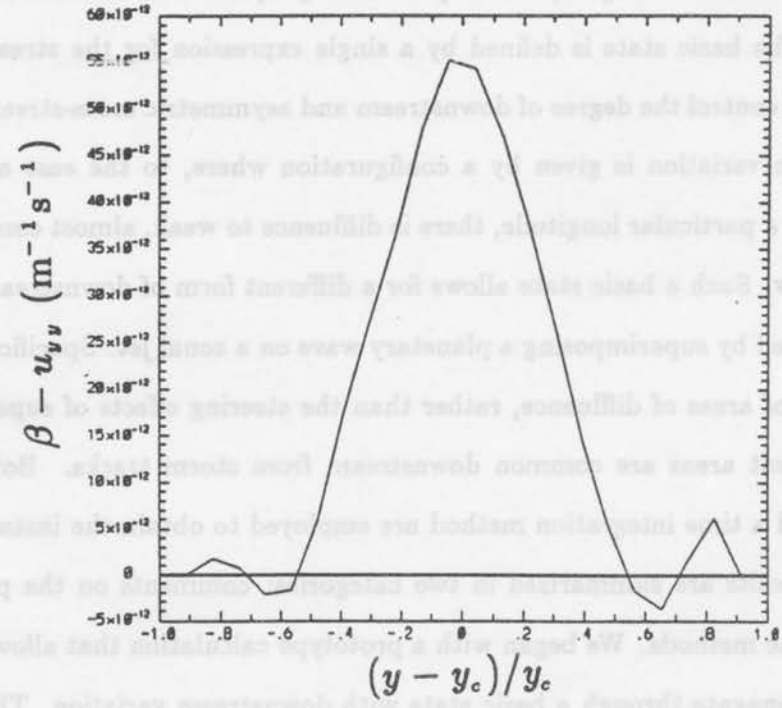

(b)

Figure 3.30: Profiles of $\beta - u_{yy}$ in $m^{-1}s^{-1}$ for the integration of Fig. 3.26 at $x = L_x/2$ for (a) $t = 0$ and (b) the average of day 8 through day 30.

unstable flow through which it is propagating. The more general and rigorous eigenvalue and time integration techniques yielded the following results. When only downstream variation was present, the instability structure resembled an envelope of amplitude, fixed in space, through which waves propagated. The maximum in envelope amplitude, and hence the maximum in streamfunction at any given time, was again located downstream from the point of maximum shear. This can be explained, as in Peng and Williams, by noting that the unstable disturbance lags in adjusting to the local instability characteristics. Sensitivity studies showed that the streamfunction amplitude was concentrated in a smaller region of the channel when the downstream variation was strong than when the flow was more nearly parallel. In addition, the instability had smaller east-west scales for stronger variation. Furthermore, the frequency of the most unstable mode was relatively unaffected as the degree of downstream variation increased, while the growth rate changed significantly, becoming an order of magnitude smaller than the parallel flow case. This results from the propagating disturbance being subjected to strong values of shear for only a finite time before moving into regions of lesser shear where it cannot grow as fast. In all cases, the structure exhibited the correct tilt for barotropic instability in the unstable regions.

When the cross-stream asymmetry was increased in parallel flow, the frequency and growth rate of the most unstable mode were relatively unchanged; however, the structure of the instability exhibited significant changes. There was larger amplitude and stronger tilt opposite to the shear on the side of the jet having larger shear in the basic state zonal velocity. This was shown to be theoretically consistent with the intuitive idea that barotropic instability will be most pronounced where the shear is strongest.

When both downstream and asymmetric cross-stream variation are present, the results can be understood as a combination of the individual effects of each type of variation. There is also a hint of wavelike behavior in the locations of the high and low centers of the streamfunction.

Where the instability was allowed to reach finite amplitude and interact non–linearly with the basic state, splitting of the disturbances occurred with the high centers moving

to the north and the low centers to the south. The scale of the disturbances increased and the basic state was stablized; however, the downstream variation remained.

The time integration method generally compared very favorably with the eigenvalue method. When differences occurred, it was suggested that they could be attributed to the presence of two modes with very similar growth rates. In such cases, the time integration model needed to be integrated for a very long time in order to converge on a single mode. Sometimes this mode did not agree with the eigenvalue method. The order of the eigenvalue problem was large enough that numerical problems with it could not be dismissed. Furthermore, a periodic beta-channel imposes a certain discreteness on the possible solutions that would not necessarily occur in spherical geometry. Thus the geometry may be at fault as well. Nevertheless , the discrepancies did not change the fundamental results above.

The basic character of the solutions was unchanged when time integration experiments were made with higher resolution in latitude. Similarly, instabilities obtained with the finite-difference model compared well with the previous results using spectral representation.

In conclusion, both methods have advantages and disadvantages as discussed in the Introduction. To highlight a few, resolution is limited with the eigenvalue method. While this can be overcome with the time integration method, long integration times are sometimes necessary to select the most unstable mode. Both techniques have their place implying that a thorough study of these types of instabilities may require application of both methods.

This study complements the previously quoted work of Peng and Williams by extending their results to the case of westerly flow in mid–latitudes, and by documenting similar results using the classical, temporal growth rate approach rather than spatial growth rate concepts. The study also complements Frederikson's research by emphasizing a type of downstream variation distinct from that caused by a planetary wave. In both cases, greater sensitivity to changes in the basic state is described. Moreover, the previous investigations have not directly addressed asymmetrically sheared jets, as we have done here.

The usefulness of our study lies partly in documenting some basic geophysical fluid dynamics results relating to instabilities of flows with downstream and asymmetric cross–stream variation. Although our model is one of the simplest imaginable, we have tried to develop a hierarchy of complexity in the solutions, culminating in the case combining downstream and asymmetric cross– stream variation. By doing this we have extended the catalog of theoretical results that can be used to understand observed atmospheric phenomena.

These results have some bearing on the problem of blocking. Specifically, we hypothesize (along with Frederikson, 1982) that blocks are the result of instability of the large scale flow. Typically, large scale flow patterns may support several instabilities with distinct differences in structure and behavior. Whether a block forms in any given synoptic situation may depend on whether the large scale flow favors a dominant instability with characteristics of blocking. Therefore, our understanding of blocking may depend on how well we understand the sensitivity of instabilities to various basic states. This study is a first step towards gaining that understanding.

An extension of these calculations to a baroclinic model is an obvious direction for future research. Not only can barotropic instability in a baroclinic atmosphere be investigated, but baroclinic instability can be discussed as well. Although we have postulated that blocking is a manifestation of instability, we do not want to imply that barotropic instability is the only mechanism. Blocking is likely to involve the combined effects of barotropic and baroclinic instability. Therefore, the baroclinic calculation is a necessary next step to pursue this hypothesis.

Future research should also perform similar calculations on a sphere. The variation of the beta parameter with latitude and the convergence of the meridians introduce additional asymmetry into the problem. Dispersion of energy is affected (Hoskins, *et al.*, 1977) and some results of baroclinic instability theory are changed (Simmons and Hoskins, 1976). The implication of these changes for our sensitivity studies should be addressed.

Finally, the non-linear aspects of the instabilities should be investigated more completely. Blocking undoubtedly involves a non-linear equilibration between a growing perturbation and the basic state. The non–linear calculation performed here hinted at some

blocking characteristics with the splitting of the disturbance and the increase in its scale. In contrast to Frederikson and Puri (1985), who document non–linear instabilities leading to relatively stationary patterns in a baroclinic model with an observed, time–averaged basic state we note that our unstable disturbances propagate. However, the net eastward motion of the disturbances are only 10-20% of the maximum jet speed, indicating that we are close to simulating the observed persistence of blocks. Future studies should attempt to pinpoint the variations and mechanisms responsible for transforming a growing, propagating instability into a stationary equilibrated feature.

REFERENCES

Arakawa, A., 1966: Computational design for long-term numerical integrations of the equations of atmospheric motions. *J. Comput. Phys.*, **1**, 119-143.

Brown, J.A., 1969: A numerical investigation of hydrodynamic instability and energy conversions in the quasi-geostrophic atmosphere: Part I. *J. Atmos. Sci.*, **26**, 352-365.

Charney, J.G., 1947: The dynamics of long waves in a baroclinic westerly current. *J. Meteor.*, **4**, 135-162.

Duffy, D.G., 1975: The barotropic instability of Rossby wave motion: A re- examination. *J. Atmos. Sci.*, **32**, 1271-1277.

Frederikson, J.S., 1978a: Instability of planetary waves and zonal flows in two layer models on a sphere. *Quart. J. Roy. Meteor. Soc.*, **104**, 841-872.

Frederikson, J.S., 1978b: Growth rates and phase speeds of baroclinic waves in multi-level models on a sphere. *J. Atmos. Sci.*, **35**, 1816-1826.

Frederikson, J.S., 1979a: Baroclinic instability of zonal flows and planetary waves in multi-level models on a sphere. *J. Atmos. Sci.*, **36**, 2320- 2335.

Frederikson, J.S., 1979b: The effect of long planetary waves on the regions of cyclogenesis: linear theory. *J. Atmos. Sci.*, **36**, 195-204.

Frederikson, J.S., 1982: A unified three dimensional instability theory of the onset of blocking and cyclogenesis. *J. Atmos. Sci.*, **39**, 969-987.

Frederikson, J.S., 1983a: Disturbances and eddy fluxes in northern hemisphere flows: instability of three dimensional January and July flows. *J. Atmos. Sci.*, **40**, 836-855.

Frederikson, J.S., 1983b: A unified three dimensional instability theory of the onset of blocking and cyclogenesis. II. Teleconnection patterns. *J. Atmos. Sci.*, **40**, 2593-2609.

Frederikson, J.S. and K. Puri, 1985: Non–linear instability and error growth in northern hemisphere three–dimensional flows: cyclogenesis, onset-of-blocking and mature anomalies. *J. Atmos. Sci.*, **42**, 1374–1397.

Gall, R., 1976: Structural changes of growing baroclinic waves. *J. Atmos. Sci.*, **33**, 374–390.

Grotjahn, R., 1984: Baroclinic instability in a long wave environment. Part I: Review. *Quart. J. Roy. Meteor. Soc.*, **110**, 663-668.

Grotjahn, R., 1987: Three-dimensional linear instability on a sphere: resolution experiments with a model using vertical orthogonal basis functions. *J. Atmos. Sci.*, **44**, 3734-3752.

Haltiner, G.J. and R.T. Song, 1963: Dynamic instability in barotropic flow. *Tellus*, **14**, 383-393.

Haltiner, G.J. and R.T. Williams, 1980: *Numerical Prediction and Dynamic Meteorology.* Wiley, 477p.

Hoskins, B.J., 1973: Stability of the Rossby-Haurwitz wave. *Quart. J. Roy. Meteor. Soc.*, **99**, 723-745.

Hoskins, B.J. and A. Hollingsworth, 1973: On the simplest example of the barotropic instability of Rossby wave motion. *J. Atmos. Sci.*, **30**, 150- 153.

Hoskins, B.J., A.J. Simmons and D.G. Andrews, 1977: Energy dispersion in a barotropic atmosphere. *Quart J. Roy. Meteor. Soc.*, **103**, 553-567.

Kuo, H.L., 1949: Dynamical instability of two dimensional non-divergent flow in a barotropic atmosphere. *J. Meteor.*, **6**, 105-122.

Lorenz, E.., 1972: Barotropic instability of Rossby wave motion. *J. Atmos. Sci.*, **29**, 258-264.

Niehaus, M.C.W., 1980: Instability of non-zonal baroclinic flows. *J. Atmos. Sci.*, **37**, 1447-1463.

Orszag, S.A., 1970: Transform method for the calculation of vector-coupled sums: application to the spectral form of the vorticity equation. *J. Atmos. Sci.*, **27**, 890-895.

Palmén, E. and C.W. Newton, 1969: *Atmospheric Circulation Systems*, Academic Press, New York, 1969.

Pedlosky, J., 1987: *Geophysical Fluid Dynamics*. Springer-Verlag, 710p.

Peng, M.S. and R.T. Williams, 1986: Spatial instability of the barotropic jet with slow streamwise variation. *J. Atmos. Sci.*, **43**, 2430-2442.

Peng, M.S. and R.T. Williams, 1987: Spatial instability of a baroclinic current with slow streamwise variation. *J. Atmos. Sci.*, **44**, 1681- 1695.

Schutts, G.J., 1983: The propagation of eddies in diffluent jetstreams: eddy vorticity forcing of blocking flow fields. *Quart. J. Roy. Meteor. Soc.*, **109**, 737-762.

Simmons, A.J. and B.J. Hoskins, 1976: Baroclinic instability on the sphere: normal modes of the primitive and quasi-geostrophic equations. *J. Atmos. Sci.*, **33**, 1454-1477.

Simmons, A.J. and B.J. Hoskins, 1978: The life cycles of some non–linear baroclinic waves. *J. Atmos. Sci.*, **35**, 414-432.

Tupaz, J.B., R.T. Williams and C.-P. Chang, 1978: A numerical study of barotropic instability in a zonally varying easterly jet. *J. Atmos. Sci.*, **35**, 1265-1280.

Williams, R.T., H. Lim, and C.-P. Chang, 1984: On-linear and linear effects in an easterly jet with downstream variation. *J. Atmos. Sci.*, **41**, 621- 636.

APPENDIX

Details of the Eigenvalue Method

Here we present some additional detail of the formulation of the eigenvalue problem which we generally described in Section 3. Specifically, we concentrate on the matrix equation (3.2)

For notational convenience, we define the operators

$$\mathcal{L}_o = \frac{\partial^o}{\partial y^o} \ , \tag{1a}$$

$$\mathcal{L}_1 = \frac{\partial}{\partial y} \ , \tag{1b}$$

$$\mathcal{L}_{2m} = \frac{\partial^2}{\partial y^2} - k_m^2 \tag{1c}$$

$$\mathcal{L}_{3m} = \frac{\partial^3}{\partial y^3} - k_m^2 \frac{\partial}{\partial y} \ . \tag{1d}$$

Second order, centered differences are used to discretize the operators. When necessary near the walls, first order, one-sided differences are employed. Using these operators, the basic state terms appearing in (2.6) may be written

$$\bar{u}(x,y) = \hat{u}(y) + \sum_{n=1}^{N} (\bar{u}_n^c(y) \cos k_n x + \bar{u}_n^s(y) \sin k_n x), \tag{2a}$$

$$\bar{v}(x,y) = \sum_{n=1}^{N} (\bar{v}_n^c(y) \cos k_n x + \bar{v}_n^s(y) \sin k_n x), \tag{2b}$$

$$\frac{\partial \bar{\zeta}(x,y)}{\partial x} = \sum_{n=1}^{N} (\bar{\zeta}^c_{xn}(y) \cos k_n x + \bar{\zeta}^s_{xn}(y) \sin k_n x), \tag{2c}$$

$$\frac{\partial \bar{\zeta}(x,y)}{\partial y} = \hat{\zeta}_y(y) + \sum_{n=1}^{N} (\bar{\zeta}^c_{yn}(y) \cos k_n x + \bar{\zeta}^s_{yn}(y) \sin k_n x), \tag{2d}$$

where

$$\begin{aligned}
&\bar{u}^c_n = -\mathcal{L}_1 \bar{\psi}^c_n \ , \quad \bar{u}^s_n = -\mathcal{L}_1 \bar{\psi}^s_n \ , \quad \hat{u} = -\partial \hat{\psi}/\partial y \ , \\
&\bar{v}^c_n = k_n \bar{\psi}^s_n \ , \quad \bar{v}^s_n = -k_n \bar{\psi}^c_n \ , \\
&\bar{\zeta}^c_{xn} = k_n \mathcal{L}_{2n} \bar{\psi}^s_n \quad \bar{\zeta}^s_{xn} = k_n \mathcal{L}_{2n} \bar{\psi}^c_n \ , \\
&\bar{\zeta}^c_{yn} = \mathcal{L}_{3n} \bar{\psi}^c_n \ , \quad \bar{\zeta}^s_{yn} = \mathcal{L}_{3n} \bar{\psi}^s_n \ , \quad \hat{\zeta} = \partial^2 \hat{\psi}/\partial y^2 \ ,
\end{aligned} \tag{3}$$

and the perturbation terms may be written

$$\frac{\partial \psi'}{\partial x} = \sum_{m=1}^{M} k_m (-\psi^c_m \sin k_m x + \psi^s_m \cos k_m x) \ , \tag{4a}$$

$$\frac{\partial \psi'}{\partial y} = \sum_{m=1}^{M} (\mathcal{L}_1 \psi^c_m \cos k_m x + \mathcal{L}_1 \psi^s_m \sin k_m x) \ , \tag{4b}$$

$$\nabla^2 \frac{\partial \psi'}{\partial y} = \sum_{m=1}^{M} k_m (-\mathcal{L}_{2m} \psi^c_m \sin k_m + \mathcal{L}_{2m} \psi^s_m \cos k_m x) \ , \tag{4c}$$

$$\nabla^2 \frac{\partial \psi'}{\partial y} = \sum_{m=1}^{M} (\mathcal{L}_{3m} \psi^c_m \cos k_m x + \mathcal{L}_{3m} \psi^s_m \sin k_m x) \ . \tag{4d}$$

With this notation, substitution of (3.1 a, b) into (2.6) followed by application of the orthogonality of sines and cosines yields the following two equations for the time dependence of ψ^c_m and ψ^s_m ,

$$\mathcal{L}_{2\ell} \frac{\partial \psi^c_\ell}{\partial t} = -k_\ell \, \hat{u} \, \mathcal{L}_{2\ell} \, \psi^s_\ell - k_\ell \, \hat{\zeta}_y \, \psi^s_\ell - k_\ell \, \beta \psi^s_\ell$$

$$+ \sum_{m=1}^{M} \left[\sum_{n=1}^{N} k_m \bar{\zeta}^s_{yn} \mathrm{CSS}(\ell, m, n) \right] \mathcal{L}_o \psi^c_m - \sum_{m=1}^{M} \left[\sum_{n=1}^{N} k_m \bar{\zeta}^c_{yn} \mathrm{CCC}(m, \ell, n) \right] \mathcal{L}_o \psi^s_m$$

$$+\sum_{m=1}^{M}\left[\sum_{n=1}^{N}\bar{\zeta}_{zn}^{c}\,\mathrm{CCC}(m,\ell,n)\right]\mathcal{L}_1\psi_m^c+\sum_{m=1}^{M}\left[\sum_{n=1}^{N}\bar{\zeta}_{zn}^{s}\,\mathrm{CSS}(\ell,m,n)\right]\mathcal{L}_1\psi_m^s$$

$$+\sum_{m=1}^{M}\left[\sum_{n=1}^{N}k_m\bar{u}_n^{s}\,\mathrm{CSS}(\ell,m,n)\right]\mathcal{L}_{2m}\psi_m^c-\sum_{m=1}^{M}\left[\sum_{n=1}^{N}k_m\bar{u}_n^{c}\,\mathrm{CCC}(m,\ell,n)\right]\mathcal{L}_{2m}\psi_m^s$$

$$-\sum_{m=1}^{M}\left[\sum_{n=1}^{N}\bar{v}_n^{c}\,\mathrm{CCC}(m,\ell,n)\right]\mathcal{L}_{3m}\psi_m^c-\sum_{m=1}^{M}\left[\sum_{n=1}^{N}\bar{v}_n^{s}\,\mathrm{CSS}(\ell,m,n)\right]\mathcal{L}_{3m}\psi_m^s\ , \tag{5a}$$

$$\mathcal{L}_{2\ell}\frac{\partial\psi_\ell^s}{\partial t}=k_\ell\,\hat{u}\,\mathcal{L}_{2\ell}\,\psi_\ell^c+k_\ell\,\hat{\zeta}_y\,\psi_\ell^c+k_\ell\,\beta\,\psi_\ell^c$$

$$+\sum_{m=1}^{M}\left[\sum_{n=1}^{N}k_m\bar{\zeta}_{yn}^{c}\,\mathrm{CSS}(n,m,\ell)\right]\mathcal{L}_0\psi_m^c+\sum_{m=1}^{M}\left[\sum_{n=1}^{N}k_m\bar{\zeta}_{yn}^{s}\,\mathrm{CSS}(m,\ell,n)\right]\mathcal{L}_o\psi_m^s$$

$$+\sum_{m=1}^{M}\left[\sum_{n=1}^{N}\bar{\zeta}_{zn}^{s}\,\mathrm{CSS}(m,\ell,n)\right]\mathcal{L}_1\psi_m^c+\sum_{m=1}^{M}\left[\sum_{n=1}^{N}\bar{\zeta}_{zn}^{c}\,\mathrm{CSS}(n,m,\ell)\right]\mathcal{L}_1\psi_m^s$$

$$+\sum_{m=1}^{M}\left[\sum_{n=1}^{N}k_m\bar{u}_n^{c}\,\mathrm{CSS}(n,m,\ell)\right]\mathcal{L}_{2m}\psi_m^c-\sum_{m=1}^{M}\left[\sum_{n=1}^{N}k_m\bar{u}_n^{s}\,\mathrm{CSS}(m,\ell,n)\right]\mathcal{L}_{2m}\psi_m^s$$

$$-\sum_{m=1}^{M}\left[\sum_{n=1}^{N}\bar{v}_n^{s}\,\mathrm{CSS}(m,\ell,n)\right]\mathcal{L}_{3m}\psi_m^c-\sum_{m=1}^{M}\left[\sum_{n=1}^{N}\bar{v}_n^{c}\,\mathrm{CSS}(n,m,\ell)\right]\mathcal{L}_{3m}\psi_m^s \tag{5b}$$

Here,

$$\mathrm{CCC}(m_1,m_2,m_3)=\frac{1}{L_x}\int_o^{L_x}\cos m_1x\cos m_2x\cos m_3x\,dx \tag{6a}$$

and

$$\mathrm{CSS}(m_1,m_2,m_3)=\frac{1}{L_x}\int_o^{L_x}\cos m_1x\sin m_2x\sin m_3x\,dx \tag{6b}$$

Upon replacing the operators by their finite difference approximations, (5) defines the matrices **A** and **B** in the matrix equation

$$\mathbf{A}\frac{d\mathbf{w}}{dt} = \mathbf{B}\mathbf{W} \tag{7}$$

The unknown vector **w** consists of the two vectors

$$(\psi^c_{1,2}\ \ \psi^c_{1,3}\cdots\psi^c_{1,J-1}\ \ \psi^c_{2,2}\cdots\psi^c_{2,J-1}\cdots\psi^c_{M,J-1})^T$$

and

$$(\psi^s_{1,2}\ \ \psi^s_{1,3}\cdots\psi^s_{1,J-1}\ \ \psi^s_{2,2}\cdots\psi^s_{2,J-1}\cdots\psi^s_{M,J-1})^T$$

placed end to end. The first subscript is the value of m and the second subscript an index of points in the y direction where $j = 1$ corresponds to the southern wall and $j = J$ to the northern wall. Note that for each value of m only the coefficients corresponding to the interior points are included in the unknown vector. Boundary conditions are incorporated by using $\psi^c_{m,1} = \psi^c_{m,J} = \psi^s_{m,1} = \psi^s_{m,J} = 0$ for all m whenever they are needed in the finite difference expressions of the operators.

Each row of the matrix equation corresponds to one of the $2M(J-2)$ equations defined by (5). The equation for a given (m, j) pair involves the surrounding j's for the same m on the left hand side but the surrounding j's for all the m's on the right hand side. Thus **A** is a tri- diagonal matrix, but **B** is considerably more complicated. In fact, not only is **B** a full matrix, but each element involves a sum over all the coefficients of the basic state. In the special case where the basic state is independent of x, **B** is much simpler because of the disappearance of all the double summation terms.

Chapter 4

SUMMARY AND CONCLUSIONS

The low frequency variability of the atmosphere is presently a subject of considerable interest. Phenomena such as blocks can influence the weather in a rather large region for a week to ten days and sometimes longer. Thus a better understanding of these phenomena can lead to improved medium range forecasting. In this study, we have investigated blocking from both an observational and a theoretical viewpoint. The climatological and synoptic descriptions of blocks were summarized. Then a review of blocking theories was presented consisting of a detailed critique of the multiple-equilibria and modon theories. The relevance of multiple equilibria theory is disputed, but we think it still holds significant promise for understanding large scale, low frequency behavior.

Modons offer an explanation for the structure and persistence of blocking events. However, the present development of the theory has several flaws. Until recently, the modon solutions with a high north of a low were obtainable in a barotropic context only with the *equivalent* barotropic vorticity equation. We are not convinced of the relevance of this equation despite several attempts at deriving it from a more justifiable starting point. In a baroclinic model, modons have an even more serious flaw: no solutions have been found with a vertical structure like that of blocks. Finally, there is little understanding of how modons evolve from more general flows. Thus, despite their attraction as an explanation of observed, long- lived, coherent structures such as blocks, progress has been slow in extending the modon concept to realistic situations.

The main body of the study is in two parts, the first of which is an examination of an individual blocking case using isentropic analysis. We particularly emphasize the distribution and evolution of potential vorticity on isentropic surfaces in light of the considerable recent interest in that subject. The principal conclusions from this case study

are as follows. Analysis of the Montgomery streamfunction on an isentropic surface is preferable to the more traditional analysis of geopotential height on a pressure surface for describing the evolution of the horizontal structure. Vertical cross sections show little tilt with height, a warm core and a high tropopause. Analysis of potential vorticity indicates that the block is a broad area of uniformly low potential vorticity. An EOF analysis added confirmation to this while illustrating well the development of the block. Both components of the potential vorticity; namely, the absolute vorticity and the static stability, evolved in the same way as the potential vorticity itself, becoming smaller or larger as the potential vorticity became smaller or larger. Subjective interpretation of the potential vorticity maps indicated that the low potential vorticity air characterizing the block originated from well south of the block. Isentropic trajectory analysis verified this and noted the relationship between the trajectories and the advection ahead of an intense cyclone that formed upstream of the block as the block developed. Selected moist trajectories differed quantitatively from the adiabatic trajectories; however, the qualitative results were unchanged.

The second part of the study is an examination of barotropic instability in the presence of downstream and asymmetric cross-stream variations in the basic state. Solutions are obtained with the non-divergent barotropic vorticity equation linearized about an arbitrary basic state. When downstream variation is present, the maximum amplitude of the unstable streamfunction is always located downstream from the location of maximum latitudinal shear. Following Peng and Williams (1986), this feature is explained by noting that the unstable disturbance lags in adjusting its structure to the local instability characteristics. The instability is sensitive to the degree of downstream variation with more concentration of streamfunction amplitude in specific regions of the channel, smaller disturbance scales and smaller growth rates when there is strong variation than when the flow is more parallel. The smaller growth rate for the downstream variation case results from the propagating disturbance being subject to strong shear for only a finite time before moving into regions of lesser shear where it cannot grow as fast. Asymmetric cross-stream variation has little effect on the growth rate and frequency of the most unstable

mode but significantly affects the structure of the instability. Larger amplitude and more pronounced tilt opposite to the shear occurrs on the side of the basic state jet with the strongest shear. This can be expected from a theoretical consideration of the energetics. It is reasonable to assume that sphericity would affect the unstable structures in a similar manner. Instabilities in the presence of both downstream and asymmetric cross-stream variations combine the effects of each of those individual kinds of variations. An eigenvalue method and a time integration method are used to obtain these results. They compare favorably and complement one another. A single non–linear calculation shows that as the disturbances grow to finite amplitude, they split, with high centers moving to the north and low centers to the south. The disturbances also increase in scale and stablize the mean flow without removing all the downstream variation.

Blocking is a complicated phenomenon undoubtedly involving several mechanisms and processes and as such is difficult to understand. The wealth of theories for its explanation is evidence of this. Our aim at the beginning of the study was to make a clear, original statement about the mechanisms important for blocking. We had hoped to be able to say something that would enable a meteorologist to evaluate a given synoptic situation and decide whether a new block was likely to form or whether an existing block would continue or decay. Unfortunately, our study has only proceeded part of the way towards this goal.

The multiple-equilibria theories were our first choice of approach. We planned to determine the "attractors" of the atmosphere, hoping to find several different regimes, each characterized by a distinct flow pattern. Presumably, one of those regimes would be similar to blocking flows. Once the attractors were identified, a diagnostic model would be used to determine the important dynamical and physical terms. If, as we hypothesized, each attractor had different characteristics, then we would have made significant progress towards determining whether a block was likely to form, continue or decay in any given situation. About this time, the work of Hoskins, *et al.* (1985) on the use and significance of isentropic potential vorticity maps became known and the preliminary data work for our study lead to the case study using isentropic analysis reported on in Chapter 2. It

was also at this time that the multiple-equilibria theories began to be disputed in the literature. Therefore, after completing the case study, we temporarily abandoned this approach.

Motivated by the case study results that lent credence to the role played by cyclones in blocking development, our efforts took a different direction. We were familiar with the modon theories which seemed to provide a particularly good explanation for the structure and persistence of blocks. We postulated that intense cyclones could transform a portion of a wavy large scale flow pattern into a dipole structure where modon dynamics could then account for its coherence and persistence. A sufficiently intense cyclone could also play a role in the destruction of the modon. Thus we were lead to investigate modons in more detail. Again, if our hypothesis was correct, we would have been able to make a significant statement about whether a block was likely to form, continue or decay in a given synoptic situation. However, we found modon theory lacking in several respects as discussed in Chapter 1.

Finally, we turned to a third prominent theory for blocks which suggest that they result from instabilities of the large scale flow. Certainly not every large scale flow is conducive to a blocking-like structure as the dominant mode of instability. The character of the instability is a strong function of the basic state upon which it grows. Therefore, it is important to document and understand the sensitivity of the instabilities to changes in the large scale flow. Only with a detailed knowledge of this sensitivity can we determine whether a block will form in any given synoptic situation. Towards this end we performed the barotropic calculations reported in Chapter 3. That research can be characterized as basic geophysical fluid dynamics, yet by documenting the sensitivity of an increasingly complex hierarchy of barotropic instabilities to basic state variations, we have taken a positive and promising step towards achieving our goal.

The effect of a diabatic heating is not explicitly included in the multiple– equlibria and modon theories nor have we considered it in this instability study. It is likely that diabatic effects play a non–negligible role in the evolution of blocking flows; however, we believe that they are not essential for qualitative understanding. We have noted observational evidence (Colucci, 1987) that rapidly intensifying cyclones ("bombs") can produce blocking

flows downstream when the planetary wave structure is suitable. Diabatic heating is involved in this process through the land–sea contrasts which help force the planetary scale stationary waves but also through the intense convection usually associated with bombs (Anthes, *et al.*, 1983). However, the effect on blocking is indirect: diabatic heating acts by determining the large–scale structure and the intensity of the cyclone instead of acting as a direct forcing of the blocking scale in a localized region. Yet the low potential vorticity and high tropopause characteristic blocks can perhaps be explained by the diabatic processes in bombs: The latent heat release and cumulus momentum mixing accompanying intense convection raises the tropopause and creates low potential vorticity air. Both the tropopause (as a boundary) and the low potential vorticity air can then be advected into the blocking region (Professor William Gray, personal communication). Whether the convection in bombs is necessary for a cyclone to significantly change the large scale flow has not yet been determined.

Blocks are high latitude, warm anomalies characterized by relatively cloud free conditions. Therefore, it is reasonable to suspect that significant radiational cooling is acting to dissipate the thermal anomaly. One or more processes must maintain the blocking anomaly by opposing this thermal sink as well as mechanical loss mechanisms. Several observational and theoretical studies (e.g. Shutts, 1986, Haines and Marshall, 1987) show that transient storms feed a nearly continual supply of low potential vorticity air into the blocking region. However, Mullen (1986) finds that this eddy forcing balances not the radiational cooling, which is small, but rather the time averaged advections. Moreover, there has been no definitive study that addresses whether breakdown of blocks is the result of weakening of the anomaly through radiational cooling, or, taking a common synoptic viewpoint, the result of the interaction of the block with an especially intense and favorably positioned synoptic scale storm. Therefore, though radiational cooling is important on the time scale of blocks, it is not clear how this process influences blocking evolution.

Even if diabatic heating in its various forms is essential to blocking flows, it is inherently difficult to include in numerical and theoretical models. On a large scale, diabatic effects must be parameterized. Though much effort has been devoted to this problem,

parameterization is still a somewhat *ad hoc* business. It is better to explain as much as possible from a purely dynamical basis where the physical laws on the large scale are well understood and appropriate techniques and simplifications are available. We believe diabatic processes are important, but not essential to a basic understanding of blocks. It is our considered opinion that in addition to sorting out the relative merits of the various dynamical theories, we also need a clear notion of how diabatic processes are acting during blocking periods. This should then be followed by the development of a reasonable parameterization.

In retrospect, multiple-equilibria and modon theories should not be dismissed as offering no hope for understanding blocks. Despite some critical evaluation of these theories, they are still receiving attention in the literature and some of their problems which inhibited our research have since been addressed and solved. (See Chapter 1.) For example, there is now considerable evidence that multiple regimes can be documented in observational data (Hansen and Sutera, 1986). Also, stationary modons with a high north of a low in a westerly background flow have been found for the non-divergent barotropic vorticity equation (Verkley, 1987).

However, we believe the instability approach holds the most promise for understanding and predicting whether a block will form in a given synoptic situation. At the end of Chapter 3, several suggestions were made regarding the future direction of this research. The first involved baroclinic calculations. We have developed a two layer, quasi-geostrophic model linearized about an arbitrary basic state. This model can be used to extend the barotropic calculation to the baroclinic case. This diabatic heating can then be included if desired. If blocking is indeed an instability, it is most likely a combined barotropic/baroclinic instability. Extensions of these calculations to the sphere should also be considered. The final suggestion involved more complete non-linear calculations. We also have at our disposal fully non-linear barotropic and two level quasi-geostrophic models. These models can be used to further our understanding of the non-linear equilibration that is undoubtedly necessary to make a more complete identification between instabilities and blocks. Moreover, non–linear instability theory may allow a better understanding of the other non–linear blocking theories of multiple–equilibria and modons.

Especially in the latter case, the splitting of high and low centers noted in our non–linear simulation may shed some light on modon generation. Perhaps a block arises from an instability which, as it reaches finite amplitude, develops an appropriate dipole structure such that modon dynamics can then account for its persistence.

REFERENCES

Anthes, R.A., Y.-H. Kuo and J.R. Gyakum, 1983: Numerical simulation of a case of explosive marine cyclogenesis. *Mon. Wea. Rev.*, **111**, 1174-1188.

Colucci, S.J., 1977: Comparitive diagnosis of blocking versus non-blocking planetary scale circulation changes during synoptic scale cyclogenesis. *J. Atmos. Sci.*, **44**, 124-139.

Haines, K. and J. Marshall, 1987: Eddy–forced coherent structures as a prototype of atmospheric blocking. *Quart. J. Roy. Meteor. Soc.*, **113**, 681-704.

Hansen, A.R. and A. Sutera, 1986: On the probability density distribution of planetary scale atmospheric wave amplitude. *J. Atmos. Sci.*, **43**, 3250- 3265.

Hoskins, B.J., M. E. McIntyre and A.W. Robertson, 1985: On the use and significance of isentropic potential vorticity maps. *Quart. J. Roy. Meteor. Soc.*, **111**, 877-946.

Peng, M.S. and R.T. Williams, 1986: Spatial instability of the barotropic jet with slow streamwise variation. *J. Atmos. Sci.*, **43**, 2430-2442.

Shutts, G.J., 1986: A case study of eddy forcing during an Atlantic blocking episode. *Adv. Geophys.*, **29**, 135-162.

Verkley, W.T.M., 1987: Stationary barotropic modons in westerly background flows. *J. Atmos. Sci.*, **44**, 2383-2398.